CLIMATE INFLUENCE ON PHYTOPLANKTON PHENOLOGY IN THE GLOBAL OCEAN

A thesis submitted to the School of Environmental Sciences of the University of East Anglia in partial fulfilment of the requirements for the degree of Doctor of Philosophy

By Marie-Fanny Racault

October 2009

À Mamie, Maman, Doudoune and Daddy,
Pour votre amour, votre soutien et votre patience,
Vous y avez toujours cru,
Merci.

Abstract

Every year, the oceans absorb one quarter of the carbon dioxide (CO_2) emitted to the atmosphere by human activities. This CO_2 sink is part of a very active, natural carbon cycle, through which phytoplankton fix CO_2 into organic matter in the surface layer of the ocean. Phytoplankton cells tend to aggregate and sink from this surface layer, exporting carbon to the deep ocean and regulating the atmospheric CO_2 on long time scales. In the light of the recent unequivocal evidence of global warming, it appears essential to assess its impact on phytoplankton community and to evaluate the subsequent feedback through the oceanic carbon cycle.

In recent years, phytoplankton phenology has been suggested as a systematic indicator to monitor the state of the pelagic ecosystem and detect changes triggered by perturbation of environmental conditions. For the first time, the phenology of phytoplankton growing season is estimated at the global scale using remote-sensing ocean colour data. The tropics and subtropics present generally long growing season (15-20 weeks) of low amplitude ($< 0.5\ mg\ m^{-3}$), whereas the high-latitudes show short growing season (< 10 weeks) of high amplitude (up to $7\ mg\ m^{-3}$). Correlation analyses suggest a close coupling between the development of the growing season and the seasonal increase in insolation in the North Atlantic and Southern Ocean. In the tropics and subtropics, light is rarely limiting and the growing season is controlled by nutrient supply enhanced by water mixing. Over the decade 1998-2008, the duration of growing season shows large interannual variability of up to $\pm$ 10 weeks. Globally, positive anomalies follow the major 1997-98 El Niño-La Niña events and persist until 2001. Positive phases of climate indices such as the North Atlantic Oscillation and the Southern Annular Mode, associated with enhanced water mixing and nutrients supply, generally sustain longer growing season.

Using *in-situ* observations, we show that the export of carbon can be related to the length of the phytoplankton growing season, with largest export in regions where the growing season is shortest and the blooms most intense. Using satellite observations, from the sensors CZCS and SeaWiFS, we estimate that North of 45°S, the phytoplankton growing season increased by 2.4 weeks on average between the periods 1979-1986 and 1998-2008. Longer growing seasons are associated with regional patterns of surface warming on the same time scale. We infer from *in-situ* data a decrease in carbon export of 0.6 Pg C yr^{-1} (excluding the Southern Ocean) over two decades. This represents an unexpected, and important, feedback between physical and biological processes in the ocean: global warming modifies phytoplankton growth, reducing the capacity of the ocean to absorb atmospheric CO_2 leading to a probable aggravation of global warming.

Finally, phenological characteristics of the phytoplankton growing season are used to resolve Sverdrup's critical depth model. Mixed layer integrated plankton community respiration R_{mld} and net community production NCP_{mld} are estimated at the global scale using remote-sensing data of incident irradiance level and primary production, and a global mixed layer depth climatology. NCP_{mld} estimates agree with *in-situ* observations and model results in the tropical and North Atlantic regions. The model estimates a net autotrophic imbalance of + 0.65 Pg C yr^{-1} in the North Atlantic and a net heterotrophic imbalance of − 1 Pg C yr^{-1} for the whole tropics and subtropics.

Acknowledgements

I would like to express my sincere appreciation to my supervisor Corinne Le Quéré for giving me the chance to work on this project and to achieve a PhD. You have been particularly motivating, inspiring and challenging over the last three years. I will always remember your great optimism, incredible enthusiasm and cutting perspicacity towards science. Thank you for giving me the freedom to explore areas of research I was interested in.

I would like to thank Trevor Platt and Shubha Sathyendranath for their continuous encouragement, for their helpful advice and valuable discussions regarding my work. I also thank Erik Buitenhuis for his time and patience in answering my random and spontaneous science questions, and for giving me the chance to analyse some model results. I would like to thank Sergio for his interest in my work and for discussing my results with me. I thank Clare Enright for programming support on the remote-sensing data. I also thank the members of the Dynamic Green Ocean Project for discussions and D. Wolf-Gladrow for providing the MATLAB code for the maximum likelihood estimate of the linear model parameters and their uncertainties.

I would like to give a giant thank you to Amandine for being such a wonderful friend throughout this PhD. It has been so much fun in your company and you gave a real french touch to the whole UEA experience. Thank you for all your encouragement and your deep understanding of any situation. I have really appreciated all the time we have spent together and all the long conversations we have had. Surely, you have expanded my feminist point of view. I would like to give a very big thank to Libby for being such a great office mate. I'll remember with a happy smile the crazyness that went on in the late evenings when we were so tired of working. You

have been such a wonderful running partner. I am really looking forward to the days when we both have time to train and run a marathon together. I thank Matt, James and Lee for always having a nice word to me every time I came to the office, and even when I was looking horrendously stressed. It was highly appreciated. I would like to thank Janina for being such a great climbing partner, for all the fun we had on Monday and Thursday evenings spent at the climbing wall; it's just been awesome. Thanks to Janina, Alba, Sophie, Eva, Andy and Roland for all the happy climbing weekends in the Peaks and Dorset. I have definitely improved my camping skills in the cold and damp english weather. Alba, I must say that you are surely the kindest spanish girl I'll ever meet. You are so nice and care so much for everyone in the office, thank you. I thank Jim for his patience in explaining to me some of the finer points of statistics. I would also like to thank Eva and Michael for their constant optimism. I thank the chemist team of Karine, Hicham and Thomas for all those light-hearted french conversation we had on at lunch time.

In addition, I would like to express thanks to the staff in ENV for giving me the chance to undertake some demonstrating, I found it a really positive experience. I also thank them for discussions about my research, the PhD and the future after the PhD.

I am indebted to my family for all their encouragement and support throughout the hard times. You have been incredibly patient and understanding. A big thank to my cousins Delphine, Ingrid and Olivier for your enthusiasm about my PhD, your sincere encouragement and for always making me feel I was doing something special.

Contents

List of tables

List of figures

Chapter 1

Introduction

1.1 Climate

Climate is the average condition of the atmosphere and underlying land or water on seasonal, decadal, centennial and longer timescales (Le Treut et al., 2007). Climate is typically characterised by a set of variables such as temperature, precipitation, wind, cloud cover, humidity, sea surface temperature (SST), sea ice extent and thickness. Although the variables are usually described in terms of their mean and variability, other measures such as maximum seasonal temperature, minimum annual sea ice extent, frequency of storms or floods, and the length of the growing season may also provide useful information. The Earth's climate evolves in time under the influence of its intrinsic variability, and because of changes in external forcings, either long-term or abrupt.

1.1.1 Variability

Large-scale patterns of climate variability (so called teleconnection patterns) are characterised by various climatic modes or indices. The El Niño Southern Oscillation (ENSO) is the most important pattern of climate variability in the tropics. The northern and southern annular modes are the dominant patterns of climate variability in the northern and southern hemispheres. Whereas ENSO owes its existence to coupled ocean-atmosphere interaction in the tropical Pacific, the annular modes are related to fluctuations in the position of atmospheric masses between the mid- and high-latitudes.

El Niño Southern Oscillation (ENSO)

El Niño events lead to warming of surface temperature in the equatorial Pacific from the International Date Line to the western coast of South America. Atmospheric variations are linked to the Southern Oscillation, which describes the fluctuations in the sign difference of air pressure between the eastern (i.e. Tahiti) and western (i.e. Darwin) tropical and subtropical Pacific. The atmospheric fluctuations induce changes in the Trade Winds, tropical circulation and precipitation (Trenberth et al.,

2007). In the historical record of the ENSO cycle, warm SST El Niño or cold La Niña events occur every 3 to 7 years. The particularly strong El Niño in 1997-1998 followed by the La Niña in 1998-1999 altered dramatically the upwelling of nutrient-enriched deep waters in the tropical Pacific. Phytoplankton biomass increased by 10% during the El Niño to La Niña transition and the high biomass persisted until 2000 (Behrenfeld et al., 2001).

North Atlantic Oscillation (NAO)

The NAO is a climatic phenomenon of the North Atlantic (NA) that exercises its influence throughout the Northern Hemisphere (NH). The NAO is characterised by fluctuations in the difference of atmosphere pressure between the Icelandic Low and the Azores High pressure systems (Hurrell, 1995). The variability of the NAO is largest during the winter months (December to March) (Hurrell et al., 2003). Alternations between positive and negative NAO phases produce large changes in the mean wind speed and direction between 40°N and 60°N, the associated heat and moisture transport from the Atlantic to the neighbouring continents, and the intensity and frequency of storms and their paths (Hurrell et al., 2003). Changes in the NAO also induce significant changes in SST, ocean heat content and currents, and sea-ice extent and thickness (Williams, 2000; Hu et al., 2002).

Southern Annular Mode (SAM)

The SAM is the leading mode of variability in the atmospheric circulation of the Southern Hemisphere (SH) (Marshall, 2003). The SAM is characterised by the difference in atmospheric pressure zonal mean at 40°S and 65°S. The variability of the SAM is largest during the austral summer months (December to March) (Ciasto and Thompson, 2008). Oscillations in the position of atmospheric mass between the polar regions and the midlatitudes influence the position and strength of the circumpolar winds and the corresponding heat and moisture transport. Changes in the dynamic of atmospheric forcings affect the Southern Ocean (SO) meridional

overturning circulation, the pathways of intermediate water ventillation and leave a strong signature in the SST (Sen Gupta and England, 2006).

The amplitude and patterns in which climatic modes influence the ocean-atmosphere system have been shown to vary markedly over multi-decadal timescales (Trenberth et al., 2007). Knowledge of the natural modes of variability is therefore critical to detect and attribute climate change.

1.1.2 Changes

Anthropogenic and natural changes

Climate is governed by the amount of energy entering and escaping the Earth's system. Changes in the energy balance will induce directional changes in the Earth's climate. The concentration of greenhouse gases in the atmosphere has increased since the industrial era. Greenhouse gases absorb the heat that would otherwise escape to space, and thus warm the planet. Carbon dioxide (CO_2) is the main anthropogenic greenhouse gas. It increased by 105 ppm between 1750 and 2008 (nearly 40%) in response to human activities, especially burning of fossil fuels and deforestation (Le Treut et al., 2007).

The largest climate changes detected in Antarctic ice cores showing paleoclimatic records of the past 800,000 years, reveal an alternation between glacial and inter-glacial periods (Jouzel et al., 2007). Such dramatic changes in the Earth's surface temperature have resulted from small variations in the Earth's orbit and axis of rotation (Milankovitch, 1941; Varadi et al., 2003). These variations modulate the amount and location of solar radiation reaching the Earth and lead to a global cooling or warming of the Earth's system. An additional, more abrupt but short-lasting changes in climate are caused by volcanic eruptions. Large quantities of particles are ejected into the atmosphere, enhancing reflection of the incident solar radiation and creating a global cooling effect. The violent eruption of Mount Pinatubo in 1991 resulted in cooler-than-average global surface temperatures that lasted for

years (Soden et al., 2003).

Part of the challenge in understanding the recent changes in climate has been to distinguish between natural and anthropogenic-induced climate changes. The present CO_2 concentration is the highest compared with any time in the last half-million years (Petit et al., 1999), and nearly one million years (Jouzel et al., 2007). The Intergovernmental Panel on Climate Change (IPCC) stated in the 2007 report that *the warming of the planet is unequivocal* and that *the observed increase in global average over the past 50 years is very likely due to the observed increase in anthropogenic greenhouse gas concentrations* (IPCC, 2007).

Recent oceanic climate change

The oceans have the largest heating capacity on Earth. During the past 50 years, the net heat uptake by the world ocean has been more than 20 times greater than that by the atmosphere (Levitus et al., 2005). Thus, the oceans play a major buffer role in the variability and change of the Earth's climate system. The temperature of the upper 3,000 m of the world ocean has increased on average by 0.037°C over the past 50 years (Levitus et al., 2005). Changes in the ocean heat content are not uniformly distributed. Whereas most regions of the world ocean present a global warming trend, the North Pacific, the western tropical Pacific, and the subarctic gyre of the North Atlantic show a global cooling trend (Bindoff et al., 2007). The origin of this variability is not well understood. Global warming of the world ocean temperature is expected to enhance vertical stratification especially in the tropics and subtropics (Sarmiento et al., 2004).

Although the global warming in ocean temperatures tend to reduce gas solubility, the recent large increase in atmospheric CO_2 concentrations has led to greater uptake of CO_2 by the oceans. Increased CO_2 concentration reduce ocean pH and carbonate ion concentrations, which in turn reduce the capacity of the ocean to take up additional CO_2. Rapid ocean acidification (over decadal timescale) has a detrimental impact on marine calcifying organisms (Feely et al., 2004; Orr et al.,

2005). The response of marine ecosystems to ocean acidification is difficult to assess as a whole and may cause a weakening in the biological part of the oceanic carbon cycle (see section 1.3.2). Weakening of the oceanic sink of CO_2 has been observed in SO in response to an increase in winds resulting from human activities (Le Quéré et al., 2007).

1.2 Tools to monitor biological responses to the changes

1.2.1 Ocean colour remote sensing

General introduction

Synoptic fields of phytoplankton biomass indexed as concentration of chlorophyll-a have been available from remote sensing for more than 20 years. They provide long-time series data with a global coverage at high spatial resolution (1 km) and frequency (1 day). Ocean colour remote sensing is based on passive radiometers or sensors measuring in the visible wavelengths the light emerging from the surface after passing through the sea. Particulate and dissolved substances interact with the sunlight penetrating the sea. Scattering and absorption of the incident light by particulate and dissolved substances influence the colour of the light leaving the sea. In general, phytoplankton cells contain a suite of pigments that absorb strongly in the blue and red regions of the visible spectrum, but weakly in the green. Thus, when the abundance of phytoplankton cells in the surface layer increases, the colour of the water will appear increasingly green.

Most of the radiation reaching the sensor is contributed by atmospheric backscatter, mainly from aerosols and air molecules (Martin, 2004). The remaining fraction ($\approx$ 10-20%) of the radiation reaching the sensor under cloud-free conditions depends on the pigment concentrations. Algorithms have been developed to remove this contamination and allow retrieval of the information about the constituents of

the upper surface layer of the sea.

Ocean colour sensors

The Coastal Zone Color Scanner (CZCS) was flown on the Nimbus-7 satellite launched in October 1978. CZCS was a demonstration mission designed to operate for one year. In fact, the sensor remained operational for seven and a half years, until June 1986. CZCS was the first sensor specifically developed to study ocean colour properties. Its mission had two main objectives: (1) "to establish the technological and scientific feasibility of mapping ocean phytoplankton pigment concentrations from satellite" and (2) "to determine the improvements that must be made for successful follow-on ocean colour missions" (Gregg et al., 2002). CZCS was a multi-spectral line scanner which measured reflected radiations in six spectral bands (Table 1.1; IOCCG (1998)). Ocean colour was monitored in four bands of the visible spectra: band one (blue) for chlorophyll absorption; band two (green) for chlorophyll concentration; band three (yellow) for dissolved organic coloured matter or suspended sediments; and band four (red) for aerosol absorption. A fifth band in the near infrared (NIR) monitored land vegetation and band six in the thermal infrared sensed SST (Martin, 2004). The temporal and spatial coverage of CZCS data was limited by power restrictions, clouds, darkness and sensor saturation over ice or snow masses.

The next major satellite instrument was the Sea-viewing Wide Field-of-View Sensor (SeaWiFS), launched in August 1997 aboard the OrbView-2 satellite. The sensor began acquiring data on 16th September 1997 and continued to operate in 2009. SeaWiFS measures reflected radiations in eight spectral bands (Table 1.1; IOCCG (1998)). The six bands in the visible spectra were adjusted on the better understanding of the spectral absorption characteristics of common water constituents (Martin, 2004). The addition of one spectral band in the NIR compared with CZCS improved information to remove more accurately aerosol and atmospheric contamination (Table 1.1).

Merging of ocean colour products from different sensors

Detection of the response of marine ecosystems to changing climatic conditions requires the construction of long-time series, which in turn requires the merging of ocean-colour data from different sensors.

Building-on the experience of CZCS, significant improvements on processing algorithms and calibration techniques have been applied to follow-on sensors, such as SeaWiFS. CZCS and SeaWiFS are relatively different instruments and intercomparison of their ocean colour products is not a straightforward process. Gregg et al. (2002) reanalysed comprehensively the CZCS archive in an effort called the NOAA-NASA CZCS Reanalysis (NCR). NCR applied modern atmospheric correction and bio-optical algorithms to improve the precision and accuracy of the retrieved ocean colour information. The data were then blended with *in-situ* chlorophyll measurements to minimise possible bias in the satellite-derived fields. NCR chlorophyll showed remarkable correspondence with SeaWiFS data and decadal changes in global ocean chlorophyll could be quantified (Gregg and Conkright, 2002). Antoine et al. (2005) adopted a different approach that remained relatively independent from *in-situ* observations. The authors revised the CZCS data processing algorithms to generate an improved "revised CZCS" chlorophyll data set. To allow intercomparison between the CZCS and SeaWiFS sensors, they applied the same revised algorithms to SeaWiFS data over the period 1998-2002.

The above data merging efforts aimed to allow quantitative comparisons of satellite-derived field of chlorophyll over decadal timescales. Recent approaches to monitor temporal changes in ecosystems have relied on ecological indicators (Platt and Sathyendranath (2008); see section 1.2.2 below). Some of these indicators relate to the timing of pelagic events such as the duration, initiation or peak of the phytoplankton growing season. These events can be calculated using relative methods of analysis of the field of chlorophyll (as opposed to methods based on absolute chlorophyll concentration). Such a relative approach has been implemented in the present study and allowed to compare information from both CZCS and SeaWiFS.

1.2.2 Development of ecological indicators from ocean-colour remote sensing

Ecological indicators have been developed to provide systematic, economical and objective metrics of the state of the ecosystems. Indicators aim to detect temporal (seasonal to decadal) as well as spatial (local to global) changes in ecosystems. Indicators must therefore be comparable between years and sites. Given the frequency and spatial resolution of ocean colour remote sensing data, they provide an excellent basis for the development and implementation of ecological indicators. Platt and Sathyendranath (2008) set out the rational and approach to the development of pelagic ecological indicators. The authors described 14 ecological indicators that can be retrieved from ocean colour remote sensing (Table 1.2). The first four characterise the phytoplankton growing season with respect to its amplitude, time of initiation, time of maximum and duration. The next four describe production and losses of organic matter by phytoplankton, either on an annual scale or integrated over the duration of the growing season. The f-ratio is defined as new production/total production (Eppley and Peterson, 1979; Laws et al., 2000), with new production being to a first approximation the integrated production over the growing season. Spatial variance in biomass and production fields are then considered. Qualitative aspects of the phytoplankton community are pictured through the phytoplankton functional types (PFTs) and size structure. Recent advances in the use of remotely-sensed ocean colour data now allow global mapping of some of the PFTs, including diatoms, Coccolithophores, *Phaeocystis*, Haptophytes, *Prochlorococcus* and *Synechococcus*-like cyanobacteria (Brown and Yoder, 1994; Sathyendranath et al., 2004; Alvain et al., 2005; Uitz et al., 2006; Aiken et al., 2007). Finally, combining ecological indicators with ocean biogeochemical characteristics is possible with the partitioning the ocean into biogeographic provinces, as proposed by Longhurst (1998); Devred et al. (2007).

Amongst the indicators mentioned above, some have been investigated for more than two decades, such as the annual phytoplankton production (Platt and Sathyendranath, 1988; Sathyendranath et al., 1989; Antoine et al., 1996; Behrenfeld and

Falkowski, 1997; Mélin, 2003), while others such as community losses (Zhai et al., 2008) or timing of pelagic events (Siegel et al., 2002; Platt et al., 2003; Henson et al., 2006) have been applied only recently to ocean colour remote sensing data.

1.2.3 Phytoplankton phenology

Definition

Phenology is derived from the Greek *phaino* meaning to appear, to come into view. Hence, phenology relates to the study of the timing of periodic biological events as influenced by the environment (Schwartz, 2003). The seasonal development of phytoplankton population is defined as the phytoplankton growing season. Events of particularly rapid production and accumulation of phytoplankton biomass are described as phytoplankton blooms (Cloern, 1996). The timing of phytoplankton development is strongly related to environmental conditions, such as day length, temperature, the timing of spring/fall stratification/de-stratification or the timing of ice break-up. Thus, phytoplankton phenology provides a pertinent tool to the analysis of long-term trends.

Detection and calculation

Phenologically important phases of the phytoplankton growing season include: (1) the time of initiation b_i; (2) the time of maximum amplitude b_t; (3) the time of end b_e; and (4) the duration b_d. Most studies of phytoplankton phenological characteristics have focused on the retrieval of b_i and b_t. The latter because it is readily identified, and the former for its predictive value of differing biological responses. Two distinct approaches have been implemented to the identification of b_i: either the timing of changes in the physical conditions is estimated and then b_i is retrieved (Platt et al., 1991; Nelson and Smith Jr., 1991; Obata and Ishizaka, 1996; Follows and Dutkiewicz, 2002); or b_i is estimated directly from the seasonal signal of chlorophyll and coherence with the changes in physical conditions is then examined (Siegel et al., 2002; Henson et al., 2006; Platt et al., 2009a). Only the second approach

remains independent of the physical variables, permitting investigation of changes in phytoplankton phenology in relation to the physical environment.

Several different methods have been developed to estimate b_i from *in-situ* and remotely-sensed observations of chlorophyll concentration in marine or freshwater ecosystems. The choice of method depended essentially on the shape of the phytoplankton growing season (exponential or not) and the sampling frequency. Conventionally, the methods involve: (1) estimating the inflexion points (Rolinski et al., 2007; Wiltshire et al., 2008); (2) fitting a density function such as the Weibull or Gaussian distribution (Platt et al., 2003; Rolinski et al., 2007; Platt et al., 2009b); (3) defining a fixed or relative threshold chlorophyll level (Siegel et al., 2002; Fleming and Kaitala, 2006; Henson et al., 2006; Platt et al., 2009b). The relative threshold method is particularly suitable for work on a global scale because it encompasses the large variability of shapes in the phytoplankton growing season. Using interannual remotely-sensed chlorophyll data, Siegel et al. (2002) proposed the median chlorophyll plus 5% as a suitable relative threshold for the NA. The authors found little quantitative differences in b_i when using thresholds ranging from 1 to 30%. Henson et al. (2006) applied this same median plus 5% threshold in the Irminger Basin. She demonstrated basin-scale coherence in b_i and the timing of mixed layer stratification. After fitting a shifted-Gaussian curve to the chlorophyll data, Platt et al. (2009b) defined a relative threshold for initiation as the time when the amplitude of the fitted curve reached 20% of the maximum amplitude of the Gaussian.

In the present study, the relative threshold of Siegel et al. (2002) (i.e. median plus 5%) was selected because of its pertinence on global scale, its direct applicability to remotely-sensed chlorophyll data, and because it had been successfully implemented in other studies (Henson et al., 2006, 2009). The end of the growing season is estimated using the same threshold as the initiation. The duration of the growing season is simply calculated as the difference between initiation and end.

1.3 Observed biological responses to the changes

Phytoplankton play a major role in pelagic ecosystems because they are at the base of the food chain. Coherence in the timing of larval release and phytoplankton population development is critical to the survival and year-class strength of zooplankton and fish populations (Cushing, 1990; Platt et al., 2003; Koeller et al., 2009). Phytoplankton are also extremely important in the oceanic carbon cycle. They consume CO_2 by photosynthesis and export carbon to the deep ocean, thus regulating the oceanic uptake of CO_2 on long time-scales. Hence, changes in abundance, timing and composition of the phytoplankton will have a critical impact on pelagic community structure and composition as well as on ocean biogeochemistry.

1.3.1 Observed changes in phenology

Numerous terrestrial studies have treated the phenological importance and more recently of the phenological shifts, in the life cycles of plants, birds, insects, amphibians, fish and mammals (see Hughes (2000) and Parmesan and Yohe (2003) for a review). Hence, on land, phenology is not a particularly recent field of study, being probably as old as civilisation itself (Schwartz, 2003). In a recent assessment of the biological response to climate warming, Parmesan and Yohe (2003) reported that 87% of the observed shifts in phenologies occurred in the direction expected from climate change. Although changes in the length of land vegetation growing season are well established (Hughes, 2000; Parmesan and Yohe, 2003; Menzel et al., 2006) and have now reached the interpretation stage (Steltzer and Post, 2009), global scale marine phytoplankton growing season remains to be characterised.

The critical importance of the timing of the onset of phytoplankton spring bloom for larval and fish recruitment was suggested almost 100 years ago (Hjort, 1914) and further characterised with the match/mismatch hypothesis of Cushing (1975). Yet the validation of this hypothesis (Platt et al., 2003) had to wait for advances in remote-sensing technologies and the availability of high spatial and temporal resolution of chlorophyll measurements. Egg development and larval release are dependent

on water temperature. Hence, some zooplankton and fish species have significantly advanced their seasonal cycles in response to climate warming in the NA (Edwards and Richardson, 2004). However, in this region, the seasonal development of phytoplankton is triggered by the increase in insolation rather than changes in temperature (Sverdrup, 1953; Platt et al., 2009a), leading to decoupling of phenological relationships between phytoplankton and larvae.

Analysis of large-scale, decadal and long-term variability in phytoplankton phenology in relation to environmental conditions has been only recently possible. In the NA, the latitudinal progression of the spring bloom follows the increase in insolation and extends over almost five months, from an initiation in January in the subtropics to May in the subpolar region (Siegel et al., 2002). Interannual variability in the timing of initiation of the spring bloom in the Irminger Basin was shown to be related to the preceding winter's mean wind speed and net heat flux (Henson et al., 2006). Decadal (from remote-sensing) and long-term (from model) estimations of the timing of initiation show no particular trends toward earlier or delayed bloom in the NA (Henson et al., 2009). However, the particularly strong periodicity in the bloom timing in the subpolar region correlates positively with the NAO index.

1.3.2 Role of biology in the oceanic carbon cycle

The oceans absorb one quarter of the CO_2 emitted into the atmosphere by human activities every year (Canadell et al., 2007). Understanding the factors affecting the variability of the ocean carbon cycle is therefore particularly important to assess possible changes in its efficiency as a natural carbon sink.

The oceanic carbon cycle

The global ocean contains approximately 50 times more CO_2 compared with the atmosphere (Raven and Falkowski, 2002). Air-sea exchange of CO_2 occurs through molecular diffusion in the direction of the difference between the CO_2 gas partial pressure (pCO_2) in the oceans and the atmosphere. CO_2 solubility decreases with

increasing temperature. Hence, in equatorial regions, upwelling of cold deep waters to the surface result in CO_2 being outgassed from the ocean to the atmosphere. The equatorial regions act as a net source of CO_2 (Le Quéré and Metzl, 2004). Low-latitude warm surface waters are then transported by ocean currents towards mid- and high-latitudes, where they cool. The formation of deep-water occurs at high-latitudes where waters are cooler and CO_2 solubility is higher. Thus, the high-latitudes act as particularly strong net sink of CO_2 (Le Quéré and Metzl, 2004). As the deep ocean is mainly filled with high latitude waters, the deep ocean carbon concentration is then on average higher than the surface concentration because of the cool surface temperatures at high latitudes. The enhanced deep ocean carbon concentration resulting from this process is called the solubility pump.

In the sunlit surface layer of the oceans, phytoplankton cells fix dissolved CO_2 by photosynthesis, to produce organic matter. This is known as the primary production (PP). A number of processes contribute to the remineralisation of organic matter: (1) phytoplankton maintenance and dark respiration; (2) phytoplankton excretion; (3) zooplankton grazing; and (4) bacterial degradation. Hence, dead phytoplankton cells or fragments of tissue can either be recycled or sink through the water column in particulate form. The downward flux of particulate organic carbon (POC) is called the export production. The organic carbon exported to the deep-waters becomes isolated from the atmosphere for decades to centuries, until the deep-waters are transported back to the surface by mixing, currents and upwelling. The enhanced deep ocean carbon concentration resulting from the downward export and upward transport of organic matter is called the biological pump.

Under normal conditions of temperature and alkalinity, the dissolution of CO_2 in seawater decreases carbonate ($CO_3{}^{2-}$) ion concentration and increases bicarbonate ($HCO_3{}^{-}$) ion concentration according to the reaction:

$$CO_2 + H_2O + CO_3{}^{2-} \longleftrightarrow 2HCO_3{}^{-} \tag{1.1}$$

Some species of phytoplankton such as the coccolithophores and foraminiferans produce calcium carbonate ($CaCO_3$) tests. The downward export of these cells removes

carbonate ions from the surface waters and drives the equilibrium of the reaction 1.1 toward the left, increasing surface CO_2 concentration. This process partly counters the effects of the biological pump and is known as the carbonate pump.

Characterisation of export production

Net community production (NCP) is the difference between PP and community respiration (i.e. described in section 1.3.2 as the remineralisation processes). NCP represents the *potential* of the plankton community for organic carbon export (Williams, 2000). The term *potential* is employed because the effects of advection and mixing might transport away part of NCP and modify the net export production in one site. Although the first estimations of PP from ocean colour remote-sensing were obtained three decades ago (Platt and Sathyendranath, 1988) and have been thoroughly investigated ever since, knowledge about the rates of community respiration (R) and NCP is still relatively limited (del Giorgio and Duarte, 2002; Robinson and Williams, 2005; Robinson, 2008). *In-situ* measurements of R and NCP have increased over the last two decades (see Robinson and Williams (2005) for a review). Unfortunately, empirical relationships between PP and R are not straightforward (del Giorgio et al., 1997; Williams, 1998; Duarte and Augusti, 1998), and the nature of the trophic balance of the global ocean remains difficult to assess (Williams et al., 1999; del Giorgio and Duarte, 2002).

Preliminary estimates of export using sediment traps (Eppley and Peterson, 1979) have suggested an explicit link between the rates of new production (i.e. the fraction of PP supported by "new" inputs of nutrients and not by recycled nutrients) and the flux of particles out of the surface layer. In the 1980s, the Joint Global Ocean Flux Study (JGOFS) was launched with the specific aim to advance understanding and estimation of export flux throughout the global ocean (Buesseler, 2001). *In-situ* measurements of export flux can be determined using a range of methods (Berelson, 2001) including: (1) ^{14}C estimation of POC produced during

PP; (2) Thorium isotope budgets of POC export from the surface to the few hundreds metres of the water-column; (3) sediment traps that collect the rain of POC at different depths; and (4) estimation of sea-floor remineralisation rates. Trap collection biases have been reduced recently with the conception of neutrally buoyant sediment traps (Buesseler et al., 2007) as opposed to the previously "fixed" traps (i.e. tethered to surface flotation). The Underwater Video Profiler is amongst the newest technology developed to sample particle-size distributions along the water-column (Gorsky et al., 2000). The particularly large sampling effort carried out over the last three decades has highlighted the large spatial and temporal variability in export flux and unravelled the unprecedented complexity of the functioning of the biological pump.

Basin-scale or global estimates of export production can only be achieved by: (1) extrapolation of *in-situ* carbon flux measurements from sediment traps (using Martin et al. (1987) power function to describe the decrease in vertical flux with depth); (2) model studies that simulate the rates of new production and then estimates export flux (Laws et al., 2000); and (3) model studies based on inverse methods of calculation to retrieve export flux from observed changes in ocean biogeochemical tracers such as nutrients, oxygen or dissolved inorganic carbon (Schlitzer, 2002). Global export production estimated from these methods ranges between 3 and 20 PgC yr^{-1} (see Najjar et al. (2007) for a review). Such variability occurs because the biological processes responsible for export production are not yet fully resolved or quantified.

Variability in biological export production

The strength and efficiency of the biological pump depends on the PFTs present in surface waters. Diatoms appear as the major contributors to carbon export (Bopp et al., 2005) because they form particularly intense blooms that aggregate into large particles. The opal content of their shells act as a mineral ballast, increasing their sinking speed through the water column (Klaas and Archer, 2002). Coccolithophores

also form large blooms in the NA (Brown and Yoder, 1994). The calcium carbonate making up their shells is denser than opal and therefore, coccolithophores contribution to export production is high (Klaas and Archer, 2002). Picophytoplankton aggregate into smaller particles (Guidi et al., 2009), which sink more slowly and are more likely to be remineralised. Thus, smaller phytoplankton tend to be associated with low export production.

1.4 Aims of the thesis

This study seeks to assess the influence of climate on the spatial and temporal variability of phytoplankton phenology at the global scale.

The specific aims of this thesis are:

- To determine the spatial and interannual variability of phytoplankton phenology at the global scale.
- To assess the control by environmental conditions on phytoplankton phenology.
- To investigate the relationship between large-scale patterns of climate variability and variations in phytoplankton phenology.
- To explore the links between phytoplankton phenology and export production.
- To evaluate the decadal variation in phytoplankton growing season and estimate its impact on the oceanic carbon cycle.
- To calculate plankton community respiration and net community production using Sverdrup's critical depth model at a global scale.

References

Aiken, J., Fishwick, J., Lavender, S., Barlow, R., Moore, G., and Sessions, H. (2007). Validation of MERIS reflectance and chlorophyll during the BENCAL cruise October, 2002: Preliminary validation of new products for phytoplankton functional types and photosynthetic parameters. *Int. J. Remote Sens.*, 28:497–516.

Alvain, S., Moulin, C., Dandonneau, Y., and Bréon, F. (2005). Remote sensing of phytoplankton groups in case 1 waters from global SeaWiFS imagery. *Deep Sea Res., Part I*, 52:1989–2004.

Antoine, D., André, J.-M., and Morel, A. (1996). Oceanic primary production 2. Estimates at global scale from satellite (coastal zone color scanner) chlorophyll. *Global Biogeochem. Cycles*, 10:57–69.

Antoine, D., Morel, A., Gordon, H., Banzon, V., and Evans, R. (2005). Bridging ocean color observations of the 1980s and 2000s in search of long-term trends. *J. Geophys. Res.*, 110:doi:10.1029/2004JC002620.

Behrenfeld, M. and Falkowski, P. G. (1997). Photosynthetic rates derived from satellite-based chlorophyll concentration. *Limnol. Oceanogr.*, 42:1–20.

Behrenfeld, M. J., Randerson, J. T., McClain, C. R., Feldman, G. C., Los, S. O., Tucker, C. J., Falkowski, P. G., Field, C. B., Frouin, R., Esaias, W. E., Kolber, D. D., and Pollack, N. H. (2001). Biospheric primary production during an ENSO transition. *Science*, 291:doi:10.1126/science.1055071.

Berelson, W. (2001). The Flux of Particulate Organic Carbon Into the Ocean Interior: A Comparison of Four U.S. JGOFS Regional Studies. *Oceanography*, 14:59–67.

Bindoff, N., Willebrand, J., Artale, V., A, C., Gregory, J., Gulev, S., Hanawa, K., Le Quéré, C., Levitus, S., Nojiri, Y., Shum, C., Talley, L., and Unnikrishnan, A. (2007). Oceanic climate change and sea level. In Solomon, S., Qin, D., Manning, M., Chen, Z., Marquis, M., Averyt, K., Tignor, M., and Miller, H., editors, *Climate Change 2007: The Physical Science Basis. Contribution of Working Group I to the Fourth Assessment*

Report of the Intergovernmental Panel on Climate Change, pages 385–432. Cambridge University Press, Cambridge, UK and New York, USA.

Bopp, L., Aumont, O., Cadule, P., Alvain, S., and Gehlen, M. (2005). Response of diatoms distribution to global warming and potential implications: A global model study. *Geophys. Res. Lett.*, 32:doi:10.1029/2005GL023653.

Brown, C. and Yoder, J. (1994). Coccolithophorid blooms in the global ocean. *J. Geophys. Res.*, 9:7467–7482.

Buesseler, K. O. (2001). Ocean Biogeochemistry and the Global Carbon Cycle: An Introduction to the U.S. Joint Global Ocean Flux Study. *Oceanography*, 14:5.

Buesseler, K. O., Lamborg, C., Boyd, P., Lam, P., Trull, T., Bidigare, R., Bishop, J., Casciotti, K., Dehairs, F., Elskens, M., Honda, M., Karl, D., Siegel, D., Silver, M., Steinberg, D., Valdes, J., Van Mooy, B., and Wilson, S. (2007). Revisiting Carbon Flux Through the Oceans Twilight Zone. *Science*, 316:doi:10.1126/science.1137959.

Canadell, J., Le Quéré, C., Raupach, M., Field, C., Buitenhuis, E., Ciais, P., Conway, T., Gillett, N., Houghton, R., and Marland, G. (2007). Contributions to accelerating atmospheric CO_2 growth from economic activity, carbon intensity, and efficiency of natural sinks. *Proc. Natl. Acad. Sci. USA*, 104:doi:10.1073/pnas.0702737104.

Ciasto, L. and Thompson, D. (2008). Observations of Large-Scale Ocean-Atmosphere Interaction in the Southern Hemisphere. *J. of Clim.*, 21:1244–1259.

Cloern, J. (1996). Phytoplankton bloom dynamics in coastal ecosystems: a review with some general lessons from sustained investigation of San Francisco Bay, California. *Rev. Geophys.*, 34:127–168.

Cushing, D. (1975). Fish stocks and the production cycles. In Cushing, D., editor, *Marine ecology and fisheries*, pages 133–163. Cambridge University Press, Cambridge, UK.

Cushing, D. (1990). Plankton production and year-class strength in fish populations: an update of the match/mismatch hypothesis. *Adv. Mar. Biol.*, 26:142–155.

del Giorgio, P., Cole, J., and Cimbleris, A. (1997). Respiration rates in bacteria exceed phytoplankton production in unproductive aquatic ecosystems. *Nature*, 385:148–151.

del Giorgio, P. and Duarte, C. (2002). Respiration in the open ocean. *Nature*, 420:doi:10.1038/nature01165.

Devred, E., Sathyendranath, S., and Platt, T. (2007). Delineation of ecological provinces using ocean colour radiometry. *Mar. Ecol. Prog. Ser.*, 346:1–13.

Duarte, C. and Augusti, S. (1998). The CO_2 Balance of Unproductive Aquatic Ecosystems. *Science*, 281:doi:10.1126/science.281.5374.234.

Edwards, M. and Richardson, A. (2004). Impact of climate change on marine pelagic phenology and trophic mismatch. *Nature*, 430:doi:10.1038/nature02808.

Eppley, R. W. and Peterson, B. J. (1979). Particulate organic matter flux and planktonic new production in the deep ocean. *Nature*, 282:677–680.

Feely, R., Sabine, C., Lee, K., Berelson, W., Kleypas, J., Fabry, V., and Millero, F. (2004). Impact of Anthropogenic CO_2 on the $CaCO_3$ System in the Oceans. *Science*, 305:doi:10.1126/science.1097329.

Fleming, V. and Kaitala, S. (2006). Phytoplankton spring bloom intensity index for the Baltic Sea estimated for the years 1992 to 2004. *Hydrobiologia*, 554:doi:10.1007/s10750–005–1006–7.

Follows, M. and Dutkiewicz, S. (2002). Meteorological modulation of the North Atlantic spring bloom. *Deep Sea Res., Part II*, 49:321–344.

Gorsky, G., Picheral, M., and Stemmann, L. (2000). Use of the underwater video profiler for the study of aggregate dynamics in the North Mediterranean. *Estuar. Coast. Shelf Sci.*, 50:121–128.

Gregg, W., Conkright, M., O'Reilly, J., Patt, F., Wang, M., Yoder, J., and Casey, N. (2002). NOAA-NASA Coastal Zone Color Scanner Reanalysis Effort. *Appl. Opt.*, 41:doi:10.1364/AO.41.001615.

Gregg, W. W. and Conkright, M. E. (2002). Decadal changes in global ocean chlorophyll. *Geophys. Res. Lett.*, 29:doi:10.1029/2002GL014689.

Guidi, L., Stemmann, L., Jackson, G., Ibanez, F., Claustre, H., Legendre, L., Picheral, M., and Gorsky, G. (2009). Effects of phytoplankton community on production, size and export of large aggregates: A world-ocean analysis. *Limnol. Oceanogr.*, 54:1951–1963.

Henson, S., Dunne, J., and Waniek, J. (2009). Decadal variability in North Atlantic phytoplankton blooms. *J. Geophys. Res.*, 114:doi:10.1029/2008JC005139.

Henson, S., Robinson, I., Allen, J., and Waniek, J. (2006). Effect of meteorological conditions on interannual variability in timing and magnitude of the spring bloom in the Irminger Basin, North Atlantic. *Deep Sea Res., Part I*, 53:1601–1615.

Hjort, J. (1914). Fluctuations in the great fisheries of northern Europe. *Rapp. Conserv. Explor. Mer*, 20:1–228.

Hu, A., Rooth, C., Bleck, R., and Deser, C. (2002). NAO influence on sea ice extent in the Eurasian coastal region. *Geophys. Res. Lett.*, 29:doi:10.1029/2001GL014293.

Hughes, L. (2000). Biological consequences of global warming: is the signal already apparent? *Trends Ecol. Evol.*, 15:56–61.

Hurrell, J. W. (1995). Decadal trends in the North Atlantic Oscillation: Regional temperatures and precipitation. *Science*, 269:676–679.

Hurrell, J. W., Kushnir, Y., Ottersen, G., and Visbeck, M. (2003). The North Atlantic Oscillation: Climatic Significance and Environmental Impact. *Geophysical Monograph*, 134:doi:10.1029/134GM01.

IOCCG (1998). Report Number 1: Minimum Requirements for an Operational, Ocean-Colour Sensor for the Open Ocean. In Morel, A., editor, *Reports of the International Ocean-Colour Coordinating Group (IOCCG)*, pages 1–50. Dartmouth, Canada.

IPCC (2007). Summary for policymakers. In Solomon, S., Qin, D., Manning, M., Chen, Z., Marquis, M., Averyt, K., Tignor, M., and Miller, H., editors, *Climate Change 2007: The Physical Science Basis. Contribution of Working Group I to the Fourth Assessment*

Report of the Intergovernmental Panel on Climate Change, pages 1–18. Cambridge University Press, Cambridge, UK and New York, USA.

Jouzel, J., Masson-Delmotte, V., Cattani, O., Dreyfus, G., Falourd, S., Hoffmann, G., Minster, B., Nouet, J., Barnola, J. M., Chappellaz, J., Fischer, H., Gallet, J. C., Johnsen, S., Leuenberger, M., Loulergue, L., Luethi, D., Oerter, H., Parrenin, F., Raisbeck, G., Raynaud, D., Schilt, A., Schwander, J., Selmo, E., Souchez, R., Spahni, R., Stauffer, B., Steffensen, J., Stenni, B., Stocker, T., Tison, J., Werner, M., and Wolff, E. W. (2007). Orbital and Millennial Antarctic Climate Variability over the Past 800,000 Years. *Science*, 317:doi:10.1126/science.1141038.

Klaas, C. and Archer, D. E. (2002). Association of sinking organic matter with various types of mineral ballast in the deep sea: Implications for the rain ratio. *Global Biogeochem. Cycles*, 16:doi:10.1029/2001GB001765.

Koeller, P., Fuentes-Yaco, C., Platt, T., Sathyendranath, S., Richards, A., Ouellet, P., Orr, D., Skúladóttir, U., Wieland, K., Savard, L., and Aschan, M. (2009). Basin-Scale Coherence in Phenology of Shrimps and Phytoplankton in the North Atlantic Ocean. *Science*, 324:doi:10.1126/science.1170987.

Laws, E. A., Falkowski, P. G., Jr., W. O. S., Ducklow, H., and McCarthy, J. J. (2000). Temperature effects on export production in the open ocean. *Global Biogeochem. Cycles*, 14:1231–1246.

Le Quéré, C. and Metzl, N. (2004). Natural processes regulating the oceanic uptake of CO_2. In Field, C. and Raupach, M., editors, *The Global Carbon Cycle: Integrating Humans, Climate, and the Natural Wolrd*, pages 243–255. Island Press, Washington, D.C.

Le Quéré, C., Rödenbeck, C., Buitenhuis, E., Conway, T., Langenfelds, R., Gomez, A., Labuschagne, C., Ramonet, M., Nakazawa, T., Metzl, N., gillett, N., and Heimann, M. (2007). Saturation of the Southern Ocean CO_2 sink due to recent climate change. *Science*, 316:doi:10.1126/science.1136188.

Le Treut, H., Somerville, R., Cubasch, U., Ding, Y., Mauritzen, C., Mokssit, A., Peterson, T., and Prather, M. (2007). Historical overview of climate change. In Solomon, S.,

Qin, D., Manning, M., Chen, Z., Marquis, M., Averyt, K., Tignor, M., and Miller, H., editors, *Climate Change 2007: The Physical Science Basis. Contribution of Working Group I to the Fourth Assessment Report of the Intergovernmental Panel on Climate Change*, pages 93–128. Cambridge University Press, Cambridge, UK and New York, USA.

Levitus, S., Antonov, J., and Boyer, T. (2005). Warming of the world ocean, 1955-2003. *Geophys. Res. Lett.*, 32:doi:10.1029/2004GL021592.

Longhurst, A. (1998). *Ecological Geography of the Sea*. Academic Press, Califoria.

Marshall, G. (2003). Trends in the Southern Annular Mode from observations and reanalyses. *J. of Clim.*, 16:4134–4143.

Martin, J. H., Knauer, G. A., Karl, D. M., and Broenkow, W. W. (1987). VERTEX: Carbon cycling in the northeast Pacific. *Deep Sea Res.*, 34:267–285.

Martin, S. (2004). Ocean Color. In Martin, S., editor, *An Introduction to Ocean Remote Sensing*, pages 124–165. Cambridge University Press, Cambridge, UK.

Mélin, F. (2003). *Potentiel de la télédétection pour l'analyse des propriétés optiques du système océan-atmosphère et application à l'estimation de la photosynthèse phytoplanctonique*. PhD thesis, Université Toulouse III.

Menzel, A., Sparks, T., Estrella, N., Koch, E., Aasa, A., Ahas, R., Alm-kübler, K., Bissolik, P., Braslavaskà, O., Briede, A., Chmielewski, F., Crepinsek, Z., Curnel, Y., Dahl, A., Defila, C., Donnelly, A., Filella, Y., Jatczak, K., Måge, F., Mestre, A., Nordli, Ø., Penũelas, J., Pirinen, P., Remišová, V., Scheifinger, H., Striz, M., Susni, A., Van Vliet, A., Wielgolaski, F.-E., Zach, S., and Zust, A. (2006). European phenological response to climate change matches the warming pattern. *Glob. Change Biol.*, 12:doi:10.1111/j.1365–2486.2006.01193.x.

Milankovitch, M. (1941). Canon of Insolation and the Ice-Age Problem. *K. Serb. Akad. Beogr. Spec. Publ.*, 132. English translation by the Israel program for Scientific Translations, 1969.

Najjar, R. G., Jin, X., Louanchi, F., Aumont, O., Caldeira, K., Doney, S. C., Dutay, J.-C., Follows, M., Gruber, N., Joos, F., Lindsay, K., Maier-Reimer, E., Matear, R., Matsumoto, K., Monfray, P., Mouchet, A., Orr, J., Plattner, G.-K., Sarmiento, J., Schlitzer, R., Slater, R., Weirig, M.-F., Yamanaka, Y., and Yool, A. (2007). Impact of circulation on export production, dissolved organic matter, and dissolved oxygen in the ocean: Results from Phase II of the Ocean Carbon-cycle Model Intercomparison Project (OCMIP-2). *Global Biogeochem. Cycles*, 21:doi:10.1029/2006GB002857.

Nelson, D. M. and Smith Jr., W. (1991). Sverdrup Revisited: Critical Depths, Maximum Chlorophyll Levels, and the Control of Southern Ocean Productivity by the Irradiance-Mixing Regime. *Limnol. Oceanogr.*, 36:1650–1661.

Obata, A. and Ishizaka, J. (1996). Global verification of critical depth theory for phytoplankton bloom with climatological in situ temperature and satellite color data. *J. Geophys. Res.*, 101:20657–20667.

Orr, J., Fabry, V., Aumont, O., Bopp, L., Doney, S., Feely, R., Gnanadesikan, A., Gruber, N., Ishida, A., Joos, F., Key, R., Lindsay, K., Maier-Reimer, E., Matear, R., Monfray, P., Mouchet, A., Najjar, R., Plattner, G., Rodgers, K., Sabine, C., Sarmiento, J., Schlitzer, R., Slater, R., Totterdell, I., Weirig, M., Yamanaka, Y., and Yool, A. (2005). Anthropogenic ocean acidification over the twenty-first century and its impact on calcifying organisms. *Nature*, 437:doi:10.1038/nature04095.

Parmesan, C. and Yohe, G. (2003). A globally coherent fingerprint of climate change impacts across natural systems. *Nature*, 421:doi:10.1038/nature01286.

Petit, J., Jouzel, J., Raynaud, D., Barkov, N. I., Barnola, J., Basile, I., Bender, M., Chappellaz, J., Davis, M., Delaygue, G., Delmotte, M., Kotlyakov, V. M., Legrand, M., Lipenkov, V., Lorius, C., Pépin, L., Ritz, C., Saltzman, E., and Stievenard, M. (1999). Climate and atmospheric history of the past 420,000 years from the Vostok ice core, Antarctica. *Nature*, 399:doi:10.1038/20859.

Platt, T., Bird, D., and Sathyendranath, S. (1991). Critical depth and marine primary production. *Proc. R. Soc. Lond., Ser. B*, 246:205–217.

Platt, T., Fuentes-Yaco, C., and Frank, K. (2003). Spring algal bloom and larval fish survival. *Nature*, 423:398–399.

Platt, T. and Sathyendranath, S. (1988). Oceanic Primary Production: Estimation by Remote Sensing at Local and Regional Scales. *Science*, 241:doi:10.1126/science.241.4873.1613.

Platt, T. and Sathyendranath, S. (2008). Ecological indicators for the pelagic zone of the ocean from remote sensing. *Remote Sens. Environ.*, 112:3426–3436.

Platt, T., Sathyendranath, S., White II, G., Fuentes-Yaco, C., Zhai, L., Devred, E., and Tang, C. (2009a). Diagnostic Properties of Phytoplankton Time Series from Remote Sensing. *Estuaries and Coasts*, 32:doi:10.1007/s12237–009–9161–0.

Platt, T., White II, G., Zhai, L., Sathyendranath, S., and Roy, S. (2009b). The phenology of phytoplankton blooms: Ecosystem indicators from remote sensing. *Ecol. Model.*, In press:doi:10.1016/j.ecolmodel.2008.11.022.

Raven, J. and Falkowski, P. (2002). Oceanic sinks for atmospheric CO_2. *Plant, Cell and Environment*, 22:741–755.

Robinson, C. (2008). Heterotrophic Bacterial Respiration. In Kirchman, D., editor, *Microbial Ecology of the Oceans, Second Edition*, pages 299–334. Wiley, New York.

Robinson, C. and Williams, P. (2005). Respiration and its measurement in surface marine waters. In del Giorgio, P. and Williams, P., editors, *Respiration in Aquatic Ecosystems*, pages 147–180. Oxford University Press, Oxford.

Rolinski, S., Horn, H., Petzoldt, T., and Paul, L. (2007). Identifying cardinal dates in phytoplankton time series to enable the analysis of long-term trends. *Oecologia*, 153:doi:10.1007/s00442–007–0783–2.

Sarmiento, J. L., Slater, R., Barber, R., Bopp, L., Doney, S., Hirst, A., Kleypas, J., Matear, R., Mikolajewicz, U., Monfray, P., Soldatov, V., Spall, S., and Stouffer, R. (2004). Response of ocean ecosystems to climate warming. *Global Biogeochem. Cycles*, 18:doi:10.1029/2003GB002134.

Sathyendranath, S., Platt, T., Caverhill, C., Warnock, R., and Lewis, M. (1989). Remote sensing of oceanic primary production: computations using a spectral model. *Deep Sea Res.*, 36:431–453.

Sathyendranath, S., Watts, L., Devred, E., Platt, T., Caverhill, C., and Maass, H. (2004). Discrimination of diatom from other phytoplankton blooms using ocean-colour data. *Mar. Ecol. Prog. Ser.*, 272:59–68.

Schlitzer, R. (2002). Carbon export fluxes in the Southern Ocean: results from inverse modeling and comparison with satellite-based estimates. *Deep Sea Res., Part II*, 49:1623–1644.

Schwartz, M. (2003). Introduction. In Schwartz, M., editor, *Phenology: An Integrative Environmental Science*, pages 1–7. Kluwer Academic Publishers, New York.

Sen Gupta, A. and England, M. (2006). Coupled ocean-atmosphere-ice response to variations in the Southern Annular Mode. *J. of Clim.*, 19:4457–4486.

Siegel, D., Doney, S., and Yoder, J. (2002). The North Atlantic spring phytoplankton bloom and Sverdrup's critical depth hypothesis. *Science*, 296:730–733.

Soden, B., Wetherald, R., Stenchikov, G., and Robock, A. (2003). Global Cooling After the Eruption of Mount Pinatubo: A Test of Climate Feedback by Water Vapor. *Science*, 296:doi:10.1126/science.296.5568.727.

Steltzer, H. and Post, E. (2009). Seasons and Life Cycles. *Science*, 324:doi:10.1126/science.1171542.

Sverdrup, H. U. (1953). On conditions for the vernal blooming of phytoplankton. *Cons. Int. Expor. Mer.*, 18:287–295.

Trenberth, K., Jones, P., Ambenje, P., Bojariu, R., Easterling, D., Klein Tank, A., Parker, D., Rahimzadeh, F., Renwick, J., Rusticucci, M., Soden, B., and Zhai, P. (2007). Observations: Surface and atmospheric climate change. In Solomon, S., Qin, D., Manning, M., Chen, Z., Marquis, M., Averyt, K., Tignor, M., and Miller, H., editors, *Climate Change 2007: The Physical Science Basis. Contribution of Working Group I to the*

Fourth Assessment Report of the Intergovernmental Panel on Climate Change, pages 235–336. Cambridge University Press, Cambridge, UK and New York, USA.

Uitz, J., Claustre, H., Morel, A., and Hooker, S. (2006). Vertical distribution of phytoplankton communities in open ocean: An assessment based on surface chlorophyll. *Geophys. Res. Lett.*, 111:10.1029/2005JC003207.

Varadi, F., Runnegar, B., and Ghil, M. (2003). Successive refinements in long-term integrations of planetary orbits. *Astrophys. J.*, 592:620–630.

Williams, P. (1998). The balance of plankton respiration and photosynthesis in the open oceans. *Nature*, 394:55–57.

Williams, P. (2000). Net production, gross production and respiration: what are the interconnections and what controls what? In Hanson, R. B., Ducklow, H. W., and Field, J. G., editors, *The changing ocean carbon cycle: a midterm synthesis of the Joint Global Ocean Flux Study*, pages 37–60. Cambridge University Press, Cambridge.

Williams, P., Bowers, D., Duarte, C., Augusti, S., del Giorgio, P., and Cole, J. (1999). Regional Carbon Imbalances in the Oceans. *Science*, 284:doi:10.1126/science.284.5421.1735b.

Wiltshire, K., Malzahn, A., Wirtz, K., Greve, W., Janisch, S., Mangelsdorf, P., Manly, B., and Boersma, M. (2008). Resilience of North Sea phytoplankton spring bloom dynamics: An analysis of long-term data at Helgoland Roads. *Limnol. Oceanogr.*, 53:1294–1302.

Zhai, L., Platt, T., Tang, C., Dowd, M., Sathyendranath, S., and Forget, M. (2008). Estimation of phytoplankton loss rate by remote sensing. *Geophys. Res. Lett.*, 35:doi:10.1029/2008GL035666.

1.5 Tables

Table 1.1: Comparison of the spectral bands used for ocean-colour applications for the CZCS and SeaWiFS instruments. Adapted from IOCCG (1998) and Martin (2004).

Wavelength range (nm)	
CZCS	SeaWiFS
–	402-422
433-453	433-453
–	480-500
510-530	500-520
540-560	545-565
660-680	660-680
–	745-785
700-800	845-885

Table 1.2: Ecological indicators proposed by Platt and Sathyendranath (2008) for the pelagic ocean. Indicators have been developped from ocean-colour remote-sensing.

Indicator	Label	Dimensions
Initiation of growing season	b_i	[T]
Timing of maximum amplitude	b_t	[T]
Duration of growing season	b_d	[T]
Amplitude of growing season	b_a	[M L^{-3}]
Total production in growing season	b_p	[M L^{-2}]
Annual phytoplankton production	P_y	[M L^{-2}]
Generalised phytoplankton loss rate	L	[M L^{-3} T^{-1}]
Integrated phytoplankton loss	L_T	[M L^{-3}]
Annual-scale *f*-ratio	f	Dimensionless
Spatial variance in biomass field	${\sigma^2}_B$	[M L^{-6}]
Spatial variance in production field	${\sigma^2}_P$	[M L^{-4}]
Phytoplankton functional types	NA	NA
Phytoplankton size structure	s	Dimensionless
Delineation of biogeochemical provinces	NA	NA

Chapter 2

Phenology of phytoplankton growing season in the global ocean

2.1 Abstract

Ecological indicators have received much attention in recent years as systematic tools to monitor the state of the pelagic ecosystem and detect changes triggered by perturbation of the environmental conditions. Here we describe the phenology of phytoplankton growing season for the world ocean using remote-sensing ocean colour data, and analyse its variability between 1998 and 2007. The tropics and subtropics present generally longer duration ($\approx$ 15-20 weeks) and lower amplitude ($< 0.5\ mg\ Chl\ m^{-3}$), while the high-latitudes show shorter duration ($<$ 10 weeks) and higher amplitude (up to 7 $mg\ Chl\ m^{-3}$). Correlation analyses suggest a close coupling between the development of the growing season and the seasonal increase in insolation in the North Atlantic and Southern Ocean. In the tropics and subtropics, light is rarely limiting and the growing season is controlled by nutrient supply occurring when mixing increases and surface waters are cooling. Over the decade 1998-2008, the duration of growing season shows large interannual variability of up to $\pm$ 10 weeks. Globally, positive anomalies follow the major 1997-98 El Niño-La Niña events and persist until 2001. As a result, negative linear trends in duration ($-$ 10 % yr^{-1} on average) are observed over a large fraction of the ocean. Positive phases of climate indices such as the North Atlantic Oscillation and the Southern Annular Mode, associated with enhanced water mixing and nutrients supply, generally sustain longer growing season.

2.2 Introduction

Diversity in the pelagic ecosystem is driven by the variability of physical conditions over the global ocean. At the base of the food chain, autotrophic phytoplankton require light and nutrients to grow. Supply of essential nutrients to the illuminated zone is modulated by changes in the depth of the mixed layer. Large seasonal changes in the depth of the mixed layer occur at mid and high latitudes. In autumn and winter, the mixed layer deepens, allowing transfer of nutrients from the rich deep water and subsequent replenishment of the mixed layer. In spring and summer, the mixed layer shallows, allowing phytoplankton cells to receive sufficient light for net positive growth. In the tropics, light is rarely a limiting factor. However, permanent stratification of the mixed layer limits nutrient supply and phytoplankton growth.

In the global ocean, phytoplankton growth conditions are controlled by regional and seasonal changes in physical forcings (such as sea-surface temperature, winds storminess, cloud cover and precipitations), which are in turn forced by climatic patterns. Extratropical, large-scale climate patterns are characterised by indices of climatic modes such as the North Atlantic Oscillation (NAO) and Southern Annular Mode (SAM). Properties of the pelagic ecosystem are affected by the variability of such climatic modes, through changes in grazer abundance and community composition (Beaugrand and Reid, 2003), integrated primary production (Bates, 2001), and phytoplankton community composition (Lomas and Bates, 2004; Leterme et al., 2005).

To allow regional and interannual comparison of the effect of changes in physical forcing or climatic modes on the pelagic ecosystem, ecological indices have been developed. Ecological indices are quantitative metrics of the pelagic ecosystem introduced as objective alternatives to more subjective concepts such as ecosystem health, vigour and resilience (Platt and Sathyendranath, 2008). The indices must therefore be comparable between years and sites because of the large spatial and temporal variability in the annual phytoplankton growing season. One systematic

approach to characterise the phytoplanktonic ecosystem is to quantify the phenology of phytoplankton growing season. Phenology is defined as the study of seasonal timing of phytoplankton growth events. For pelagic ecosystem, the seasonal timing of phytoplankon growth can be critical to survival and recruitment of fish and invertebrate populations (Platt et al., 2003; Koeller et al., 2009).

Phytoplankton growth can be approximated at a global scale from remotely sensed changes in chlorophyll concentrations (biomass). The annual phytoplankton growing season corresponds to more or less rapid and intense changes in biomass, where the most rapid and intense increase in biomass were defined as bloom (Sverdrup, 1953; Cushing, 1959; Yoder et al., 1993).

In the present study, a decade of remote-sensing ocean colour data from 1998 to 2007 are used to: (1) describe the regional and interannual variability in the phenology of phytoplankton growing season for the global ocean; (2) explore the relationships between the phenology of growing season and the changes in climate and physical conditions.

2.3 Data and methods

2.3.1 The remotely-sensed data

Satellite measurements of sea-surface concentrations of chlorophyll-*a* (Chla) and photosynthetically active radiation (PAR) are made by sensing the ocean-leaving radiation in the visible part of the electromagnetic spectrum, while the sea-surface temperature (SST) measurement are made in the infra-red part of the spectrum.

The Sea-viewing Wide Field-of-view Sensor (SeaWiFS) weekly level 3 data of Chla and PAR with a global area coverage at 9 km resolution were retrieved from http://oceancolor.gsfc.nasa.gov/ for the period 1998-2007. A fortran programming code was written to read all the input files in HDF format and to write a unique output file in NetCDF format. To estimate the timing of various ecological events, gaps were eliminated from the time series using the Ferret NOAA PMEL software as

follows. Missing values were substituted by interpolating spatially-adjacent values (from the 9 km grid), if these were not missing. Otherwise the value was not filled. The remaining missing values were filled by interpolating temporally-adjacent values, if these were not missing. Otherwise the value was not filled. A three-weeks running mean was applied to remove small peaks in Chla. The data were then averaged to one degree resolution.

NOAA Optimum Interpolation SST V2 weekly data products were downloaded on a one-degree global grid from the National Oceanic-Atmospheric Administration/Office of Oceanic and Atmospheric Research/Earth System research Laboratory at http://www.cdc.noaa.gov/ for the period 1998-2007.

2.3.2 Ecological and physical indices

The ecological indices considered in this paper are summarised in Table 2.1. The timings of initiation (b_i) and end (b_e) of the phytoplankton growing season were detected as the weeks when the chlorophyll concentration in a particular year rose above the long-term median value plus 5% and later fell below this same threshold (Siegel et al., 2002). The duration (b_d) of the growing season is defined as the number of weeks between initiation and end. The present method of analysis captures only the characteristics of the main phytoplankton growing season that is associated with the timing (b_t) and value (b_a) of the maximum amplitude of the chlorophyll signal. The method does not account for sub-surface chlorophyll maxima or secondary blooms. The chlorophyll integrated over the duration (b_s) provides a useful metric to compare different regions of the ocean that display similar durations of growing season.

Physical indices were derived from the PAR and SST datasets. PAR and SST values were retrieved at the times of initiation (l_i and t_i) and end (l_e and t_e) of the growing season in a particular year. The average PAR and SST indices were calculated over the duration of the growing season (l_d and t_d).

Interannual variability in the indices were highlighted by subtracting the 10-year

mean from each annual estimate to show the annual anomalies.

2.3.3 Climate indices

The North Atlantic Oscillation (NAO) index was obtained from the NOAA Climate Prediction Center at http://www.cpc.ncep.noaa.gov/data/teledoc/nao.shtml for the period 1998-2007. The NAO index (Hurrell, 1995) describes basin scale patterns of climate variability. Anomalies in the index are characterised by: (1) changes in the intensity of the surface westerly winds across the North Atlantic towards Europe and (2) shifts in atmospheric mass over the North Atlantic between high pressures centred on the Azores and low pressures around Iceland. Winter (December-March) NAO anomalies were computed by removing the 1998-2007 mean winter signal.

The Southern Annular Mode (SAM) was derived from Marshall (2003) reanalysis available at http://www.nerc-bas.ac.uk/icd/gjma/sam.html. The SAM (Kidson, 1988) describes large-scale climate variability in the Southern Hemisphere. Anomalies in the mode are characterised by: (1) north-south shifts in atmospheric mass between the polar regions and the midlatitudes and (2) north-south oscillations in the latitude of the midlatitude westerly winds. The amplitudes of the midlatitude dynamics and climate patterns have been shown to be largest during the warm season (Ciasto and Thompson, 2008). Hence, in the present study, austral summer (December-March) SAM anomalies were computed by removing the 1998-2007 mean warm season signal.

2.3.4 Statistical analyses

Spearman rank correlation analysis was performed over the 10-year time-series between anomalies of: (1) b_i and l_i; (2) b_i and t_i; (3) b_d and b_i; (4) b_d and b_e and (5) b_i and b_e. Autocorrelation between the time-series generates artificially high correlation coefficients. The results are therefore used only to distinguish geographical patterns of positive, negative or absence of correlations.

The differences between means of anomalies of duration during positive and negative anomalies of SST or climate indices were analysed using Welch *t*-test. Unlike the Student *t*-test that is based on a pooled variance estimate, the Welch *t*-test allows to compare variables with unequal size and variance.

2.4 Results and discussion

2.4.1 Phenology of the phytoplankton growing season

Spatial patterns of the phenology of the phytoplankton growing season are illustrated in Fig. 2.1 for the global ocean. Regional variability is observed in the timing, duration and amplitude of the growing season. Poleward of 30°N and S the propagation in the timing of initiation of the growing season follows the latitude-dependent progression in light intensity. In the tropics and subtropics (30°S-30°N), light supply is usually not limiting and the latitudinal propagation is not observed. This pattern is summarised in Table 2.2 and further evidenced in section 2.4.2 (Fig. 2.2). The method of detection of the timing events is centred around the main peak of Chla in a particular year. It allows detection of initiation and end times outside of that particular year, when such cases occur. Thus, the "negative" initiation times found in the tropics (Fig. 2.1) correspond to a growing season with a peak amplitude in April (i.e. week 15) of the year n and an initiation in December (i.e. week -4) of the year n - *1*. Initiation, peak and end of the growing season succeed one another in time with almost identical latitudinal propagation trends.

The phenological importance and variability in the timing of events is emphasised in the duration index where regional patterns of short and long growing seasons can be discerned. Longer growing season between 15-20 weeks are found at low and mid-latitudes, where the water column is permanently stratified (Sarmiento et al., 2004). The duration decreases towards higher latitudes and becomes shorter than 10 weeks in the subpolar regions. In these regions, phytoplankton growth is mostly limited by light availability and by the depth of the mixed layer. High-latitude

short growing seasons display both the highest amplitude and highest average integrated chlorophyll concentration over the duration period with individual values as high as 5-7 $mg\ m^{-3}$ and 1-2 $mg\ m^{-3}$ respectively. The phytoplankton growth is extremely rapid and intense in these regions. Similar growth conditions are also encountered in coastal and equatorial upwelling regions where nutrient-rich deep waters are brought up to the surface and enhance extensive development of phytoplankton biomass. However, a short growing season is not always associated with blooming conditions. The short growing seasons observed in some of the tropical and sub-tropical permanently stratified waters correspond to ultra oligotrophic conditions where the seasonality is so low that no phytoplankton growth can be calculated. Combined observations of duration and amplitude are essential to diagnose the type of growth conditions occurring in a specific region of the global ocean.

2.4.2 Physical conditions determining the variability of phytoplankton growing season

Relation between regional changes in the physical environment and variability in the timing of growing season

Initiation of rapid phytoplankton growth, as described by Sverdrup (1953), is related to the seasonal increase in insolation and the stratification of surface waters. This hypothesis was established from observations of a station in the North Atlantic (NA). However, the global ocean presents large variability in phytoplankton biomass (Fig. 2.1), in associated ecosystem structure and in ambient conditions. How might these variations control the growing season?

We investigate the regional variability in the relation between changes in physical conditions and in timing of initiation of the growing season using global maps of correlation between interannual anomalies of: (a) the timing of initiation and the incident PAR flux at initiation and (b) the timing of initiation and the SST at initiation (Fig. 2.2).

In the NA and Southern Ocean (SO), strong positive correlations between timing of initiation and PAR are observed. In these regions, the development of the growing season follows closely the seasonal increase in insolation. The weak correlation with surface temperature is consistent with a recent stratification which did not allow enough time for the surface water to warm significantly. Conventionally, verification of Sverdrup's critical conditions of stratification and surface irradiance for phytoplankton bloom involved estimation of the timing of changes in the physical conditions, and then retrieving the chlorophyll concentration (Platt et al., 1991; Nelson and Smith Jr., 1991; Obata and Ishizaka, 1996; Follows and Dutkiewicz, 2002). Only recently in the NA, estimation of the timing of bloom initiation was performed directly from changes in the seasonal signal of chlorophyll, and coherence with the changes in physical conditions was then examined (Siegel et al., 2002; Henson et al., 2006; Platt et al., 2009).

In the central North Pacific (NP) ocean, the initiation of the growing season occurs on average in June, three months later than in the NA. The method employed in the present study detects systematically the timing of maximum amplitude in the seasonal surface chlorophyll signal, and subsequently the related timings of initiation and end. Considerable interannual variability in the phytoplankton seasonal cycle has been reported in the central NP (Ondrusek et al., 1991; Karl et al., 2001; Peña and Varela, 2007) and is also observed in the present time series with chlorophyll maxima detected from early spring to late summer. In this region, seasonal cycles in surface and deeper living phytoplankton species develop independently and possible perturbations of vertical structure make the seasonal cycles in biomass difficult to establish (Venrick, 1993; Campbell et al., 1997). Pulses in surface chlorophyll might also be triggered following episodic falls of volcanic dust (Banse and English, 1999). Thus, the estimated timing of initiation in the central NP does not appear to be positively related to incident light supply as it is clearly the case in the NA and in the regions surrounding the central NP (Fig. 2.2). The strong positive correlations shown between the timing of initiation and the SST indicate that surface waters

have warmed subsequent to stratification.

The negative correlations observed at mid-latitudes between the timing of initiation and the incident PAR flux imply that in these regions, the highest clorophyll values are observed in winter. The cooling of surface waters (negative correlations with SST) increase vertical mixing and nutrient supply in winter, which may enhance phytoplankton growth. However, it is recognised that in these regions, photoacclimation in response to lower light level imposed by deeper mixing is the most probable cause of chlorophyll enhancement (McClain et al., 2004).

Low-latitude oligotrophic regions are characterised by low or non-existent seasonality of phytoplankton biomass, permanent surface water stratification and sufficient light supply (Sarmiento et al., 2004). Changes in incident PAR and SST are therefore only weakly related with the estimated timing of initiation.

The conditions leading to the end of the growing season depend on complex factors including not only physical changes in the environment (such as reduction of insolation, water column destratification, intensity and frequency of storms) but also surface macro- and micronutrient depletion and grazing pressure from higher trophic levels. Global estimations of surface nutrient and grazer concentrations with sufficient spatial coverage are available as climatologies only (Levitus, 1982; Levitus et al., 1993; Buitenhuis et al., 2006). As a result, interannual correlation analyses could not be performed.

Timing influence on the duration of the growing season

Considerable regional and interannual variability occurs in the timing of initiation and end, but is this reflected in the duration of the growing season? Does an early start or late end result in a long duration and vice versa? Fig. 2.3 presents global maps of correlation between interannual anomalies of: (a) the timing of initiation and the duration of the growing season and (b) the timing of end and the duration of the growing season. A global observation reveals that the later the start, the shorter the growing season (negative correlation, Fig. 2.3a) and the later the end the longer

the growing season (positive correlation, Fig. 2.3b). Thus both the anomalies in intiation and end influence the duration.

The timing of initiation is generally positively correlated with the timing of end (Fig. 2.3c), except in the NA and most of the SO, where the duration appears to be strongly limited by the conditions occurring at the end of the growing season. Amongst the previously-stated factors leading to termination of phytoplankton growth, a combination of surface nitrate and silicate-depletion with increasing grazing pressure is likely to determine the ending of the NA spring bloom (Barlow et al., 1993; Gregg et al., 2003; Moore et al., 2004). The SO is part of the high-nutrient-low-chlorophyll (HNLC) regions; iron availability is likely to be the controlling factor in this region. Effect of iron-limitation on HNLC pelagic ecosystems has been extensively investigated using biogeochemical models (Gregg et al., 2003; Aumont and Bopp, 2006; Moore and Doney, 2007) and mesoscale in-situ iron fertilisation experiments (de Baar et al., 2005; Boyd et al., 2007; Moore et al., 2007). In the subtropical gyres of the Southern Hemisphere, the duration of the growing season appears to be regulated by both the timing of initiation and end, which indicates a close relation with changes in physical conditions and vertical supply of nutrients (McClain et al., 2004).

The regional differences observed in the timing response to SST anomalies (Fig. 2.2) and in the duration response to timing anomalies (Fig. 2.3), suggest a mechanistic connection between anomalies of duration and changes in the environmental conditions. In the next section, we seek to understand the effect of interannual variability in physical variables and their climate proxies, such as SST anomalies or the NAO and SAM indices, on the duration of the growing season.

2.4.3 Interannual variability in the duration of phytoplankton growing season

A decade of anomalies

On a global scale, maximum duration anomalies were associated with a major El Niño event in 1997 followed by La Niña in 1998 (Fig. 2.4). Positive anomalies have persisted until 2001. From 2003 onwards, the duration was shorter than average.

The largest variations in duration anomalies are observed in the central Pacific and Indian Ocean, with extremes reaching ± 10 weeks or more. In low productivity regions, large variations in duration of growing season do not necessarily reflect large variations in biomass. The variations in duration are interpreted as follows: (1) in years of positive anomalies, phytoplankton biomass is not null and apparently long growing seasons are estimated as a consequence of the very low seasonality encountered in the region; (2) in years of negative anomalies, phytoplankton biomass remains in general extremely low and very short pulses of phytoplankton growth of two to three weeks are detected. In 1998, the cold La Niña conditions supported an intense upwelling of limiting nutrients. The subsequent enhancement in biological productivity (Boyd et al., 1998; Chavez et al., 1999) resulted in a longer growing season, which appears as a strong positive anomaly.

The NA shows strong positive anomalies between 5-10 weeks at the beginning of the time series from 1998 to 2000 and similarly strong negative anomalies at the end of the time series from 2005 to 2007. A tripole pattern is observed in the basin in years 1997, 2005 and 2006 with two zonal bands of positive (negative) anomalies between 0-25°N and 35-60°N separated by a zonal band of negative (positive) anomalies between 25-35°N. This tripole pattern is reported in the interaction between the NAO and the SST (Cayan, 1992; Czaja and Frankignoul, 2002).

The SO presents less distinct patterns of anomalies. In 1998 and 1999, anomalies are positive and range between 5-10 weeks. In 2000, anomalies tend to be negative in the Pacific part of the SO, while they are positive in the Atlantic and Indian parts of the SO. The 30-45°S zonal band displays clearer patterns of positive and negative

anomalies in 2002 and 2006 and in 2004 and 2005 respectively.

Statistically significant trends ($P < 0.05$) in the duration anomalies, computed as the slope of the linear regression (in % yr^{-1}) for 10-years of data, are presented in Fig. 2.5. The observed trends in duration match closely with the trends in chlorophyll signal reported by Vantrepotte and Mélin (2009) for the same period. Globally, negative trends are dominant. A decrease in the duration of the growing season is observed in parts of the Pacific tropical gyres, the northern tropical Atlantic, the southern part of the South Atlantic gyre, the southern Indian Ocean gyre. Negative trends are also shown in the eastern subarctic Pacific, the eastern NA, as well as the SO 50-60°S band. Significant increase in the duration of the growing season is observed in the northern part of the South Atlantic gyre, the Greenland Sea, the northern Indian Ocean, in coastal and offshore areas of the Pacific side of North and South America and in the SO 35-45°S band on the eastern and western side of New Zealand. The marked influence of the major 1997/1998 El Niño/La Niña event on prevailing global negative trends might not correspond to the long-term trends (Yoder and Kennelly, 2003).

Regional patterns in anomalies of SST and duration of growing season

The relationship between temperature and duration of the growing season is explored by calculating the difference between means of anomalies of duration during positive and negative anomalies of SST averaged over the growing season: (SST^+ minus SST^-). SST^+ denotes the mean of anomalies of duration for the years when anomalies of the average SST index were positive. SST^- denotes the mean of anomalies of duration for the years when anomalies of the average SST index were negative.

Two distinct regimes of temperature and duration dynamics are captured between the high-latitude high-production regions and the low- and midlatitudes low-production regions (Fig. 2.6, Fig. 2.7). In the latter, and especially in the tropical and subtropical Pacific, when the duration is very short (negative anomalies), the SST index is higher than average. Higher SST suggests complete stratification, only

allowing extremely low and short pulses of biomass. At high latitudes, in the Bearing Sea, the NA and most of the SO, when the growing season is longer (positive anomalies), the SST index is higher than average. The SST anomalies are higher because the duration of the growing season extends into the summer, when surface waters are more stratified and have warmed. Fig. 2.3 shows that the conditions in the surface waters at the end of the growing season appeared to have the strongest influence on the duration. Accounting for the large regional variability in environmental conditions, the following alternative scenarios are suggested to explain the longer duration/higher SST dynamic: (1) strong winter mixing and large nutrient supply allow higher amplitude of biomass, which takes longer to decrease for a given loss rate; (2) strong mixing and large nutrient supply are followed by early surface water stratification at the onset of the growing season. Large nutrient supply and early stratification allow for rapid development of phytoplankton biomass followed immediately by rapid development of grazers, which "regulate" the phytoplankton population to a relatively low concentration, that persists as a result of the reduced demand for the available nutrients; (3) relatively strong and persistent water stratification over the duration of the growing season reduces the availability of limiting nutrients such as silicate. As a result, large phytoplankton species (i.e. diatoms) develop for a shorter period of time, leaving more macronutrients in the surface waters, which is then followed by the development of smaller phytoplankton species for a longer period of time. The SST index alone lacks information to identify the regional and interannual variability in the underlying mechanisms leading to longer growing season.

Regional patterns in anomalies of climate indices and duration of the growing season

Part of the physical and associated biogeochemical variability at middle and high latitudes is driven by large-scale low frequency variability in ocean-atmosphere interactions. The natural variability in these interactions is dominated by patterns of

climate variability represented notably in the NAO and SAM. The effect of large-scale climate variability on the duration of the growing season is examined by calculating the difference between the means of anomalies of duration during the positive and negative phases of the NAO and SAM.

In the NA, the NAO influence on SST is described as a horseshoe or tripole pattern with the subpolar gyre (north of 55°N) and the southern part of the subtropical gyre (south of 25°N) being positively correlated with the NAO. The western part of the subtropical gyre (around 35°N) appears negatively correlated with the NAO while the eastern part shows weak correlation (Cayan, 1992; Williams, 2000; Czaja and Frankignoul, 2002). Positive phases of the NAO are characterised by enhanced heat loss, deep winter mixing, enhanced surface wind intensity, reduced SST over the subpolar gyre and southern part of the subtropical gyre. The opposite effects are encountered over the western part of the subtropical gyre. This tripole pattern is partially observed in the duration anomalies (Fig. 2.8a). When the NAO index is positive, the growing season is longer in the southern part of the subtropical gyre and shorter in both the western part of the subtropical gyre and the northern part of the subpolar gyre. The influence of the NAO is reported to be stronger in the NA subtropics (Oschlies, 2001) and this may account for the mixed response in duration anomalies observed north of 40°N. The enhanced and deeper winter mixing reported during higher NAO bring more nitrate to the surface waters of the southern part of the subtropical gyre and permit the development of a longer growing season (Fig. 2.8b). The shorter growing season observed in the western part of the subtropical gyre coincides with reduced winter mixing and reduced nitrate supply to the surface waters. In the Sargasso Sea, at the Bermuda Atlantic Time Series (BATS) site, changes in the biogeochemical dynamics have been shown to correlate with NAO variability (Bates, 2001; Oschlies, 2001; Bates and Hansell, 2004; Lomas and Bates, 2004; Bates, 2007). Reduced integrated primary production (Bates, 2001) and enhanced diatom abundance in the phytoplankton community (Lomas

and Bates, 2004) occur during high NAO. Thus, the reduced concentration of nutrients is rapidly consumed and depleted, leading to a short growing season. In the Labrador Sea and Irminger Basin, where a short growing season is also observed in high NAO, changes in the physical properties are also influenced by the variability in sea-ice formation. During positive phase of NAO, enhanced net sea-ice production injects more salt into the ocean (Hu et al., 2002), which deepens the mixed layer depth and reduces water stratification. The latter conditions, combined with stronger winds, have been shown to delay the initiation of phytoplankton growing season, reduce chlorophyll maximum (Henson et al., 2006, 2009), and thus in the present study, shorten the duration.

The effect of large-scale patterns of climate variability on the physical properties and biogeochemical dynamics has been less extensively documented in the SH (Reynolds and Smith, 1994). Distinct and opposite SAM influences on the physical properties are observed between the bands 30° to 45°S and 50° to 65°S (Hall and Visbeck, 2002; Sen Gupta and England, 2006). Positive phases of the SAM are characterised by enhanced westerly winds, enhanced heat loss, cooler SST, deeper mixed layer depth, enhanced upwelling, enhanced sea-ice extension at latitudes southward of 50°S. The opposite characteristics are encountered at latitudes northward of 45°S. The regional differences in duration anomalies only partially show the zonally symmetric response reported in the physical properties (Fig. 2.9a). When the SAM index is positive, zonally symmetric changes are observed from the east of the Antarctic Peninsula to 100°E with longer growing season in the south band (50-65°S) and shorter growing season in the north band (35-50°S). The enhanced upwelling and deeper mixed layer reported during high SAM in the south band enhance iron and silicate supply to surface waters. The reduced micronutrient-limitation (Boyd, 2002) combined with the low algal growth rates recorded in polar waters (Boyd et al., 2002) result in the development of a longer growing season (Fig. 2.9b). The shorter growing season recorded in the north band coincides with reduced upwelling and reduced supply of limiting nutrients. In the rest of the SO, during positive

SAM phases, the growing season is longer and the north/south zonal symmetry is not seen. The SAM index varies markedly on decadal timescales. Thus, the changes in physical properties associated with ten years of SAM anomalies might be weak in some parts of the SO and might not be the primary source of variability that explains the observed anomalies in duration of growing season.

2.5 Conclusions

Large regional variability is observed in the phenology of the phytoplankton growing season. The timings of initiation, peak and end of the growing season show a latitudinal propagation from low- to high-latitudes in both hemispheres. The duration of the growing season is longer in the tropics and subtropics ($\approx$ 15-20 weeks) where biomass remains low throughout the seasonal cycle. The duration shortens towards the poles ($<$ 10 weeks) where seasonality is clearly defined and biomass maxima are high.

In the NA and SO, the timing of initiation follows closely the seasonal increase in insolation. Over most of these regions, the duration appears to be limited by the conditions occurring at the end of the growing season, which indicate nutrients-depletion in surface waters. In the tropics and subtropics, light is rarely limiting and initiation is triggered by increased nutrients supply supported by the deepening of the mixed layer. The duration is controlled by both the timing of initiation and end, which suggest a close relation with the availability of nutrients brought up by mixing.

Large interannual variability in the duration of the growing season is observed over the decade 1998-2007. Globally, maximum anomalies (+ 10 weeks) occur at the beginning of the time series associated with a major El Niño event in 1997 followed by La Niña in 1998. Positive anomalies tend to persist until 2001, while the data from 2003 onwards is dominated by negative anomalies. Significant negative linear trends in duration ($-$ 10 % yr^{-1} on average) are observed in the tropics and subtropics, the eastern NA and the SO south of 50°S. Regions showing a significant

increase in duration (+ 8 % yr^{-1} on average) occupy a smaller fraction of the ocean and include essentially the Greenland Sea and part of the SO 35-45°S band. The trends, estimated over the 1998-2007 period, are dominated largely by the major El Niño event that occured at the beginning of the time series, and therefore might not reflect the long-term trend.

Higher SST over the duration of the growing season is associated with longer duration at high-latitudes indicating an extension of the growing season over the summer months. The opposite is observed at low- and mid-latitudes, where the duration is shorter when higher SST indicate increased stratification.

Positive anomalies in the NAO and SAM climate indices are generally associated with enhanced winter mixing and nutrients supply. These conditions tend to favour the development of longer growing season.

References

Aumont, O. and Bopp, L. (2006). Globalizing results from ocean in situ iron fertilization studies. *Global Biogeochem. Cycles*, 20:doi:10.1029/2005GB002591GB2017.

Banse, K. and English, D. (1999). Comparing phytoplankton seasonality in the eastern and western subarctic Pacific and the western Bering Sea. *Prog. Oceanogr.*, 43:235–288.

Barlow, R., Mantoura, R., Gough, M., and Fileman, T. (1993). Pigment signatures of the phytoplankton composition in the northeastern Atlantic during the 1990 spring bloom. *Deep Sea Res., Part II*, 40:459–477.

Bates, N. (2007). Interannual variability of the oceanic CO_2 sink in the subtropical gyre of the North Atlantic Ocean over the last 2 decade. *J. Geophys. Res.*, 112:doi:10.1029/2006JC003759.

Bates, N. R. (2001). Interannual variability of oceanic CO_2 and biogeochemical properties in the Western North Atlantic Subtropical Gyre. *Deep Sea Res., Part II*, 48:1507–1528.

Bates, N. R. and Hansell, D. (2004). Temporal variability of excess nitrate in the subtropical mode water of the North Atlantic Ocean. *Mar. Chem.*, 84:225–241.

Beaugrand, G. and Reid, P. C. (2003). Long-term changes in phytoplankton, zooplankton and salmon related to climate. *Glob. Change Biol.*, 9:801–817.

Boyd, P. W. (2002). The role of iron in the biogeochemistry of the Southern Ocean and equatorial Pacific: a comparison of in situ iron enrichments. *Deep Sea Res., Part II*, 49:1803–1821.

Boyd, P. W., Jackson, G., and Waite, A. (2002). Are mesoscale perturbation experiments in polar waters prone to physical artefacts? Evidence from algal aggregation modelling studies. *Geophys. Res. Lett.*, 29:10.1029/2001GL014210.

Boyd, P. W., Jickells, T., Law, C., Blain, S., and Buesseler, E. B. K. (2007). Mesoscale iron enrichment experiments 1993-2005: synthesis and future directions. *Science*, 315:612–617.

Boyd, P. W., Wong, C., Merrill, J., Whitney, F., Snow, J., Harrison, P., and Gower, J. (1998). Atmospheric iron supply and enhanced vertical carbon flux in the NE subarctic Pacific: Is there a connection? *Global Biogeochem. Cycles*, 12:429–441.

Buitenhuis, E. T., Le Quéré, C., Aumont, O., Beaugrand, G., Bunker, A., Hirst, A., Ikeda, T., O'Brien, T., Piontkovski, S., and Straile, D. (2006). Biogeochemical fluxes mediated by meso-zooplankton. *Global Biogeochem. Cycles*, 20:doi:10.1029/2005GB002511.

Campbell, J. W., Liu, H., Nolla, H., and Vaulot, D. (1997). Annual variability of phytoplankton and bacteria in the subtropical North Pacific Ocean at Station ALOHA during the 1991-1994 ENSO event. *Deep Sea Res., Part I*, 44:167–192.

Cayan, D. (1992). Latent and sensible heat flux anomalies over the northern oceans: The connection to monthly atmospheric circulation. *J. of Clim.*, 5:354–369.

Chavez, F. P., Strutton, P. G., Friederich, G. E., Feely, R. A., Feldman, G. C., Foley, D. G., and Mcphaden, M. J. (1999). Biological and chemical response of the Equatorial Pacific ocean to the 1997-98 El Niño. *Science*, 286:2126–2131.

Ciasto, L. and Thompson, D. (2008). Observations of Large-Scale Ocean-Atmosphere Interaction in the Southern Hemisphere. *J. of Clim.*, 21:1244–1259.

Cushing, D. (1959). The seasonavla riationin oceanic productioans a problemin population dynamics. *J. Cons. Int. Explor. Mer.*, 24:455–464.

Czaja, A. and Frankignoul, C. (2002). Observed impact of Atlantic SST anomalies of the North Atlantic Oscillation. *J. of Clim.*, 15:606–623.

de Baar, H., Boyd, P., Coale, K., Landry, M., Tsuda, A., Assmy, P., Bakker, D., Bozec, Y., Barber, R., Brzezinski, M., Buesseler, K., Boye, M., Croot, P., Gervais, F., Gorbunov, M., Harrison, P., Hiscock, W., Laan, P., Lancelot, C., Law, C., Levasseur, M., Marchetti, A., Millero, F., Nishioka, J., Nojiri, Y., van Oijen, T., Riebesell, U., Rijkenberg, M., Saito, H., Takeda, S., Timmermans, K., Veldhuis, M., Waite, A., and Wong, C.-S. (2005). Synthesis of iron fertilization experiments: from the iron age in the age of enlightenment. *J. Geophys. Res.*, 110:doi:10.1029/2004JC002601.

Follows, M. and Dutkiewicz, S. (2002). Meteorological modulation of the North Atlantic spring bloom. *Deep Sea Res., Part II*, 49:321–344.

Gregg, W. W., Ginoux, P., Schopf, P. S., and Casey, N. W. (2003). Phytoplankton and iron: validation of a global three-dimensional ocean biogeochemical model. *Deep Sea Res., Part II*, 50:3143–3143.

Hall, A. and Visbeck, M. (2002). Synchronous variability in the Southern Hemisphere atmosphere, sea ice, and ocean resulting from the annular mode. *J. of Clim.*, 15:3043–3057.

Henson, S., Dunne, J., and Waniek, J. (2009). Decadal variability in North Atlantic phytoplankton blooms. *J. Geophys. Res.*, 114:doi:10.1029/2008JC005139.

Henson, S., Robinson, I., Allen, J., and Waniek, J. (2006). Effect of meteorological conditions on interannual variability in timing and magnitude of the spring bloom in the Irminger Basin, North Atlantic. *Deep Sea Res., Part I*, 53:1601–1615.

Hu, A., Rooth, C., Bleck, R., and Deser, C. (2002). NAO influence on sea ice extent in the Eurasian coastal region. *Geophys. Res. Lett.*, 29:doi:10.1029/2001GL014293.

Hurrell, J. W. (1995). Decadal trends in the North Atlantic Oscillation: Regional temperatures and precipitation. *Science*, 269:676–679.

Karl, D., Bidigare, R., and Letelier, R. (2001). Long-term changes in plankton community structure and productivityin the North Pacific Subtropical Gyre: The domain shift hypothesis. *Deep Sea Res., Part II*, 48:1449–1470.

Kidson, J. W. (1988). Interannual variations in the Southern Hemisphere circulation. *J. of Clim.*, 1:1177–1198.

Koeller, P., Fuentes-Yaco, C., Platt, T., Sathyendranath, S., Richards, A., Ouellet, P., Orr, D., Skúladóttir, U., Wieland, K., Savard, L., and Aschan, M. (2009). Basin-Scale Coherence in Phenology of Shrimps and Phytoplankton in the North Atlantic Ocean. *Science*, 324:doi:10.1126/science.1170987.

Leterme, S., Edwards, M., Seuront, L., Attrill, M., Reid, P., and John, A. (2005). Decadal basin-scale changes in diatoms, dinoflagellates, and phytoplankton color across the North Atlantic. *Limnol. Oceanogr.*, 50:1244–1253.

Levitus, S. (1982). Climatological atlas of the world ocean. Technical Report 13, U.S. Govt. Print. Office, Washington D. C.

Levitus, S., Conkright, M. E., Reid, J. L., Najjar, R. G., and Mantyla, A. (1993). Distribution of nitrate, phosphate and silicate in the world oceans. *Prog. Oceanogr.*, 31:245–273.

Lomas, M. and Bates, N. (2004). Potential controls on interannual partitioning oforganic carbon during the winter/spring phytoplankton bloom at the Bermuda Atlantic time-series study (BATS) site. *Deep Sea Res., Part I*, 51:1619–1636.

Marshall, G. (2003). Trends in the Southern Annular Mode from observations and reanalyses. *J. of Clim.*, 16:4134–4143.

McClain, C. R., Signorini, S., and Christian, J. (2004). Subtropical gyre variability observedby ocean-color satellites. *Deep Sea Res., Part II*, 51:281–301.

Moore, J. and Doney, S. (2007). Iron availability limits the ocean nitrogen inventory stabilizing feedbacks between marine denitrification and nitrogen fixation. *Global Biogeochem. Cycles*, 21:doi:10.1029/2006GB002762.

Moore, J., Seeyave, S., Hickman, A. E., Allen, J. T., Lucas, M. I., Planquette, H., Pollard, R. R., and Poulton, A. J. (2007). Iron-light interactions during the CROZet natural iron bloom and EXport experiment (CROZEX) I: Phytoplankton growth and photophysiology. *Deep Sea Res., Part II*, 54:2045–2065.

Moore, J. K., Doney, S. C., and Lindsay, K. (2004). Upper ocean ecosystem dynamics and iron cycling in a global three-dimensional model. *Global Biogeochem. Cycles*, 18:doi:10.1029/2004GB002220.

Nelson, D. M. and Smith Jr., W. (1991). Sverdrup Revisited: Critical Depths, Maximum Chlorophyll Levels, and the Control of Southern Ocean Productivity by the Irradiance-Mixing Regime. *Limnol. Oceanogr.*, 36:1650–1661.

Obata, A. and Ishizaka, J. (1996). Global verification of critical depth theory for phytoplankton bloom with climatological in situ temperature and satellite color data. *J. Geophys. Res.*, 101:20657–20667.

Ondrusek, M., Bidigare, R., Sweet, S., Defreitas, D., and Brooks, J. (1991). Distribution of phytoplankton pigments in the North Pacific Ocean in relation to physical and optical variability. *Deep Sea Res.*, 38:243–266.

Oschlies, A. (2001). NAO-induced long-term changes in nutrient supply to the surface waters of the North Atlantic. *Geophys. Res. Lett.*, 28:1751–1754.

Peña, M. and Varela, D. (2007). Seasonal and interannual variability in phytoplankton and nutrient dynamics along Line P in the NE subarctic Pacific. *Prog. Oceanogr.*, 75:200–222.

Platt, T., Bird, D., and Sathyendranath, S. (1991). Critical depth and marine primary production. *Proc. R. Soc. Lond., Ser. B*, 246:205–217.

Platt, T., Fuentes-Yaco, C., and Frank, K. (2003). Spring algal bloom and larval fish survival. *Nature*, 423:398–399.

Platt, T. and Sathyendranath, S. (2008). Ecological indicators for the pelagic zone of the ocean from remote sensing. *Remote Sens. Environ.*, 112:3426–3436.

Platt, T., Sathyendranath, S., White II, G., Fuentes-Yaco, C., Zhai, L., Devred, E., and Tang, C. (2009). Diagnostic Properties of Phytoplankton Time Series from Remote Sensing. *Estuaries and Coasts*, 32:doi:10.1007/s12237–009–9161–0.

Reynolds, R. W. and Smith, T. M. (1994). Improved global sea surface temperature analyses using optimum interpolation. *J. of Clim.*, 7:929–948.

Sarmiento, J. L., Slater, R., Barber, R., Bopp, L., Doney, S., Hirst, A., Kleypas, J., Matear, R., Mikolajewicz, U., Monfray, P., Soldatov, V., Spall, S., and Stouffer, R. (2004). Response of ocean ecosystems to climate warming. *Global Biogeochem. Cycles*, 18:doi:10.1029/2003GB002134.

Sen Gupta, A. and England, M. (2006). Coupled ocean-atmosphere-ice response to variations in the Southern Annular Mode. *J. of Clim.*, 19:4457–4486.

Siegel, D., Doney, S., and Yoder, J. (2002). The North Atlantic spring phytoplankton bloom and Sverdrup's critical depth hypothesis. *Science*, 296:730–733.

Sverdrup, H. U. (1953). On conditions for the vernal blooming of phytoplankton. *Cons. Int. Expor. Mer.*, 18:287–295.

Vantrepotte, V. and Mélin, F. (2009). Temporal variability of 10-year global SeaWiFS time-series of phytoplankton chlorophyll *a* concentration. *ICES Journal of Marine Science*, 66:1547–1556.

Venrick, E. (1993). Phytoplankton seasonality in the central North Pacific: The endless summer reconsidered. *Limnol. Oceanogr.*, 38:1135–1149.

Williams, P. (2000). Net production, gross production and respiration: what are the interconnections and what controls what? In Hanson, R. B., Ducklow, H. W., and Field, J. G., editors, *The changing ocean carbon cycle: a midterm synthesis of the Joint Global Ocean Flux Study*, pages 37–60. Cambridge University Press, Cambridge.

Yoder, J. and Kennelly, M. (2003). Seasonal and ENSO variability in global ocean phytoplankton chlorophyll derived from 4 years of SeaWiFS measurements. *Global Biogeochem. Cycles*, 17:doi:10.1029/2002GB001942.

Yoder, J., McClain, C., Feldman, G., and Esaias, W. (1993). Annual cycles of phytoplankton chlorophyll concentrations in the global ocean: a satellite view. *Global Biogeochem. Cycles*, 7:181–193.

2.6 Tables

Table 2.1: Ecological and physical indices developed and adapted from Platt and Sathyendranath (2008). Indices are derived from remotely-sensed radiances in the visible (ocean colour) and infra-red (SST) spectra.

Index	Label	Units
Initiation of growing season	b_i	*week*
Timing of maximum amplitude	b_t	*week*
End of growing season	b_e	*week*
Duration of growing season	b_d	*weeks*
Amplitude of growing season	b_a	$mg\ m^{-3}$
Average integrated Chla over duration	b_s	$mg\ m^{-3}$
PAR at initiation of growing season	l_i	$mol\ photon\ m^{-2}\ d^{-1}$
PAR at end of growing season	l_e	$mol\ photon\ m^{-2}\ d^{-1}$
Average PAR over duration	l_d	$mol\ photon\ m^{-2}\ d^{-1}$
SST at initiation of growing season	t_i	°C
SST at end of growing season	t_e	°C
Average SST over duration	t_d	°C

Table 2.2: Zonal statistics of ecological and physical indices for the global ocean. Ten years mean values of each index are estimated for each zonal band of latitudes. (Top) Ecological indices include timing of initiation (b_i), maximum amplitude (b_t) and end (b_e), duration (b_d), amplitude (b_a) and average integrated Chla over the duration (b_s) of the growing season. (Bottom) Physical indices include PAR and SST values estimated at the time of initiation (l_i, t_i) and end (l_e, t_e), and averaged over the duration (l_d, t_d) of the growing season.

Zone (°)	b_i ($week$)	b_t ($week$)	b_e ($week$)	b_d ($weeks$)	b_a ($\frac{mg}{m^3}$)	b_s ($\frac{mg}{m^3}$)
60-70N	16	20	25	10	2.2	1.2
50-60N	16	21	27	12	2.6	1.3
40-50N	15	22	28	14	1.1	0.6
30-40N	3	14	22	20	0.5	0.3
20-30N	20	28	35	16	0.3	0.2
10-20N	22	28	35	14	0.4	0.2
0-10N	16	23	30	15	0.4	0.3
0-10S	21	28	35	15	0.5	0.3
10-20S	21	29	37	17	0.2	0.2
20-30S	18	27	35	18	0.2	0.1
30-40S	21	31	39	19	0.3	0.2
40-50S	29	36	44	16	0.5	0.3
50-60S	34	41	47	14	0.5	0.3
60-70S	33	38	43	11	0.6	0.3

Zone (°)	l_i ($\frac{mol\ photon}{m^2\ d}$)	l_e ($\frac{mol\ photon}{m^2\ d}$)	l_d ($\frac{mol\ photon}{m^2\ d}$)	t_i (°C)	t_e (°C)	t_d (°C)
60-70N	27.9	30.8	32.6	3.4	4.6	3.8
50-60N	30.8	29.5	33.4	4.9	7.2	5.7
40-50N	27.0	32.2	31.4	10.3	11.4	10.6
30-40N	23.2	46.5	30.7	22.5	16.6	18.9
20-30N	35.5	46.0	37.3	26.2	23.3	24.7
10-20N	44.8	47.9	45.5	27.6	27.0	27.3
0-10N	43.4	46.5	45.5	28.4	27.8	28.1
0-10S	45.3	49.2	47.1	28.1	26.9	27.5
10-20S	41.5	49.8	44.0	26.9	25.2	26.0
20-30S	33.3	47.4	35.6	24.7	21.5	23.1
30-40S	25.9	46.7	32.6	19.3	16.0	17.4
40-50S	33.3	32.2	37.4	9.3	10.5	9.7
50-60S	28.1	29.9	34.5	2.8	3.8	3.1
60-70S	25.6	24.8	29.2	-0.9	-0.0	-0.6

2.7 Figures

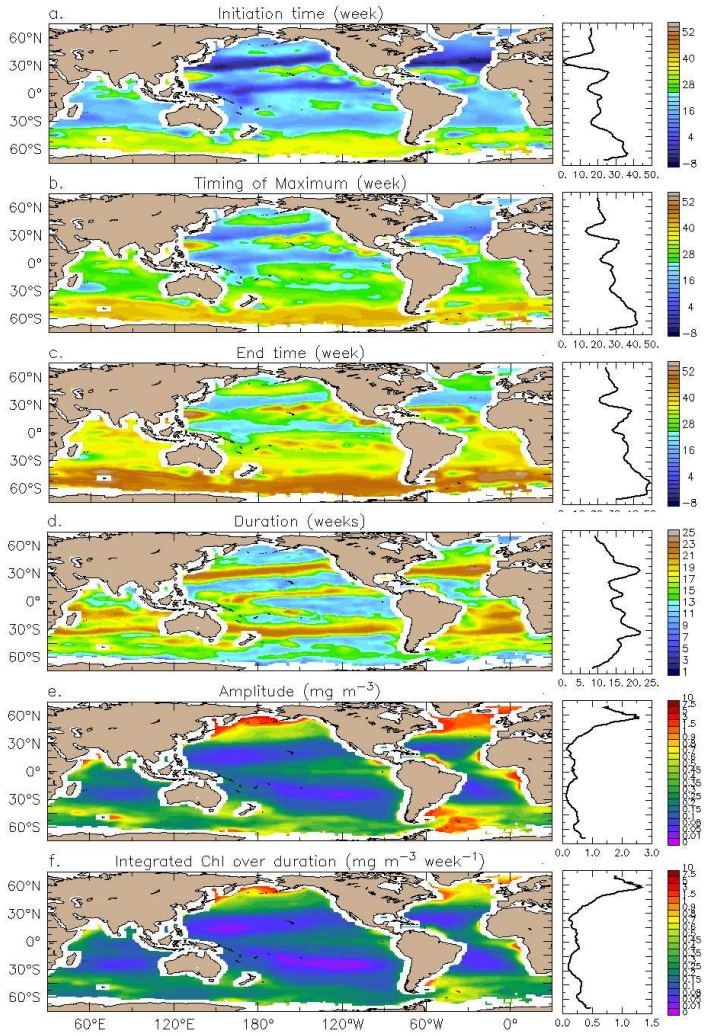

Figure 2.1: Characteristics of phytoplankton growing season. The spatial distributions are averaged over 10 years of SeaWiFS data (1998 to 2007). Data were smoothed with a running average of 8° in longitude and 5° in latitude. The right panels show the data averaged longitudinally and smoothed latitudinally with a 5° running average.

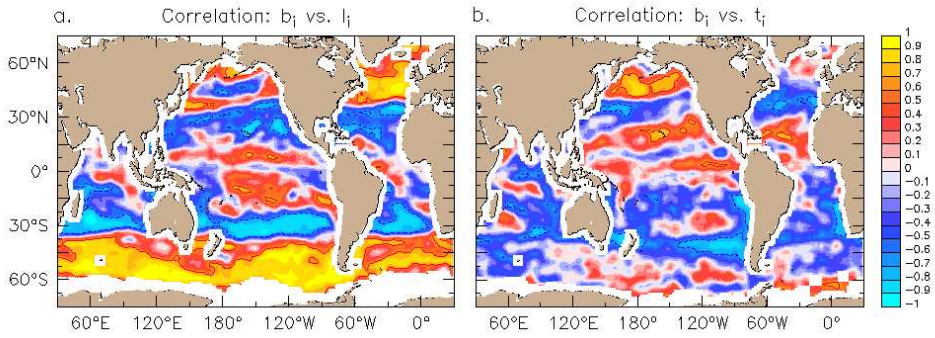

Figure 2.2: Global maps of temporal correlation between 10 years (1998 to 2007) of anomalies of (a) timing of initiation b_i and PAR at the time of initiation l_i, (b) timing of initiation b_i and SST at the time of initiation t_i. Significant correlations at 95% are indicated with red and blue contours. The correlation is positive (red) where the timing of initiation follows the increase in (a) insolation or (b) temperature and negative (blue) where the timing of initiation follows the decrease in (a) insolation or (b) temperature. Data were smoothed with a running average of 8° in longitude and 5° in latitude.

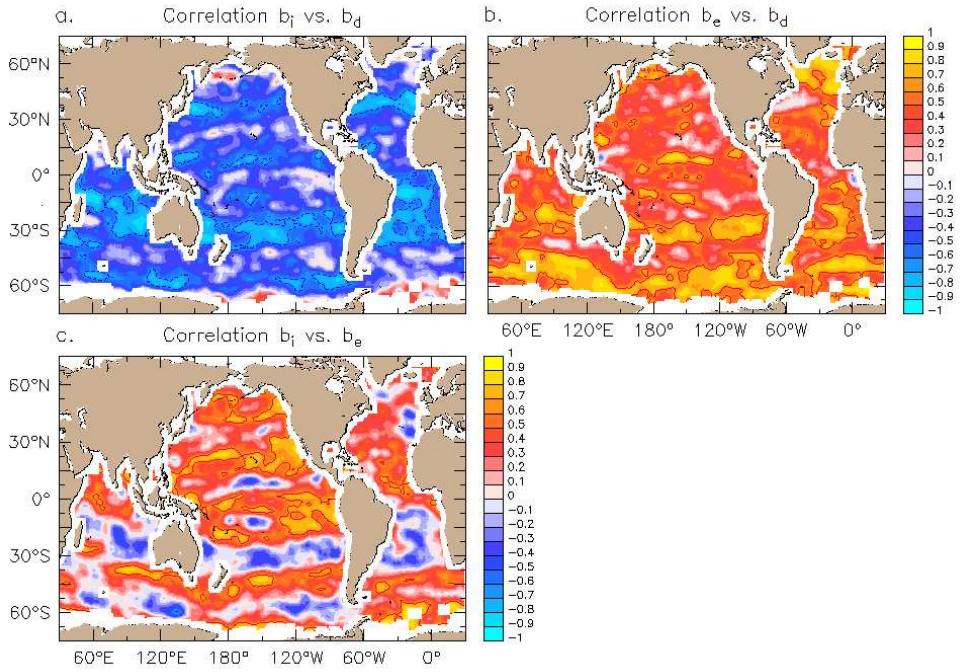

Figure 2.3: Global maps of temporal correlation between 10 years (1998 to 2007) of anomalies of (a) timing of initiation b_i and duration of growing season b_d, (b) timing of end b_e and duration of growing season b_d and (c) timing of initiation b_i and timing of end b_e. Significant correlations at 95% are indicated with red and blue contours. In (a), the correlation is negative (blue) where the earlier (later) the time of initiation, the longer (shorter) the duration of growing season. In (b), the correlation is positive (red) where the earlier (later) the time of initiation, the shorter (longer) the duration of growing season. Data were smoothed with a running average of 8° in longitude and 5° in latitude.

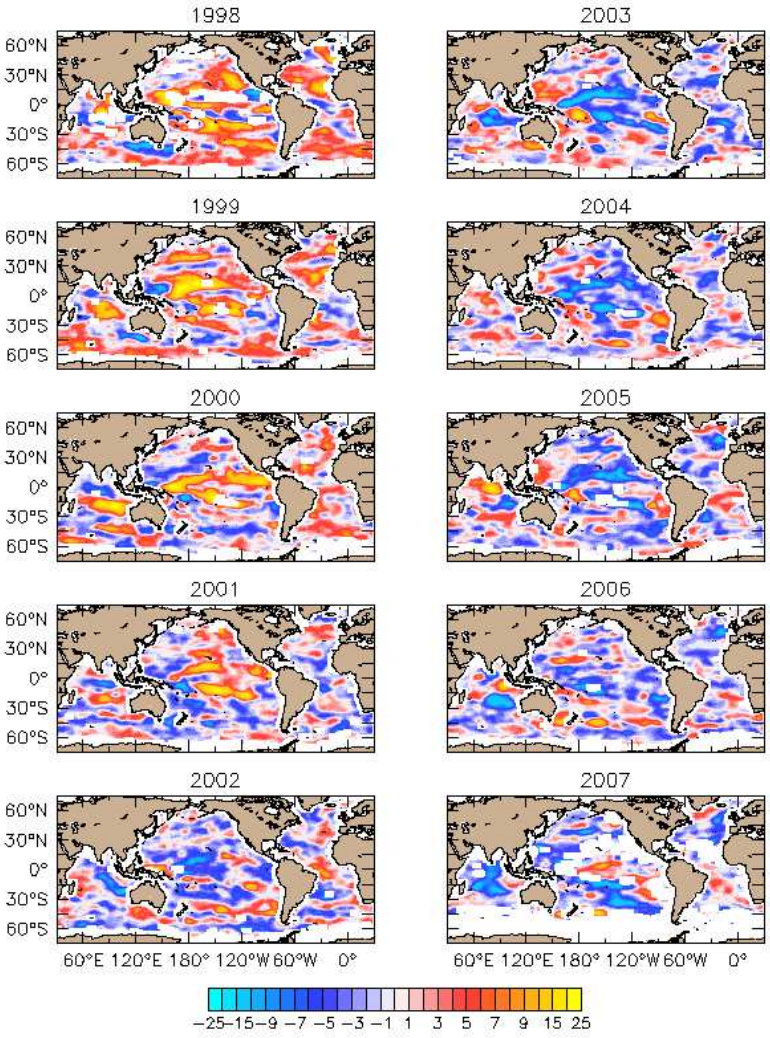

Figure 2.4: Decadal anomalies (1998 to 2007) in duration of phytoplankton growing season (weeks). The anomalies were smoothed with a running average of 8° in longitude and 5° in latitude.

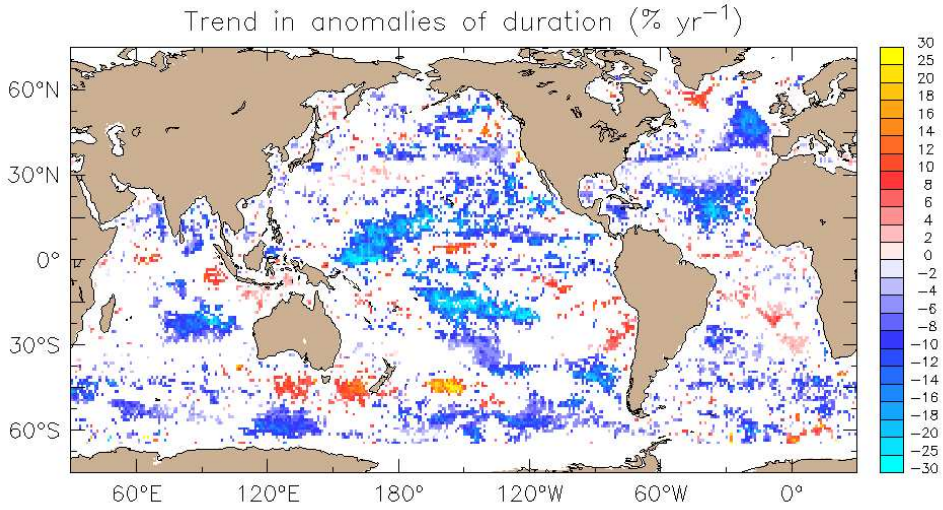

Figure 2.5: Slope of the linear regression for duration anomalies (in % yr^{-1}) over 10 years of SeaWiFS data (1998 to 2007). Only statistically significant values ($P < 0.05$) are presented.

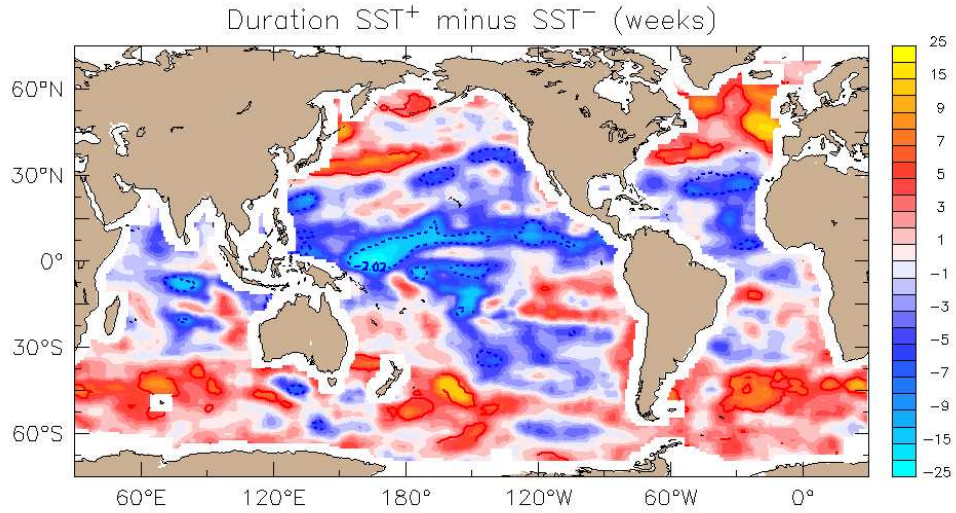

Figure 2.6: Difference between means of anomalies of duration during positive and negative anomalies of SST averaged over the growing season. A decade (1998-2007) of anomalies in duration of phytoplankton growing season (weeks) is considered. When the averaged SST over the growing season is warmer: anomalies are positive (red) where the duration is longer and negative (blue) where the the duration is shorter. The anomalies were smoothed with a running average of 8° in longitude and 5° in latitude.

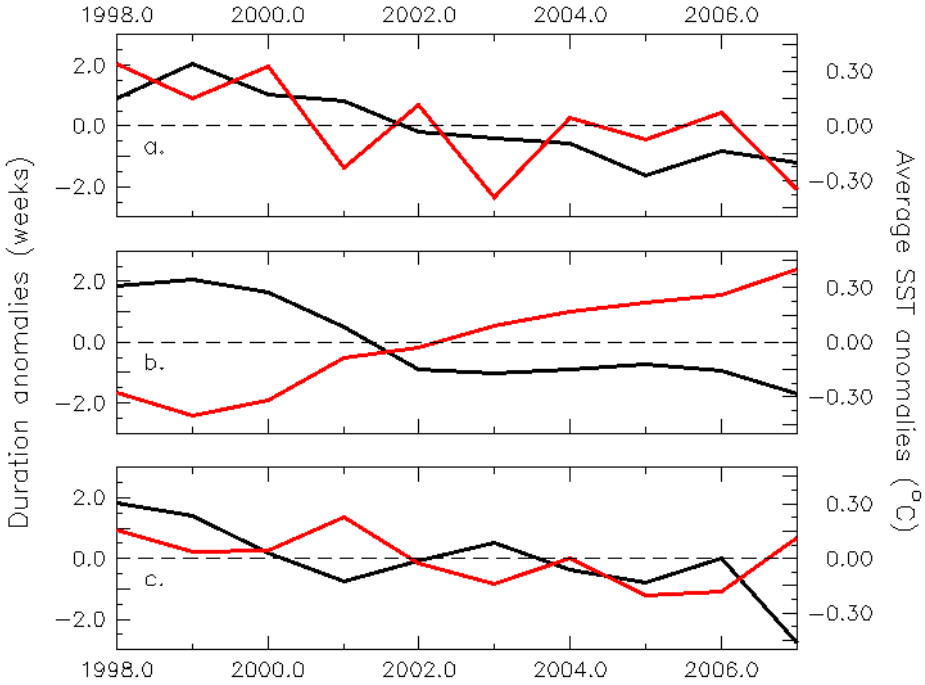

Figure 2.7: Time series from 1998 to 2007 of anomalies of duration (black line; in weeks) and anomalies of averaged SST over the growing season (red line; in °C) averaged between (a) 35°N-65°N, (b) 35°S-35°N, and (c) 65°S-35°S.

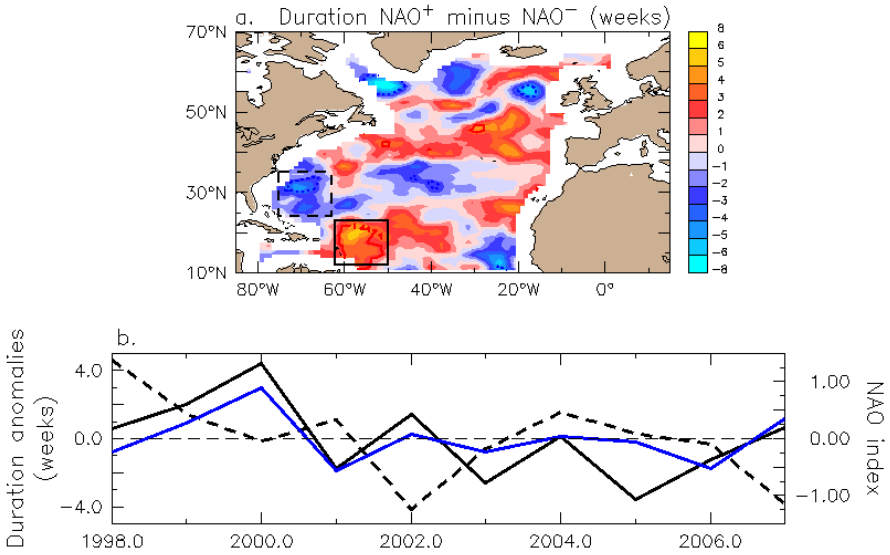

Figure 2.8: Regional patterns in NAO and duration anomalies (1998-2007). (a) Map of the difference between the means of anomalies of duration during the positive and negative phases of the NAO in the North Atlantic. Black boxes represent the areas selected in (b). During high NAO: anomalies are positive (red) where the duration of growing season is longer and negative (blue) where the the duration of growing season is shorter. The anomalies were smoothed with a running average of 8° in longitude and 5° in latitude. (b) Time series of duration anomalies (in weeks) averaged over the black box area in (a) (black line), the dashed box area in (a) (dash line) and NAO anomalies (blue line).

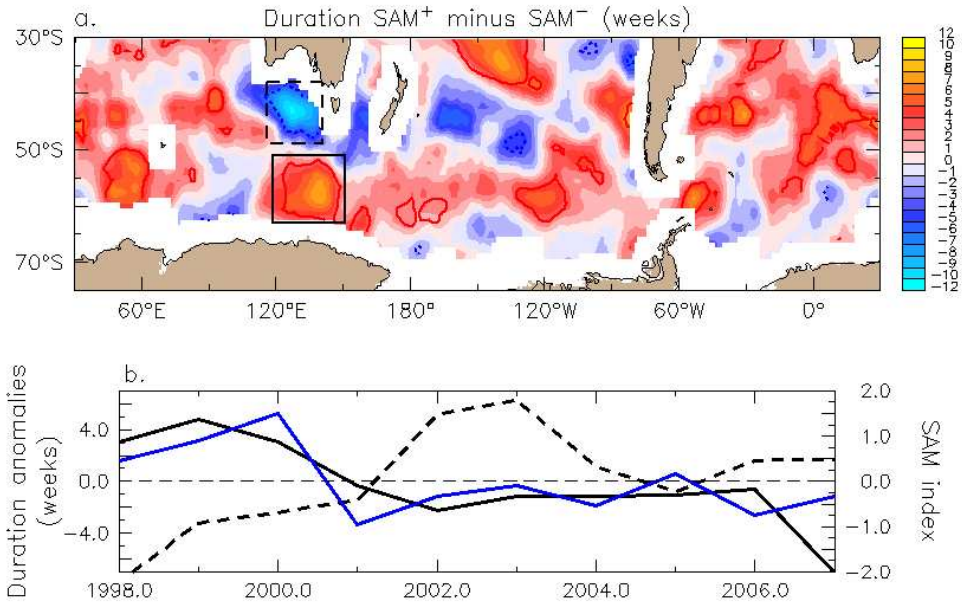

Figure 2.9: Regional patterns in SAM and duration anomalies (1998-2007). (a) Map of the difference between the means of anomalies of duration during the positive and negative phases of the SAM in the Southern Ocean. Black boxes represent the areas selected in (b). During high SAM: anomalies are positive (red) where the duration of growing season is longer and negative (blue) where the the duration of growing season is shorter . The anomalies were smoothed with a running average of 8° in longitude and 5° in latitude. (b) Time series of duration anomalies (in weeks) averaged over the black box area in (a) (black line), the dashed box area in (a) (dash line) and SAM anomalies (blue line).

Chapter 3

Decadal change in phytoplankton phenology and its impact on the oceanic carbon cycle

3.1 Abstract

Phytoplankton fix carbon dioxide into organic matter in the surface layer of the ocean. Organic matter aggregates and sinks, and thus creates a persistent "export" of carbon from the surface to the deep ocean, regulating, over long time scales, the concentration of CO_2 in the atmosphere. Using *in situ* observations, we show here that the export of carbon can be related to the length of the phytoplankton growing season, with largest export in regions where the growing season is shortest and the blooms most intense. Using satellite observations, we estimate that, North of 45°S, the phytoplankton growing season increased by 2.4 weeks on average, between the periods 1979-1986 and 1998-2008. Longer growing seasons are associated with increase in surface temperature on the same time scale. We infer from the data a decrease in carbon export of $\sim$0.6 Pg C yr^{-1} (excluding the Southern Ocean) over two decades. The implication is that the marine ecosystem has responded rapidly to global change in such a way as to weaken a sink that we have relied on to help mitigate the effect of increasing CO_2 in the atmosphere.

3.2 Introduction

Every year, the oceans absorb one quarter of the carbon dioxide (CO_2) emitted to the atmosphere by human activities, or an average of 2.2 Pg C yr^{-1} (Canadell et al., 2007). This CO_2 sink is part of a very active, natural carbon cycle, through which, phytoplankton fix CO_2 into organic matter in the surface layer of the ocean: it helps to modulate the increase in atmospheric CO_2 that results from the burning of fossil fuels. Organic matter fixed at the surface may aggregate and sink, creating a persistent "export" of carbon of ∼11 Pg C yr^{-1} from the surface to the deep ocean (Schlitzer, 2002). Eventually, carbon is remineralised at depth, and transported back to the surface by ocean currents. The magnitude of the carbon export depends on: (a) the biomass of phytoplankton, (b) the size of the phytoplankton cells, (c) the depth of the mixed layer, (d) the presence of organic polymers that enhance aggregation (Engel et al., 2004), (e) the presence of inorganic materials that act as ballast (Klaas and Archer, 2002; Ploug et al., 2008), and (f) the packaging of fecal pellets produced by large zooplankton. The intensities of these processes are ultimately governed by the physical environment, and thus they are likely to be affected by recent climate and other environmental changes. Over decadal time-scales, ∼75% of the changes in carbon export are directly reflected in changes in the oceanic CO_2 sink (Giraud et al., 2008; Moore et al., 2006). Thus, even a small change in biological export can cause a significant change in the oceanic CO_2 sink.

Notwithstanding its importance, carbon export is difficult to estimate at the global scale. *In situ* measurements from sediment traps are sparse over the world ocean, and are rarely repeated at the same place. The only large-scale biological observations of the ocean ecosystem that span more than two decades come from remote sensing of chlorophyll-*a*. A range of ecological indicators can be derived directly from remote sensing of chlorophyll-*a*, including phytoplankton biomass, productivity, and growing season characteristics such as timing, amplitude, and duration (Platt and Sathyendranath, 2008). Of these ecological indicators, only the timing and duration of the phytoplankton growing season are relative indices

that are independent of the satellite sensor type and hence can be pieced together seamlessly using data from various satellite missions. A link between the export of carbon and the phytoplankton phenology is expected because the aggregation processes provide a mechanism for transporting material to the ocean interior that is strongly dependent on the biomass (Burd and Jackson, 2009).

The aim of this chapter is to assess decadal change in phytoplankton phenology and to evaluate its impact on the oceanic carbon cycle. To maintain a the logical flow amongst the paragraphs in this chapter, details about the materials and methods are described in Appendix 3.5.

3.3 Results and discussion

3.3.1 Duration of phytoplankton growing season

We defined the duration index as the number of weeks between the initiation and the end of the phytoplankton growing season. The points are detected from a relative chlorophyll threshold, allowing the comparison of duration estimates from different satellite sensors regardless of their different chlorophyll-retrieval algorithms. We compiled global maps of duration of phytoplankton growing season using climatologies of weekly fields of chlorophyll-a from the Coastal Zone Color Scanner (CZCS, 1979-1986) and from the Sea-viewing Wide Field-of-view Sensor (SeaWiFS, 1998-2008) missions. To our knowledge, duration of the autotrophic growing season in the ocean has not been analysed at the global scale before now. The spatial distributions of duration of phytoplankton growing season calculated separately for both missions show similar patterns (Fig. 3.1a,b). The longest growing seasons (17-21 weeks) occur in subtropical and low temperate oligotrophic waters. The permanent stratification of these waters results in an extremly low nutrient supply that sustains low surface chlorophyll concentrations all year round (Sarmiento et al., 2004) (Fig. 3.2). Intermediate growing seasons (11-17 weeks) are present in equatorial and low-latitude upwelling regions, sustaining intermediate surface chlorophyll concentrations. The

shortest growing seasons (5-10 weeks) are found typically in seasonally-stratified and sub-polar waters, where upwelling or deep winter mixing brings large nutrient supplies to the surface and spring restratification triggers intense phytoplankton blooms (Sarmiento et al., 2004). The maximum chlorophyll concentrations in these waters reach 1.5 mg Chl m^{-3} or more (Fig. 3.2). Thus, embedded in the duration index of the phytoplankton growing season is a complex of various factors: the amplitude of the surface chlorophyll concentration, the depth of the mixed layer and the surface nutrient concentration.

3.3.2 Detection of decadal changes in duration

Decadal changes in duration of phytoplankton growing season were detected by subtracting the results for the period 1998-2008 (SeaWiFS) from those for the period 1979-1986 (CZCS)(Fig. 3.3). Within the extent of data coverage, we report here a significant global increase of 2.4 weeks ($P < 0.001$) in the duration of growing season between the two time periods (Table 3.3 and Table 3.1). Large increases of more than 3 weeks are observed on average in the Atlantic and Indian Oceans. The smaller increase of 1.5 weeks on average in the Pacific Ocean is caused by a dipole pattern of increasing (decreasing) duration of growing season in the western (eastern) Pacific.

Observations of changes in sea-surface temperature (SST) between the 1979-1986 and 1998-2008 periods show a global ocean warming of +0.2°C, with the changes varying regionally, including an East-West dipole in the Pacific (Fig. 3.4). Over more than 70% of the global ocean, the spatial trends in the duration of growing season are associated with the geographic differences in the trends of SST (Table 3.2). The regional increases (decreases) in SST matched significantly with the regional lengthening (shortening) of the phytoplankton growing season. The large regional increase in SST modifies upper-ocean stratification, limiting the supply of nutrient for phytoplankton growth. Similar results have been reported for the observed and simulated increase in ocean stratification (Behrenfeld et al., 2006; Bopp et al., 2001, 2005), for the observed expansion of oligotrophic waters (Polovina et al., 2008)

as well as for the simulated expansion of permanently-stratified biomes, which are characterised by shallow mixing and more nutrient-depleted conditions in the surface ocean (Sarmiento et al., 2004).

3.3.3 Relation to export production

To elucidate the relation between the duration index and the carbon export flux, we used two different export estimates. The first export estimates were produced by R. Schlitzer using an inverse modelling method (Schlitzer, 2002) based on a large global dataset of hydrographic and biogeochemical properties, including dissolved nutrients, oxygen, carbon and CFCs that contain latent information on the underlying processes. The inverse method estimates annual export fluxes of particulate organic carbon (POC) at 100 m using an ocean biogeochemistry model that is fitted systematically to the hydrographic dataset (Fig. 3.5a). The model-derived export flux is independent of the satellite-based chlorophyll data. High export values associated with eutrophic coastal systems were excluded from our analysis. We divided the surface of the globe between 65°N and 65°S into 306 boxes of 10° latitude by 20° longitude. Export estimates and calculated bloom duration were averaged for each box. A significant negative correlation ($r = -0.69$, $P < 0.0025$) was found between averaged export values at 100 m and duration of growing season with a slope$\pm 1\sigma$ of -0.062 ± 0.022 mol C m^{-2} yr^{-1} per week (Fig. 3.6a).

To evaluate the robustness of the globally-derived linear equation, we developed a series of sensitivity tests (Fig. 3.7). First, we assessed the robustness of the results to the definition of duration of the growing season: (Cases S1 and S2) we increased the relative chlorophyll threshold by 5 and 10% respectively. Then, we assessed the robustness of the results with respect to the differences in the remote-sensing data processing. We compared datasets processed by three different algorithms and calibration methods: (Case S) SeaWiFS data, (Case C) CZCS data, (Cases Sa and Ca) the "CZCS-type SeaWiFS" and "revised CZCS" produced by D. Antoine (Antoine et al., 2005). The negative correlation between annual export production

at 100 m and duration of growing season was sustained in all sensitivity tests and the linear trends ranged from -0.032 to -0.069 mol C m^{-2} yr^{-1} per week.

The second export estimates are from annual POC export flux derived from 62 sediment-traps deployed at an averaged depth of 1,100 m in various locations of the world ocean (Fig. 3.5b and Table 3.4). For each trap position, we retrieved the corresponding box-averaged duration and found a significant negative correlation ($r = -0.83$, $P < 0.0005$) between averaged trap export values and duration of growing season (Fig. 3.6b). The attenuation of the export flux with depth explains the factor of five difference in the slope value (-0.013 ± 0.005 mol C m^{-2} yr^{-1} per week) found for the trap export flux at 1,100 m compared with the model-derived export flux at 100 m.

3.3.4 Rationalisation of the relation between export and duration

A relation between export production and duration of phytoplankton growing season is observed because of the dynamics of particle aggregation and mixed-layer depth (MLD) (de Boyer Montégut et al., 2004) (Fig. 3.8a,b). Regions with a short growing season produce high phytoplankton biomass that is sustained by deep surface MLD in winter and consequently high surface nutrient concentrations in spring. This large concentration of phytoplankton biomass aggregates into flocs that sink rapidly below the MLD. The export of organic material is further enhanced by the shallower MLD present under these growth conditions, as it reduces remineralisation losses within the mixed layer. In a region with a long growing season surface nutrients and phytoplankton biomass remain low. Slow sinking of small, non-aggregated cells and the deeper MLD present under these growth conditions favour remineralisation of organic material within the mixed layer and reduce carbon export.

3.3.5 Decadal changes in export production

Decadal changes in export production were estimated from the changes in the duration of the phytoplankton growing season and the linear relation between duration and export. We infer a decrease in export production of -0.55 ± 0.20 Pg C yr^{-1} at 100 m and -0.11 ± 0.04 Pg C yr^{-1} at 1,100 m North of 45°S from the global lengthening in the duration of growing season by 2.4 weeks (Table 3.3). Regionally, the Atlantic and Indian oceans show the largest decrease in export production with $-6.9\pm2.5\%$ and $-6.1\pm2.2\%$ at 100 m and $-13.0\pm5.1\%$ and $-11.4\pm4.5\%$ at 1,100 m respectively. The dipole pattern of increasing (decreasing) duration of growing season observed in the western (eastern) Pacific led to a smaller decrease in export production of $-2.9\pm1.0\%$ at 100 m and $-5.6\pm2.2\%$ at 1,100 m. The uncertainties in the decadal changes in export production of $\pm34\%$ to $\pm39\%$ are estimated from a Maximum Likelihood analysis performed on the slope of the linear relation between duration and export data (see Appendix 3.5 for details). Different sources and levels of uncertainty can be identified from those data: (a) uncertainty associated with the SeaWiFS ocean-colour data products is estimated to range between $\pm5\%$ to $\pm35\%$, although in extreme oligotrophic waters it may reach $\pm65\%$ (Hu et al., 2001); (b) largest uncertainty in modelled POC export at 100 m comes from the SO, where it is estimated to be of $\pm21\%$ (Schlitzer, 2002); (c) uncertainty associated with analytical errors of sediment trap data reaches up to $\pm6\%$ in the literature (Klaas and Archer, 2002), although this number does not account for uncertainty associated with trapping efficiency, which may vary by a factor of three or more in shallow traps (Buesseler, 1991). The uncertainties in the data will not reflect in uncertainty in the trends if they are normally distributed and there are no bias. This is difficult to evaluate. Some bias may be present in the SO where fewer observations are available to constrain the satellite algorithms and the modelled POC export. However less than 22% of our data points originate from the Southern Ocean, and thus the influence on the trend should be minimal. We estimate the changes in the oceanic CO_2 sink that are directly associated with the changes in carbon export over decadal

time-scales using an ocean biogeochemistry model (Giraud et al., 2008). Based on the results of Giraud et al. (2008), a decrease in export of -0.55 Pg C yr^{-1} would reduce the oceanic CO_2 sink by -0.41 Pg C yr^{-1} North of 45°S.

3.3.6 Limitations

The present method of analysis accounts for the changes associated with the main phytoplankton growing season, which develop around the highest surface chlorophyll concentration of the year. The method does not allow detection of changes associated with sub-surface chlorophyll maxima or secondary blooms. Our analysis is also limited roughly to North of 45°S as the CZCS data coverage in the Southern Ocean is insufficient to estimate duration. Recent decadal increase in winds in the Southern Ocean would suggest enhanced nutrient supply (Le Quéré et al., 2007), and thus a different mechanism operating there.

3.4 Conclusions

Observations show a lengthening of the phytoplankton growing season over the last two decades that is associated mainly with ocean warming and increased stratification. Our analysis suggests that an increase in duration of the growing season North of 45°S leads to a reduction in carbon export, which has a direct effect on the global CO_2 sink over decadal time scales. In particular, it represents a reduction in the role of the ocean as a damper on the increasing concentrations of CO_2 as a result of fossil fuel burning, and the associated enhanced greenhouse effect. As such, it is an unanticipated or emergent effect of global warming on the planetary carbon cycle, specifically on the status of the ocean as a sink for CO_2 emitted to the atmosphere by the activities of man.

3.5 Appendix: Materials and Methods

3.5.1 Remote-sensing chlorophyll-*a* data

Sea-surface concentrations of chlorophyll-*a* (Chl a) were derived from level 3 data at 9 km spatial resolution available at http://oceancolor.gsfc.nasa.gov/. Weekly climatologies were constructed for the periods October 1978 to June 1986 (CZCS) and September 1997 to June 2008 (SeaWiFS). The "revised CZCS" and "CZCS-type SeaWiFS" Chl a processed daily at 9 km spatial resolution (Antoine et al., 2005) by D. Antoine were retrieved directly from the author. Weekly climatologies were constructed for the periods January 1979 to June 1986 and January 1998 to December 2002 respectively. A three-weeks running mean was applied to the original data to remove small peaks in chlorophyll-*a* concentrations generated by meteorological forcings.

When comparing the bloom durations estimated from the Chl a data of the two satellites missions SeaWiFS and CZCS, we recognise difficulties such as differences in the sensors, the temporal and spatial scale of observations, the calibration techniques and the data processing algorithms (Gregg and Conkright, 2002; Antoine et al., 2005). We therefore applied a relative method to estimate the duration of the phytoplankton growing season. We checked the Chl a data from CZCS and omitted the spatially-isolated pixels for which it was impossible to determine the standard deviation with the surrounding pixels to ensure data homogeneity (i.e. non-homogeneity in the data are potentially associated with errors in the atmospheric correction). We compared our results to the re-processed Chl a data of D. Antoine (Antoine et al., 2005), where the same algorithm and corrections have been applied to both satellite missions.

3.5.2 Remote-sensing sea-surface temperature data

NOAA ERSST V3 monthly data products (Jan 1979-Dec 1986 and Jan 1998-Dec 2008) were acquired from the National Oceanic-Atmospheric Administration/Office

of Oceanic and Atmospheric Research/Earth System research Laborartory available at http://www.cdc.noaa.gov/cdc/data.noaa.ersst.html.

3.5.3 Threshold estimation

Initiation and end points of the growing season are defined as the times when the chlorophyll-*a* concentration in a particular year period rises above the median value plus 5% and later falls below this same threshold (Siegel et al., 2002). We applied an additional criteria in the processing: data with a coefficient of variation (CV) of chlorophyll-*a* concentrations lower than 0.1 and a duration of growing season less than or equal to 10 weeks were omitted to exclude ultra-oligotrophic waters where the seasonality is so low that the chlorophyll threshold method is unlikely to detect any phytoplankton growth.

3.5.4 Statistical analyses

The global and regional average differences in duration of growing season between the 1979-1986 and 1998-2008 periods were analysed using Welch *t*-test comparisons. This test is an adaptation of the Student *t*-test for use with samples having unequal variances. Homogeneity of variances was checked using an *F*-test and the null hypothesis (i.e. equality of variances between samples) was rejected in all cases (Table 3.1). Programming codes were written to implement the Welch *t*-test and *F*-test using the Ferret NOAA PMEL software.

The influence of the changes in SST on the changes in duration of the growing season was analysed using the nonparametric Sign Test. The null hypothesis H_0: the proportion of boxes with a matching sign change in both SST and duration is equal to 0.5, is rejected with a confidence level of 99.99%, $n = 123$ (Table 3.2). A programming code was written to implement the nonparametric Sign Test using the Ferret NOAA PMEL software.

The linear relation between the export of carbon and the duration of the phytoplankton growing season was also tested on non-binned data: The Pearson correlation analysis performed on the 167 box means gives a significant negative coefficient $\rho = -0.22$ ($P < 0.005$); The Pearson correlation analysis performed on the 62 traps gives a significant negative coefficient $\rho = -0.31$ ($P < 0.01$). A Fortran programming code was written to perform the Pearson correlation analysis.

The uncertainty ($\pm 1\sigma$) in the slope of the relation between duration and export was calculated using a 1000-step Maximum Likelihood analysis (Sivia and Skilling, 2006). A MATLAB programming code was kindly provided by D. Wolf-Gladrow to perform the Maximum Likelihood analysis. The Maximum Likelihood method fits the least squares linear model to the export and duration data, to provide the most likely (and best) estimates of the linear model parameters and their uncertainties.

3.5.5 Data processing

The highest 5% of the export fluxes at 100 m were omitted in the analysis to exclude eutrophic coastal systems. This cut-off criterion corresponds roughly to an upper limit of 6 mol C m^{-2} yr^{-1}. The 10x20 one-degree-latitude-by-one-degree-longitude pixels included in each box were averaged. If the box contained data on less than 50 (1/4) of its 200 pixels, then the box was discarded from the analysis. The 10x20 degrees box size was selected to reduce variability in the duration data associated with micro- and mesoscale features such as eddies and fronts.

References

Antia, A. N., Maassen, J., Herman, P., Voss, M., Scholten, J., Groom, S., and Miller, P. (2001). Spatial and temporal variability of particle flux at the NW European continental margin. *Deep Sea Res., Part II*, 48(14-15):3083–3106.

Antia, A. N., von Bodungen, B., and Peinert, R. (1999). Particle flux across the mid-european continental margin. *Deep Sea Res., Part I*, 46:1999–2024.

Antoine, D., Morel, A., Gordon, H., Banzon, V., and Evans, R. (2005). Bridging ocean color observations of the 1980s and 2000s in search of long-term trends. *J. Geophys. Res.*, 110:doi:10.1029/2004JC002620.

Behrenfeld, M., O'Malley, R., Siegel, D., McClain, C., Sarmiento, J., Feldman, G., Milligan, A., Falkowski, P., Letelier, R., and Boss, E. (2006). Climate-driven trends in contemporary ocean productivity. *Nature*, 444:doi:10.1038/nature05317.

Bopp, L., Aumont, O., Cadule, P., Alvain, S., and Gehlen, M. (2005). Response of diatoms distribution to global warming and potential implications: A global model study. *Geophys. Res. Lett.*, 32:doi:10.1029/2005GL023653.

Bopp, L., Monfray, P., Aumont, O., Dufresne, J.-L., LeTreut, H., Madec, G., Terray, L., and Orr, J. (2001). Potential impact of climate change on marine export production. *Global Biogeochem. Cycles*, 15:81–100.

Buesseler, K. O. (1991). Do upper-ocean sediment traps provide an accurate record of particle flux? *Nature*, 353:420–424.

Burd, A. and Jackson, G. (2009). Particles aggregation. *Annu. Rev. Mar. Sci.*, 1:doi:10.1146/annurev.marine.010908.163904.

Canadell, J., Le Quéré, C., Raupach, M., Field, C., Buitenhuis, E., Ciais, P., Conway, T., Gillett, N., Houghton, R., and Marland, G. (2007). Contributions to accelerating atmospheric CO_2 growth from economic activity, carbon intensity, and efficiency of natural sinks. *Proc. Natl. Acad. Sci. USA*, 104:doi:10.1073/pnas.0702737104.

de Boyer Montégut, C., Madec, G., Fischer, A., Lazar, A., and Iudicone, D. (2004). Mixed layer depth over the global ocean: An examination of profile-based climatology. *J. Geophys. Res.*, 109:doi:10.1029/2004JC002378.

Dymond, J. and Collier, R. (1988). Biogenic particle fluxes in the equatorial Pacific: Evidence for both high and low productivity during the 1982-1983 El Niño. *Global Biogeochem. Cycles*, 2:129–137.

Engel, A., Thoms, S., Riebesell, U., Rochelle-Newall, E., and Zondervan, I. (2004). Polysaccharide aggregation as a potential sink for marine dissolved organic carbon. *Nature*, 428:929–932.

Fischer, G., Donner, B., Davenport, B., Ratmeyer, V., and Wefer, G. (1996). Distinct year-to-year particle variation off Cape Blanc during 1988-1991: Relation to ^{18}O-deduced sea-surface temperature and trade winds. *J. Mar. Res.*, 54:73–98.

Fischer, G., Gersonde, R., and Wefer, G. (2002). Organic carbon, biogenic silica and diatoms fluxes in the marginal winter sea-ice zone in the polar front region: interannual variations and differences in composition. *Deep Sea Res., Part II*, 49:1721–1745.

Fischer, G., Ratmeyer, V., and Wefer, G. (2000). Organic carbon fluxes in the Atlantic and the Southern Ocean: relationship to primary production compiled from satellite radiometer data. *Deep Sea Res., Part II*, 47:1961–1997.

Giraud, X., Le Quéré, C., and da Cunha, L. (2008). Importance of coastal nutrient supply for global ocean biogeochemistry. *Global Biogeochem. Cycles*, 22:doi:10.1029/2006GB002717.

Gregg, W. W. and Conkright, M. E. (2002). Decadal changes in global ocean chlorophyll. *Geophys. Res. Lett.*, 29:doi:10.1029/2002GL014689.

Gupta, L. and Kawahata, H. (2002). Impact of ENSO variability on the flux and composition of sinking POM in the western equatorial Pacific Ocean: Amino acids and hexosamines. *Deep Sea Res., Part II*, 49:doi:10.1016/S0967–0645(02)00057–7.

Honda, M., Imai, K., Nojiri, Y., Hoshi, F., Sugawara, T., and Kusakabe, M. (2002). Biological pump in the northwestern North Pacific based on fluxes and major components

of particulate matter obtained by sediment-trap experiments (1997-2000). *Deep Sea Res., Part II*, 49:5595–5625.

Honjo, S., Dymond, J., Collier, R., and Manganini, S. (1995). Export production of particles to the interior of the equatorial Pacific Ocean during the 1992 EqPac experiment. *Deep Sea Res., Part II*, 42:831–870.

Honjo, S., Dymond, J., Prell, W., and Ittekkot, V. (1999). Monsoon-controlled export fluxes to the interior of the Arabian Sea. *Deep Sea Res., Part II*, 46:1859–1902.

Honjo, S., Francois, R., Manganini, S., Dymond, J., and Collier, R. (2000). Particle fluxes to the interior of the Southern Ocean in the Western Pacific sector along 170°W. *Deep Sea Res., Part II*, 47:doi:10.1016/S0967–0645(00)00077–1.

Honjo, S. and Manganini, S. (1993). Annual biogenic particle fluxes to the interior of the North Atlantic Ocean; studied at 34°N 21°W and 48°N 21°W. *Deep Sea Res., Part I*, 40:587–607.

Honjo, S., Manganini, S., and Cole, J. (1982). Sedimentation of biogenic matter in the deep ocean. *Deep Sea Res., Part A*, 29:609–625.

Hu, C., Carder, K., and Muller-Karger, F. (2001). How precise are SeaWiFS ocean color estimates? Implications of digitization-noise errors. *Remote Sens. Environ.*, 76:239–249.

Ittekkot, V., Nair, R., Honjo, S., Ramaswamy, V., Bartsch, M., Manganini, S., and Desai, B. (1991). Enhanced particle fluxes in Bay of Bengal induced by injection of fresh water. *Nature*, 351:385–387.

Kawahata, H. (2002). Suspended and settling particles in the Pacific. *Deep Sea Res., Part II*, 49:5647–5664.

Kempe, S. and Knaack, H. (1996). Vertical particle flux in the western Pacific below the north equatorial current and the equatorial counter current. In Ittekkot, V., Schafer, P., Honjo, S., and Depetris, P., editors, *Particle Flux in the Ocean*, pages 313–323. John Wiley and Sons, New York.

Klaas, C. and Archer, D. E. (2002). Association of sinking organic matter with various types of mineral ballast in the deep sea: Implications for the rain ratio. *Global Biogeochem. Cycles*, 16:doi:10.1029/2001GB001765.

Kuss, J. and Kremling, K. (1999). Particle trace element fluxes in the deep northeast Atlantic Ocean. *Deep Sea Res., Part I*, 46:149–169.

Le Quéré, C., Rödenbeck, C., Buitenhuis, E., Conway, T., Langenfelds, R., Gomez, A., Labuschagne, C., Ramonet, M., Nakazawa, T., Metzl, N., gillett, N., and Heimann, M. (2007). Saturation of the Southern Ocean CO_2 sink due to recent climate change. *Science*, 316:doi:10.1126/science.1136188.

Mohiuddin, M., Nishimurab, A., Tanakab, Y., and Shimamoto, A. (2002). Regional and interannual productivity of biogenic components and planktonic foraminiferal fluxes in the Northwestern Pacific Basin. *Mar. Micropaleontol.*, 45:57–82.

Mohiuddin, M., Nishimurab, A., Tanakab, Y., and Shimamoto, A. (2004). Seasonality of biogenic particle and planktonic foraminifera fluxes: response to hydrographic variability in the Kuroshio Extension, northwestern Pacific Ocean. *Deep Sea Res., Part I*, 51:doi:10.1016/j.dsr.2004.06.002.

Moore, J., Doney, S., Lindsay, K., Mahowald, N., and Michaels, A. (2006). Nitrogen fixation amplifies the ocean biogeochemical response to decadal timescale variations in mineral dust deposition. *Tellus*, 58B:560–572.

Neuer, S., Ratmeyer, V., Davenport, R., Fischer, G., and Wefer, G. (1997). Deep water particle flux in the Canary Island region: seasonal trends in relation to long-term satellite derived pigment data and lateral sources. *Deep Sea Res., Part I*, 44:1451–1466.

Nodder, S. and Northcote, L. (2001). Episodic particulate fluxes at southern temperate and mid-latitudes (42-45°S) in the Subtropical Front region, east of New Zealand. *Deep Sea Res., Part I*, 48:833–864.

Pilskaln, C., Manganini, S., Trull, T., Armand, L., Howard, W., Asper, V., , and Massom, R. (2004). Geochemical particle fluxes in the Southern Indian Ocean seasonal ice zone: Prydz Bay region, East Antarctica. *Deep Sea Res., Part I*, 51:307–332.

Platt, T. and Sathyendranath, S. (2008). Ecological indicators for the pelagic zone of the ocean from remote sensing. *Remote Sens. Environ.*, 112:3426–3436.

Ploug, H., Iversen, M., Koski, M., and Buitenhuis, E. (2008). Production, oxygen respiration rates, and sinking velocity of copepod fecal pellets: Direct measurements of ballasting by opal and calcite. *Limnol. Oceanogr.*, 53:469–476.

Polovina, J., Howell, E., and Abecassis, M. (2008). Ocean's least productive waters are expanding. *Geophys. Res. Lett.*, 35:doi:10.1029/2007GL031745.

Sarmiento, J. L., Slater, R., Barber, R., Bopp, L., Doney, S., Hirst, A., Kleypas, J., Matear, R., Mikolajewicz, U., Monfray, P., Soldatov, V., Spall, S., and Stouffer, R. (2004). Response of ocean ecosystems to climate warming. *Global Biogeochem. Cycles*, 18:doi:10.1029/2003GB002134.

Schlitzer, R. (2002). Carbon export fluxes in the Southern Ocean: results from inverse modeling and comparison with satellite-based estimates. *Deep Sea Res., Part II*, 49:1623–1644.

Shin, K., Norikia, S., Itoua, M., and Tsunogai, S. (2002). Dynamics of sinking particles in northern Japan trench in the western North Pacific: biogenic chemical components and fatty acids biomarkers. *Deep Sea Res., Part II*, 49:doi:10.1016/S0967–0645(02)00217–5.

Siegel, D., Doney, S., and Yoder, J. (2002). The North Atlantic spring phytoplankton bloom and Sverdrup's critical depth hypothesis. *Science*, 296:730–733.

Sivia, D. S. and Skilling, J. (2006). *Data analysis: a Bayesian tutorial*. Oxford University Press, 2 edition.

Trull, T., Bray, S., Manganini, S., Honjo, S., and Francois, R. (2001). Moored sediment trap measurements of carbon export in the Subantarctic and Polar Frontal Zones of the Southern Ocean, south of Australia. *J. Geophys. Res.*, 106:31489–31509.

Waniek, J., Schulz-Bull, D., Blanz, T., Prien, R., Oschlies, A., and Müller, T. (2005). Interannual variability of deep water particle flux in relation to production and lateral sources in the northeast Atlantic. *Deep Sea Res., Part II*, 52:doi:10.1016/j.dsr.2004.08.008.

Wefer, G. and Fischer, G. (1993). Seasonal patterns of vertical particle flux in equatorial and coastal upwelling areas of the eastern Atlantic. *Deep Sea Res., Part I*, 40:1613–1645.

Wefer, G., Suess, E., Balzer, W., Leibezeit, G., Muller, P., Ungerer, C., and Zenk, W. (1982). Fluxes of biogenic components form sediment trap deployment in circumpolar waters of the Drake Passage. *Nature*, 299:145–147.

Wong, C., Whitney, F., Crawford, D., Iseki, K., Matear, R., Johnson, W., Page, J., and Timothy, D. (1999). Seasonal and interannual variability in particle fluxes of carbon, nitrogen and silicon from time series of sediment traps at Ocean Station P, 1982-1993: relationship to changes in subarctic primary productivity. *Deep Sea Res., Part II*, 46:2735–2760.

3.6 Tables

Table 3.1: Summary of statistical comparisons of the duration of the phytoplankton growing season between the periods 1979-1986 (past) and 1998-2008 (present). F is the statistic for test of homogeneity of variances with the null hypothesis H_0: variance of duration in the past = variance of duration in the present. dfn and dfd are degrees of freedom for the numerator and denominator respectively. P is the two-tailed probability of accepting H_0. t is the absolute value of the Welch t-test statistic. The significance is indicated with a confidence limit of 95% (*) and 99% (**). ν is degrees of freedom for the t-test statistic. Global Ocean coverage is restricted to North of 45°S (see Fig. 3.3).

Ocean	F test				Welch t-test	
	F	dfn	dfd	P	t	ν
Atlantic	14.01	1	70	0.001	3.796**	59.3
Indian	11.35	1	32	0.005	3.473**	26.2
Pacific	4.74	1	110	0.1	2.197*	101.6
Global	25.31	1	244	0.001	5.051**	221.9

Table 3.2: Sign changes in sea-surface temperature (SST) and duration of phytoplankton growing season for 1998-2008 (present period) minus 1979-1986 (past period), calculated for the global ocean North of 45°S (to the extent of data coverage, see Fig. 3.3).

Sign difference (present − past)		Number of
SST	Duration	boxes
+	+	81
−	−	9
+	−	24
−	+	9

Table 3.3: Changes in duration and export production for 1998-2008 minus 1979-1986. Changes in export production (Δexport) at 100 m and 1,100 m are calculated from the linear relations between duration and export for each change in duration (Δduration) of the phytoplankton growing season. The relative changes in export are displayed in parentheses (in %). The amplitude of the export variability is shown at $\pm 1\sigma$. The significance is indicated with a confidence limit of 95% (*) and 99% (**).

Ocean	Δ duration weeks	Δ export at 100m Pg C yr^{-1} (%)	Δ export at 1,100m Pg C yr^{-1} (%)
Atlantic	3.5**	-0.20±0.07 (-6.9±2.5)	-0.04±0.02 (-13.0±5.1)
Indian	3.0**	-0.09±0.03 (-6.1±2.2)	-0.02±0.01 (-11.4±4.5)
Pacific	1.5*	-0.15±0.05 (-3.0±1.0)	-0.03±0.01 (-5.6±2.2)
Global[(1)]	2.4**	-0.55±0.20 (-4.7±1.7)	-0.11±0.04 (-8.9±3.5)

[(1)]North of 45°S to the extent of data coverage (see Fig. 3.3)

Table 3.4: Location (Latitude and Longitude), water depth, trap depth, sampling year, sampling interval, code and reference of the sediment-trap data used in this study.

Lat. (deg.)	Lon. (deg.)	Water Depth (m)	Trap Depth (m)	Years	Interval (days)	Total Flux (g m^{-2} yr^{-1})	POC Flux (g m^{-2} yr^{-1})	Code (Reference)
54.39	-21.14	3074	1000	1993-1994	239	14.72	3.43	L3-93 (Kuss and Kremling, 1999)
50.01	165.01	5546	1227	1999	345	20.86	1.02	50N (Honda et al., 2002)
50.01	165.01	5546	1227	1997-1998	395	44.20	2.34	50N (Honda et al., 2002)
50.00	-145.00	4240	1000	1983-1994	1320	51.70	2.71	OSP (Wong et al., 1999)
49.60	-12.30	1500	1050	1993-1994	365	26.48	2.22	OMEX-2 (Antia et al., 1999)
48.90	-13.50	3260	1440	1993-1994	365	42.50	3.61	OMEX-3 (Antia et al., 1999)
47.73	-20.86	4451	1110[a]	1989-1990	378	20.90	2.63	NB4U (Honjo and Manganini, 1993)
47.50	-19.39	4574	1000	1992	144	26.44	2.63	L2-A-92 (Kuss and Kremling, 1999)
47.48	-19.47	4577	1030	1992-1993	350	7.49	4.16	L2-B-92 (Kuss and Kremling, 1999)
46.07	175.02	5435	1412	1993-1994	304	75.86	2.35[b]	Site-8 (Kawahata, 2002)
43.58	155.03	5375	924	1999-2000	375	62.60	4.27	KNOT (Honda et al., 2002)
43.58	155.03	5375	924	1997-1998	395	46.02	2.37	KNOT (Honda et al., 2002)
40.26	144.28	7150	1000	1994-1996	551	29.95	3.69	JT-Station B (Shin et al., 2002)
40.00	165.00	5476	953	1997-1998	395	28.38	1.53	KURU-40N (Honda et al., 2002)
40.00	165.00	5476	953	1999	365	26.11	2.05	KURU-40N (Honda et al., 2002)
39.00	146.60	5356	1371	1997-1999	625	65.71	5.46	WCT2 (Mohiuddin et al., 2002)
37.24	174.57	5105	1482	1993-1994	313	34.55	1.87[b]	Site-7s (Kawahata, 2002)
36.41	154.56	5578	1191	1999-2000	376	25.31	1.64	WTC7 (Mohiuddin et al., 2004)
35.60	147.00	5615	1108	1998-1999	345	13.30	1.64	WCT3 (Mohiuddin et al., 2004)
34.25	177.44	3365	1342	1993-1994	304	15.01	0.84[b]	Site-5s (Kawahata, 2002)
33.81	-21.04	5083	1159[a]	1989-1990	364	19.59	1.07	NB3U (Honjo and Manganini, 1993)
31.80	-64.20	4400	1500	1988-1989	361	10.93	0.74	OFP (Antia et al., 2001)
31.80	-64.20	4400	1500	1987-1988	369	15.00	0.98	OFP (Antia et al., 2001)
31.80	-64.20	4400	1500	1991-1992	365	13.94	0.96	OFP (Antia et al., 2001)
31.80	-64.20	4400	1500	1990-1991	359	16.18	0.93	OFP (Antia et al., 2001)
31.80	-64.20	4400	1500	1984-1985	366	13.62	1.01	OFP (Antia et al., 2001)
31.80	-64.20	4400	1500	1989-1990	368	10.96	0.63	OFP (Antia et al., 2001)
31.33	-55.55	5581	976	1976-1977	110	7.16	0.89	SAP-S2 (Honjo et al., 1982)
29.15	-15.44	3605	1026	1992-1993	309	14.80	1.06	CI2 (Neuer et al., 1997)
29.11	-15.45	3611	1006	1991-1992	305	5.89	0.44	CI1 (Neuer et al., 1997)
25.00	136.60	4905	917	1997-1998	613	7.08	0.98	WCT1u (Mohiuddin et al., 2002)
25.00	136.60	5308	1388	1998-1999	357	7.08	1.50	WCT1l (Mohiuddin et al., 2002)
21.08	-20.40	4108	733	1991	200	26.80	3.43	CB4u (Fischer et al., 1996)
21.08	-20.40	4094	730	1990-1991	387	32.50	1.82	CB3u (Fischer et al., 1996)
17.41	58.51	1448	999	1994-1995	408	58.44	3.84	MS1 (Honjo et al., 1999)
17.40	89.60	2263	809	1987-1988	365	11.55	3.59	BngN (Ittekkot et al., 1991)
17.24	58.48	3655	924	1994-1995	408	74.15	6.28	MS2 (Honjo et al., 1999)
17.12	59.36	3477	888	1994-1995	408	81.82	6.39	MS3 (Honjo et al., 1999)
15.30	61.30	3983	821	1994-1995	408	53.69	3.25	MS4 (Honjo et al., 1999)
15.21	-151.28	5792	978	1978	61	2.74	0.20	HAP-P1 (Honjo et al., 1982)
13.50	-54.00	5288	988	1977-1978	98	17.97	1.44	DAP-E (Honjo et al., 1982)
13.20	84.40	3259	906	1987-1988	365	14.63	2.64	BngC (Ittekkot et al., 1991)
12.02	134.29	5300	1200	1988-1989	383	1.74	0.14	NEC (Kempe and Knaack, 1996)
11.50	-21.00	4968	1003	1992-1993	181	29.81	2.31	CV1 (Fischer et al., 2002)
11.50	-21.00	4973	975	1993-1994	363	17.70	0.99	CV2 (Fischer et al., 2002)
10.00	65.00	4411	800	1994-1995	170	26.41	2.08	MS5 (Honjo et al., 1999)
9.00	-139.98	5100	1250	1992	85	13.90	0.97	EP1U (Honjo et al., 1995)
5.21	-81.53	3856	1268	1989	112	38.17	3.27	PB1 (Honjo et al., 1982)
5.02	-139.78	4493	1191	1992-1993	357	25.34	2.20	EP2U (Honjo et al., 1995)
5.01	138.83	4130	1130	1988-1989	391	6.59	0.65	ECC (Kempe and Knaack, 1996)
4.40	87.30	4017	1040	1987-1988	365	16.08	2.37	BngS (Ittekkot et al., 1991)
4.03	135.00	4762	970	1999	324	21.40	2.70	Site-M1 (Gupta and Kawahata, 2002)
1.80	-11.20	4399	953	1991	230	24.24	2.49	EA2-1991 (Fischer et al., 2000)
1.80	-11.20	4522	859	1990-1991	369	30.94	2.98	GBN6-1990 (Fischer et al., 2000)
1.48	-11.08	4481	853	1989-1990	380	29.20	3.20	GBN3-1989 (Wefer and Fischer, 1993)
1.13	160.34	3181	116	1994-1995	197	9.39	0.56[b]	Site 10 (Kawahata, 2002)
1.00	-139.00	4470	1095	1982-1984	428	1.73	1.08	MANOP-TP-C3 (Dymond and Collier, 1988)
1.00	-139.00	4470	1083	1984-1985	434	3.55	1.96	MANOP-TP-C4 (Dymond and Collier, 1988)
0.07	-139.75	4358	880	1992-1993	357	33.25	1.70	EP4U (Honjo et al., 1995)
0.02	174.56	4828	1040	1999	312	19.61	2.08	Site-M5 (Gupta and Kawahata, 2002)
0.01	145.02	3680	1020	1999	320	13.55	1.50	Site-M3 (Gupta and Kawahata, 2002)
0.00	-23.50	3744	718	1994-1995	357	23.71	2.49	WA8 (Fischer et al., 2000)
0.00	-10.80	4141	1097	1991	230	11.40	0.97	EA3c (Fischer et al., 2000)
0.00	-10.80	4580	1280	1993-1994	420	15.30	1.89	EA10 (Fischer et al., 2000)
0.00	-10.80	4563	1226	1992-1993	171	18.61	2.33	EA9 (Fischer et al., 2000)
0.00	-10.80	4255	949	1991-1992	307	32.07	1.16	EA7 (Fischer et al., 2000)
0.00	175.10	4880	1357	1992-1993	289	14.65	0.71[b]	Site-3s (Kawahata, 2002)
-2.20	-9.90	3906	1068	1991	230	11.00	0.96	EA4-1991 (Fischer et al., 2000)
-4.00	-25.70	5601	854	1994-1995	363	21.96	1.69	WA7 (Fischer et al., 2000)
-4.00	-25.70	5525	808	1993-1994	373	20.75	2.20	WA4 (Fischer et al., 2000)
-4.30	-10.30	3490	947	1991	230	11.92	0.79	EA5 (Fischer et al., 2000)
-4.95	-139.73	4198	1216	1992	204	21.02	1.04	EP6U (Honjo et al., 1995)
-11.97	-135.03	4294	1292	1992-1993	357	10.60	0.55	EP7U (Honjo et al., 1995)

[a] Averaged depth

[b] POC calculated as POC = Total flux / 2.27 (Waniek et al., 2005)

Table 3.4: Continued.

Lat. (deg.)	Lon. (deg.)	Water Depth (m)	Trap Depth (m)	Years	Interval (days)	Total Flux (g m^{-2} yr^{-1})	POC Flux (g m^{-2} yr^{-1})	Code (Reference)
-12.60	155.60	1832	1315	1995-1996	321	9.39	0.44[b]	Site-11 (Kawahata, 2002)
-17.46	154.50	2821	1298	1995-1996	245	3.98	0.30[b]	Site-12s (Kawahata, 2002)
-35.31	161.00	3174	1161	1995-1996	245	9.35	0.72[b]	Site-13 (Kawahata, 2002)
-42.42	178.38	1500	1000	1996-1997	243	161.00	7.50	NCR (Nodder and Northcote, 2001)
-44.37	178.37	1500	1000	1996-1997	340	10.50	1.80	SCR (Nodder and Northcote, 2001)
-46.77	142.07	4540	1060	1997-1998	153	18.00	1.40	SAZ-47S (Trull et al., 2001)
-50.09	5.46	3750	700	1987	351	39.56	2.70	PF1 (Fischer et al., 2002)
-53.75	141.75	2280	830	1997-1998	153	27.00	0.80	SAZ-54S (Trull et al., 2001)
-56.90	-170.17	4924	982	1996-1998	416	41.33	2.03	PFZ (Honjo et al., 2000)
-60.28	-170.06	3958	1003	1996-1998	425	65.45	2.68	APF (Honjo et al., 2000)
-60.55	-57.06	3625	965	1980-1981	52	163.00	5.41	Drake Passage (Wefer et al., 1982)
-62.29	72.59	4000	1400	1998-1999	365	25.42	0.92	PZB1 (Pilskaln et al., 2004)
-63.01	70.57	nd	1300	1994-1995	353	3.04	0.11	ANTARES-M3 (Pilskaln et al., 2004)
-63.15	-169.90	2886	1031	1996-1998	425	133.52	3.86	ACC (Honjo et al., 2000)
-66.16	-168.67	3016	985[a]	1996-1997	204	23.10	1.73	RSn (Honjo et al., 2000)

[a] Averaged depth

[b] POC calculated as POC = Total flux / 2.27 (Waniek et al., 2005)

3.7 Figures

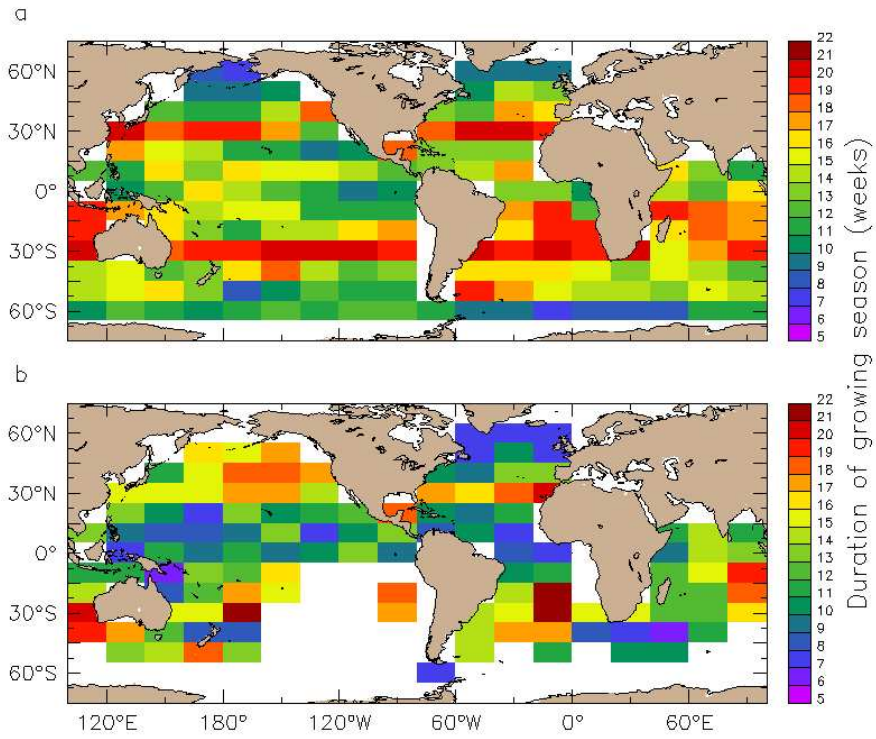

Figure 3.1: Duration of the phytoplankton growing season. (a) Climatology for the period 1998-2008 (SeaWiFS). (b) Climatology for the period 1979-1986 (CZCS). Boxes are 10° latitude by 20° longitude.

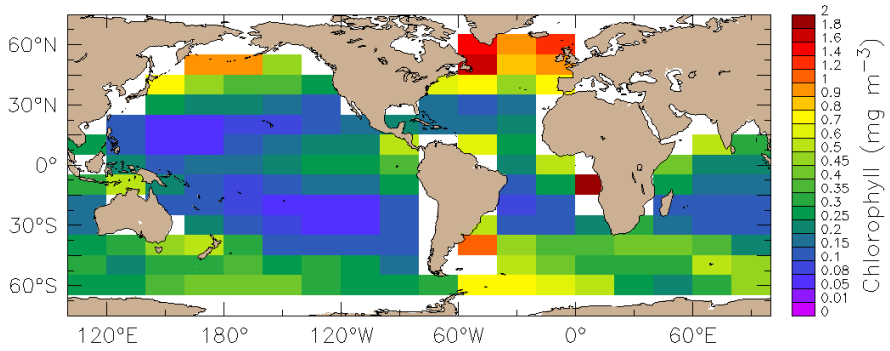

Figure 3.2: Maximum chlorophyll concentration. Climatology for the period 1998-2008 (SeaWiFS). Boxes are 10° latitude by 20° longitude.

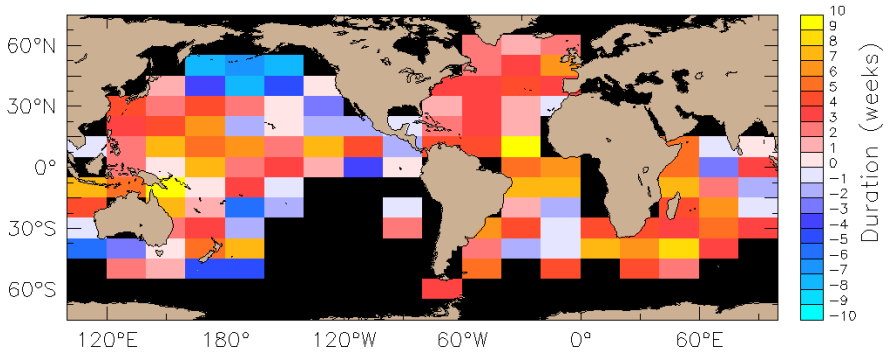

Figure 3.3: Changes in the duration of the phytoplankton growing season for 1998-2008 minus 1979-1986. Duration of growing season was estimated from climatologies of remotely-sensed chlorophyll-*a* concentrations from the Coastal Zone Color Scanner (CZCS, 1979-1986) and from the Sea-viewing Wide Field-of-view Sensor (SeaWiFS, 1998-2008) missions. Positive (negative) changes in duration correspond to longer (shorter) phytoplankton growing season in 1998-2008 compared to 1979-1986. Boxes are 10° latitude by 20° longitude. Black colour means no data.

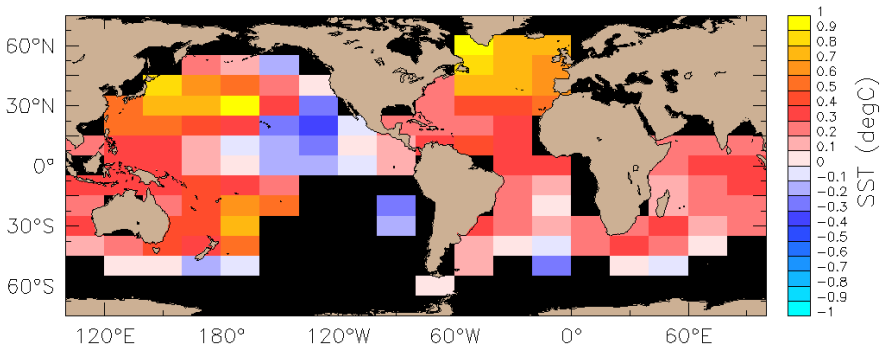

Figure 3.4: Changes in the sea-surface temperature (ΔSST) for 1998-2008 minus 1979-1986. Positive (negative) ΔSST corresponds to an increase (decrease) of the SST in 1998-2008 compared to 1979-1986. Boxes are 10° latitude by 20° longitude. Black colour means no data.

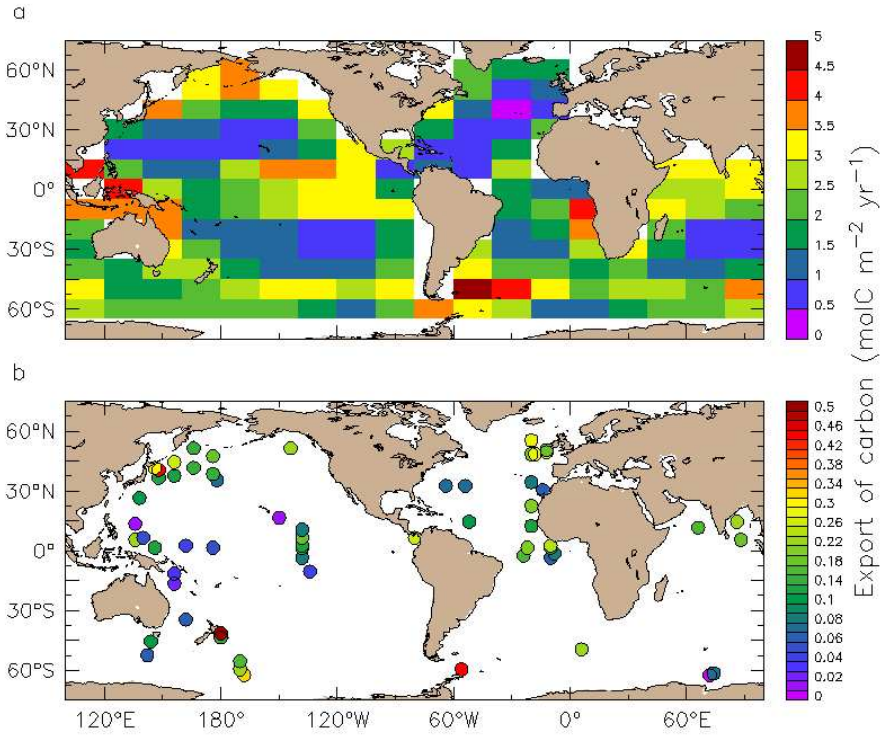

Figure 3.5: Annual estimates of Particulate Organic Carbon (POC) export. (a) Climatology of POC export at 100 m from an inverse model based on hydrographic and biogeochemical observations (Schlitzer, 2002). Boxes are 10° latitude by 20° longitude. (b) Climatology of POC export at 1,100 m from sediment trap experiments retrieved from the literature (see Table 3.4 for reference details).

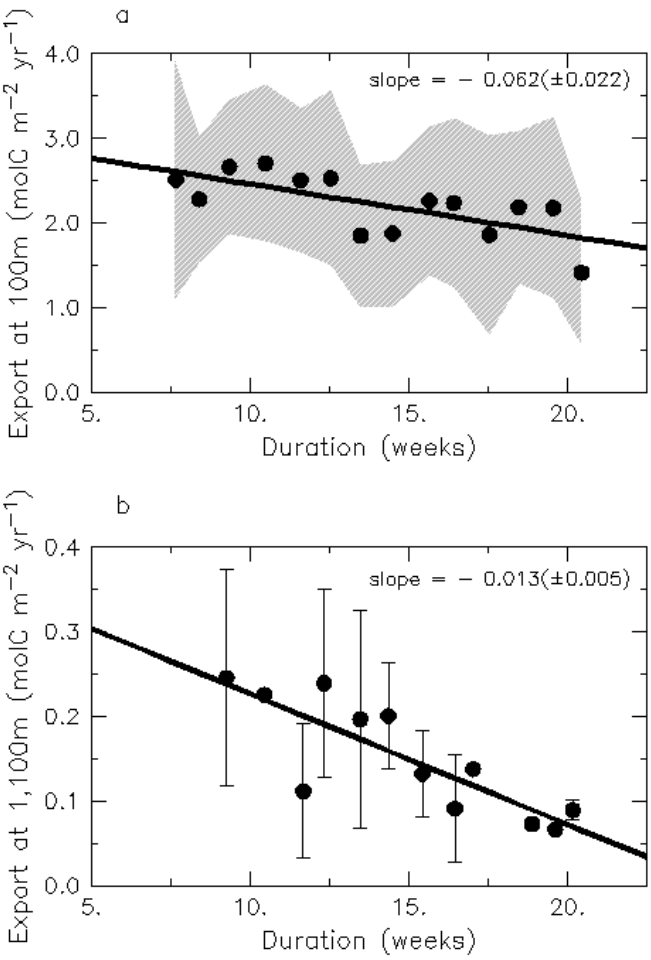

Figure 3.6: Relation between the export of carbon in the ocean interior and the duration of the phytoplankton growing season. (a) Export at 100 m from an inverse model based on hydrographic and biogeochemical observations (Schlitzer, 2002). The export data are binned at one-week duration intervals ($n = 14$, $r^2 = 0.48$). The Pearson correlation coefficient $\rho = -0.69$ is significant ($P < 0.0025$). (b) Export at 1,100 m from sediment trap data (see Table 3.4). The export data are binned at one-week duration intervals ($n = 12$, $r^2 = 0.69$). The Pearson correlation coefficient $\rho = -0.83$ is significant ($P < 0.0005$). Duration of growing season is estimated from SeaWiFS chlorophyll data climatology (1998-2008). Gray shading and error bars indicate the amplitude of the export variability for each duration (±1SD).

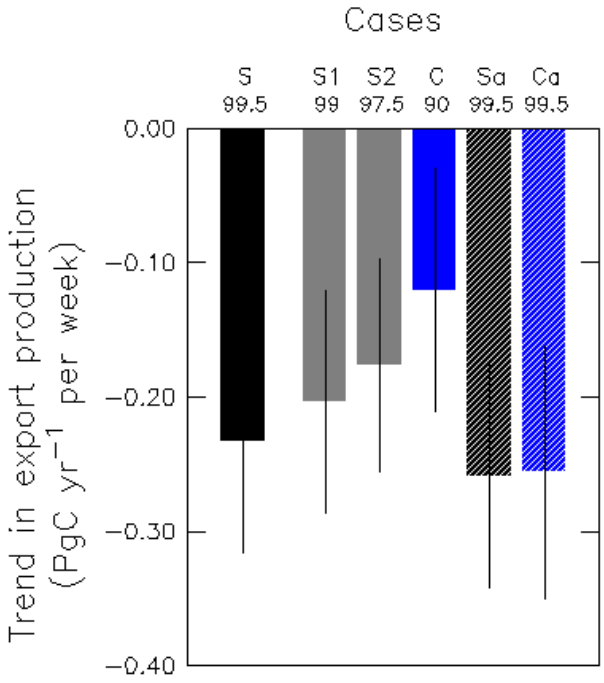

Figure 3.7: Trends in the export production at 100 m. Case S (in black) is the standard trend in export estimated from the duration of growing season derived for the period 1998-2008 (SeaWiFS). Case S1 and S2 (in gray) are sensitivity tests to the detection method for the duration of growing season. Case C (in blue) is the trend in export estimated from the duration of growing season derived for 1979-1986 (CZCS). Case Sa and Ca (in dashed black and dashed blue) are sensitivity tests to the remote sensing data-processing algorithm: durations of growing seasons are derived both from the "CZCS-type SeaWiFS" (1998-2002) and from the "revised CZCS" (1979-1986) processed by Antoine et al. (2005).

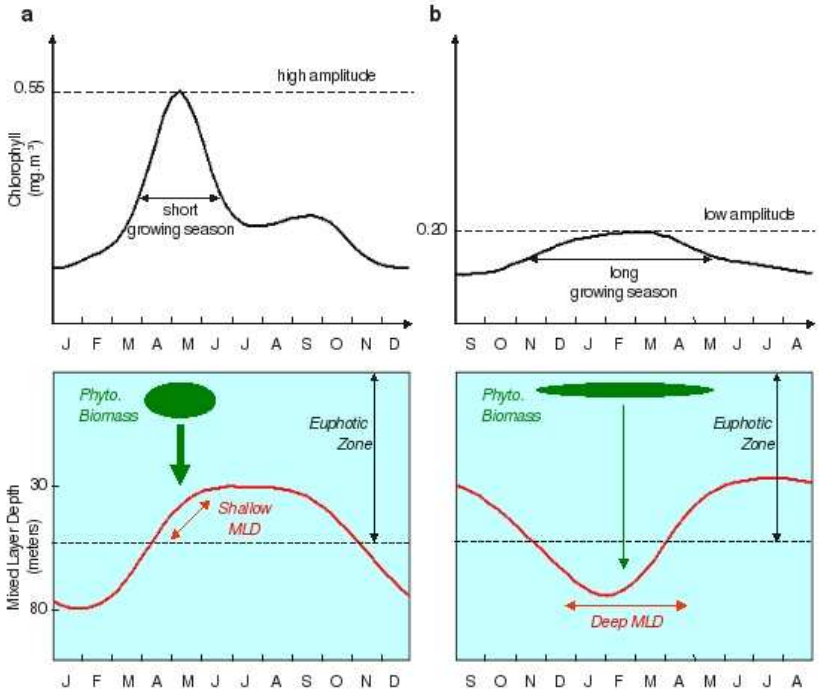

Figure 3.8: Climatology of chlorophyll-*a* and mixed layer depth (MLD) averaged over regions where the growing season is 10 weeks (a) and 20 weeks (b) in the North Hemisphere. (a) In a short growing season/high export case, the chlorophyll amplitude is high, the biomass is high and particulate aggregation is high. Furthermore under short growing season, the MLD is shallow and large phytoplankton aggregates reach more rapidly the intermediate ocean (below the MLD). (b) In a long growing season/low export case, the chlorophyll amplitude is low, the biomass is low, and particulate aggregation is low. Furthermore under long growing season, the MLD remains relatively deep and a larger fraction of organic material is likely to be remineralised before it sinks below the mixed layer. Remotely-sensed chlorophyll-*a* concentrations are from a global climatology constructed from the Sea-viewing Wide Field-of-view Sensor (SeaWiFS, 1998-2008). MLD data are from a global climatology based on both temperature and density profiles (de Boyer Montégut et al., 2004).

Chapter 4

Resolving Sverdrup's critical depth hypothesis to estimate plankton community respiration and net community production

4.1 Abstract

Mixed layer integrated plankton community respiration R_{mld} and net community production NCP_{mld} are estimated at the global scale by resolving Sverdrup's critical depth model. Key parameters of the model, i.e. community compensation irradiance I_c and critical depth z_{cr} are calculated using remote-sensing data of incident irradiance level and primary production, and a global mixed layer depth climatology. Large regional variability in I_c is observed between the tropics and subtropics (10-15 mol photon m^{-2} d^{-1}) and the high-latitudes (0.5-3 mol photon m^{-2} d^{-1}). Poleward of 35°, NCP_{mld} is positive (100-150 g C m^{-2} y^{-1}) during the phytoplankton growing season and becomes negative ($-$130-180 g C m^{-2} y^{-1}) when phytoplankton growth is limited. In contrast, equatorward of 35°, NCP_{mld} is negative ($-$50-90 g C m^{-2} y^{-1}) during the estimated growing season and positive (30-70 g C m^{-2} y^{-1}) outside of the growing season. The method overestimates R_{mld} in the North Pacific, the Southern Ocean 35-45°S band and the Arabian Sea, leading to calculation of a global annual net heterotrophic imbalance of $-$ 5.9l Pg C y^{-1}. However, the range and seasonality of NCP_{mld} estimates agree with *in-situ* and model data reported for the North Atlantic Drift province, suggesting that the present method might be of use to predict NCP in some regions of the ocean. In particular, the net autotrophic imbalance of 0.65 Pg C y^{-1} calculated for the North Atlantic matches at 85% with annual model export estimates for that region.

4.2 Introduction

In the surface layer of the ocean, the phytoplankton community fixes dissolved CO_2 by photosynthesis to produce organic matter. Photosynthetic production of organic carbon has been thoroughly investigated and can be derived at a global scale from remote-sensing measurements of surface phytoplankton biomass (Platt and Sathyendranath, 1988; Sathyendranath et al., 1989; Platt et al., 1991a,b; Antoine et al., 1996; Behrenfeld and Falkowski, 1997; Mélin, 2003; Behrenfeld et al., 2005). The processes controlling the fraction of total primary production (PP) that is recycled by plankton community respiration (R) are less well understood (del Giorgio and Duarte, 2002; Robinson and Williams, 2005; Robinson, 2008). The plankton community losses described in the variable R include phytoplankton light and dark respiration, maintenace respiration, zooplankton respiration and bacterial respiration as carbon sinks. *In-situ* measurements of R are extremely sparse compared with the large data set of PP (Williams, 2000). Empirical relationships between PP and R have been shown not to be straightforward (del Giorgio et al., 1997; Williams, 1998; Duarte and Augusti, 1998) and have generated intense debate on the nature of the trophic balance of the global ocean (Williams et al., 1999; del Giorgio and Duarte, 2002). The trophic balance of a biological community is summarised in the net community production (NCP), i.e. the difference between PP and R. Williams (2000) defined NCP as the "potential of the plankton community for organic export".

Owing to the recent improvements in detection of phytoplankton growing season (Siegel et al. (2002), chapter 2), global mixed layer depth estimates (de Boyer Montégut et al., 2004), and remote-sensing measurements of incident irradiance level and primary production, it is now possible to resolve the critical depth model of Sverdrup (1953) at a global scale. This model calculates seasonal and regional variability in plankton community respiration and net community production.

This chapter is structured as follows. Section 4.3 introduces Sverdrup's (1953) critical depth model (the list of mathematical expressions used in the model is summarised in Table 4.1). Section 4.4 describes the data and methods. Section 4.5

presents and discusses regional and seasonal variations of (1) key variables required to implement Sverdrup's critical depth model, (2) estimates of PP, R and NCP. The estimates of NCP are then compared with *in-situ* and modelled data from the literature. Summary and conclusions are given in section 4.6.

4.3 Sverdrup's critical depth model

Sverdrup (1953) proposed the fundamental hypothesis that net accumulation of phytoplankton biomass in a given layer will occur when the depth-integrated rate of production of organic matter by photosynthesis in that layer exceeds the depth-integrated rate of destruction by respiration. The model assumes that PP is linearly related to the level of irradiance in the Photosynthetically Active Range (PAR). The slope α of the Productivity-Irradiance (P-I) relationship is illustrated in the Figure 4.1). In the ocean water-column, irradiance level decreases exponentially with depth:

$$I(z) = I_o e^{-kz} \tag{4.1}$$

where *I(z)* is irradiance in the PAR at depth z, I_o is incident irradiance in the PAR and k is vertical attenuation for irradiance in the PAR. In Sverdrup's model, PP is described to decrease exponentially with depth (Fig. 4.2) such as:

$$P(z) = \alpha I(z) = \alpha I_o e^{-kz} = P_o e^{-kz} \tag{4.2}$$

where *P(z)* is PP at depth z and P_o is PP at surface. Community respiration is assumed to remain constant with depth:

$$R(z) = R_o \tag{4.3}$$

where *R(z)* is community respiration at depth z and R_o is community respiration at surface. Sverdrup (1953) explicitly included phytoplankton and zooplankton respiration in the loss term. Uncertainties about the definition and the difficulties to constrain the components of the loss term were raised by Smetacek and Passow

(1990). Platt et al. (1991a) refined the loss term in the model to include phytoplankton maintenance and dark respiration, micro- and macrozooplankton grazing, excretion and sedimentation losses. The assumption that community respiration remain constant with depth is acknowledged throughout the mixed layer (Platt et al., 1991a). Below the mixed layer depth (MLD), rates of community respiration decrease sharply (del Giorgio and Duarte, 2002) as they rely on the quantity of organic matter being exported through sinking of particles and zooplankton migrations.

The minimum level of irradiance required for production to compensate community respiration at a particular depth is defined as community compensation irradiance I_c (Fig. 4.1 and Fig. 4.2). In the water-column, the irradiance level I_c occurs at the compensation depth z_c:

$$I_c = I_o e^{-kz_c} \tag{4.4}$$

At compensation depth z_c, production and respiration are equal:

$$R_o = P_o e^{-kz_c} \tag{4.5}$$

Hence, using equations (4.4) and (4.5), I_c can be defined as:

$$I_c = \frac{I_o R_o}{P_o} \tag{4.6}$$

In the mixed layer, phytoplankton cells spend time both above and below z_c. Net growth will occur when the integrated production from the surface to the depth of the mixed layer z_{mld} is greater than the integrated respiration in the same layer. The integrated production (P_{mld}) from the surface to z_{mld} is:

$$P_{mld} = P_o \int_0^{z_{mld}} e^{-kz} dz = \frac{P_o}{k}(1 - e^{-kz_{mld}}) \tag{4.7}$$

The integrated respiration (R_{mld}) in the mixed layer is:

$$R_{mld} = R_o \int_0^{z_{mld}} dz = R_o z_{mld} \tag{4.8}$$

The depth at which integrated production and integrated respiration are equal is defined as the critical depth z_{cr}:

$$P_{z_{cr}} = R_{z_{cr}} \tag{4.9}$$

When the MLD is deeper than z_{cr}, the average irradiance received by the phytoplankton cells is insufficient. Production cannot balance respiration. As surface insolation increases and the mixed layer stratifies in spring, the MLD may shoal to depth less than z_{cr}. Production can then compensate the respiration and net growth will occur. This is the Sverdrup (1953) necessary condition for initiation of the phytoplankton growing season and the critical depth can be defined as the depth where:

$$\frac{1}{kz_{cr}}(1 - e^{-kz_{cr}}) = \frac{R_o}{P_o} = \frac{I_c}{I_o} \tag{4.10}$$

4.4 Data and methods

4.4.1 The remotely-sensed data

Global weekly Level 3 Standard Mapped Images of chlorophyll-a (Chla), photosynthetically active radiation (PAR) and diffuse attenuation coefficient at 490nm wavelength (k_{490}) were retrieved at 9 km resolution from the Sea-viewing Wide Field-of-view Sensor (SeaWiFS) for the period September 1997 to April 2009, available at http://oceancolor.gsfc.nasa.gov/. Uncertainty associated with the SeaWiFS ocean-colour data products (i.e. Chla, PAR and (k_{490}) is estimated to range between ±5% to ±35%, although in extreme oligotrophic waters it may reach ±65% (Hu et al., 2001).

The diffuse attenuation coefficient for the PAR wavelengths (k) was estimated from k_{490} using the equations of Rochford et al. (2001). The equations are adapted to the three different water classes: oligotrophic clear CASE 1 waters, intermediate CASE 1-2 waters and turbid coastal CASE 2 waters.

$$k = \begin{cases} 0.0085 + 1.6243k_{490} & k_{490} \leq 1 \\ 0.3175 + 1.2144k_{490} & 1 < k_{490} \leq 2.3 \\ 0.3570 + 1.1676k_{490} & 2.3 < k_{490} \end{cases} \tag{4.11}$$

4.4.2 The primary production data

PP was retrieved from the model of Mélin (2003), including spectral, temporal and vertical resolution. The model uses monthly remotely-sensed data from SeaWiFS and is available for the period September 1997 to December 2004 at 4 km resolution. The key parameters of the PP model (i.e. biomass distribution in the water column, carbon assimilation coefficient and light-productivity relationship) were assigned following the partitioning of the ocean into biogeographic provinces, as proposed by Longhurst (1998). In the model, the values of the P-I parameters varied seasonally. The model outputs of Mélin (2003), denoted $P_{0.1\%}$, were available as depth-integrated PP to 0.1% light level.

Mélin (2003) estimated uncertainty from his globally averaged annual PP values as ±10% of the mean of the PP values derived from Behrenfeld and Falkowski (1997), Antoine et al. (1996) and his model. The model of Mélin (2003) uses SeaWiFS Chla as input data to calculate PP. Uncertainty associated with SeaWiFS is discussed in section 4.4.1 and is assumed to be of the order of ±35% for open case 1 water. Antoine et al. (1996) have shown that vertically integrated Chla varies approximately as the square root of the surface Chla. Hence, the authors were able to estimate uncertainty in water column integrated Chla of approximately ±17%. Therefore, in Mélin (2003) model, the uncertainty in PP estimates, that is attributable only to uncertainty in the SeaWiFS Chla (and when the other parameters remain unchanged), is likely to be of the order of ±17%.

4.4.3 The mixed-layer depth data

A global monthly climatology of mixed-layer depth (MLD) was acquired from C. de Boyer-Montégut available at http://www.locean-ipsl.upmc.fr/ cdblod/mld.html. The 2° resolution climatology was constructed from approximately five million temperature profiles from the period 1941 to 2008. The MLD was defined as the temperature criterion of ± 0.2 °C change compared with the temperature at 10 m (de Boyer Montégut et al., 2004). The depth of the mixed layer is denoted z_{mld}.

Depending on the criterion selected (i.e. threshold value of temperature or density), the estimated MLD varied on average by ±30% for the global ocean, with larger standard deviation found as depth increases. The MLD climatology based on the temperature criterion is derived from approximately five million profiles, whereas the MLD climatology based on the density criterion is derived from approximately 900,000 profiles.

4.4.4 Data processing

To conform with the remotely-sensed data, $P_{0.1\%}$ and z_{mld} were interpolated to weekly temporal resolution. Because the data (i.e. Chla, I_o, k, $P_{0.1\%}$ and z_{mld}) were to be associated with phenologically important phases in the phytoplankton growing season, it was important to eliminate gaps in the time series. Missing values were substituted by interpolating spatially-adjacent values, if these were not missing. Otherwise the value was not filled. The remaining missing values were filled by interpolating temporally-adjacent values, if these were not missing. Otherwise the value was not filled. A three-weeks running mean was applied to remove small spikes in Chla and the data were then averaged to one degree resolution. Finally, global weekly climatologies of Chla, I_o, k, $P_{0.1\%}$ and z_{mld} were constructed.

4.4.5 Characterisation of the phytoplankton growing season

The timings of initiation and end of the phytoplankton growing season (b_i and b_e respectively) were detected as the weeks when the chlorophyll concentration in the year period rose above the median value plus 5% (Siegel et al., 2002) and later fell below this same threshold. The peak timing (b_t) was retrieved as the week of maximum chlorophyll concentration.

4.4.6 Calculation of the community compensation irradiance

According to Sverdrup's hypothesis, at the time b_i, depth-integrated production compensates exactly the respiration and the depth of the mixed-layer z_{mld} coincides with the critical depth z_{cr}. The values of I_o, k, and z_{mld} were retrieved at b_i. All the variables in equation (4.10) were then available to solve for I_c.

4.4.7 Calculation of the critical depth

A time series of critical depth can be calculated using equation (4.10) assuming I_c to remain constant over time. Phytoplankton compensation irradiance (I_{cphy}) may vary temporally (Smetacek and Passow, 1990; Platt et al., 1991a) as phytoplankton adapt to seasonal changes in light intensity and spectral quality. However, the seasonal variability in the community compensation irradiance is unclear. *In-situ* measurments of phytoplankton community compensation irradiance from a mooring site in the North Atlantic showed limited variability over the one week experiment interval (Marra, 2004). Henson et al. (2006) assumed constant I_c to estimate a daily time series of Sverdrup's critical depth in the Irminger Basin. Their z_{cr} estimates showed coherent seasonality and interannual variabilily in mixed layer shallowing and deepening as well as phytoplankton bloom initiation. In the present study, weekly climatologies of I_o, k and the corresponding constant I_c values were used to estimate the critical depth z_{cr} by solving iteratively equation (4.10) in the form:

$$\frac{1}{kz_{cr}}(1 - e^{-kz_{cr}}) - \frac{I_c}{I_o} = 0 \tag{4.12}$$

4.4.8 Calculation of mixed layer integrated production P_{mld} and respiration R_{mld}

The mixed layer integrated production P_{mld} was derived from Mélin's $P_{0.1\%}$ estimates of integrated PP from the surface to the depth $z_{0.1\%}$ where the irradiance level is 0.1% of the incident surface irradiance. $z_{0.1\%}$ was calculated by solving equation (4.1)

in the form:

$$I_o e^{-kz_{0.1\%}} = I_o \frac{0.1}{100} \tag{4.13}$$

$$z_{0.1\%} = -\frac{ln\frac{0.1}{100}}{k} \tag{4.14}$$

Weekly surface production P_o were estimated based on Sverdrup's assumption that PP decreases exponentially with depth, and using k, $z_{0.1}$ and $P_{0.1\%}$ such that:

$$P_o = \frac{P_{0.1\%}k}{(1 - e^{-kz_{0.1\%}})} \tag{4.15}$$

All the variables in equation (4.6) were then available to determine weekly surface respiration R_o. Finally, equations (4.7) and (4.8) were solved to determine the time series of P_{mld} and R_{mld}.

Uncertainty estimates have been discussed (sections 4.4.1, 4.4.2, 4.4.3) for each variable used to calculate P_{mld} and R_{mld}. The different levels of uncertainty associated with the variables k, $P_{0.1\%}$, $z_{0.1\%}$ and z_{mld} propagate throughout the equations (4.7), (4.8), (4.14) and (4.15). Assuming the stated uncertainties on the input variables, error propagation potentially leads to more than ±100% uncertainty on both P_{mld} and R_{mld}.

4.5 Results and discussion

4.5.1 Global estimations of the spatial distributions of Sverdrup's model key parameters z_{cr}, I_o and I_c

Timing of initiation of growing season

Spatial distribution in the timing of initiation of phytoplankton growing season is shown in Fig. 4.3a. In the Northern Hemisphere, growing season initiates in December (week 43) in the subtropical gyres. In the North Atlantic (NA), the timing of initiation then propagates steadily towards the poles from January to June (week 1 to 20), following the seasonal increase in insolation. In the North Pacific (NP), similar poleward propagation is detected along the coast of Japan, China, and in the

Bering Sea. The Central NP demarcates itself clearly with growing season setting off in June-August (week 20-30), three months later than the surrounding waters. This demarcation results from large seasonal and interannual variability in phytoplankton biomass in the Central NP (Peña and Varela, 2007). In the Southern Hemisphere, the growing season initiates in June-July (week 20-24) in the subtropical gyres. Along the 30°S band, growth starts in May (week 16) and rapidly propagates to July and August along the 40°S band. South of 45°S, the growing season initiates between September and November (week 34 and 40).

Critical depth at initiation

Following Sverdrup's hypothesis, at initiation of the growing season b_i, the depth of the mixed layer z_{mld} is equal to the critical depth z_{cr} (Fig. 4.3b). The shallowest z_{mld} are found along the West coast of Africa, America, and in the Central NP. Most of the tropics and subtropics present relatively shallow z_{mld} between 40 to 80 m depth. Deeper z_{mld} ($>$ 100 m) are found in the NA, in the NP along the coast of Japan, China and the Kurushio extension. The deepest z_{mld} at bloom initiation are encountered throughout the Southern Ocean (SO), reaching more than 200 m. The notions of deep and shallow must be considered relative to the average conditions occuring in the region. The tropics and subtropics are characterised by permanently stratifed waters (Sarmiento et al., 2004), where the seasonality in z_{mld} is limited. In fact, the shallow z_{mld} found in these regions tend to be deeper at b_i and during the growing season compared to the rest of the year (Fig. 4.4). Polewards of 35°, z_{mld} presents large seasonality and significant deepening of the mixed layer in winter. Hence, the relatively deep z_{mld}, when compared to the tropics and subtropics found at b_i, are actually shallower during the growing season than compared to the rest of the year (Fig. 4.4).

Incident irradiance level at initiation

Spatial distribution of the incident irradiance in the PAR I_o at initiation b_i is shown in Fig. 4.3c. I_o is higher than 35 mol photon m^{-2} d^{-1} in most of the tropics and subtropics. Long daylength and high irradiance levels predominate throughout the year in these regions (Hartmann, 1994). North of 30°N, I_o increases polewards at b_i, following the seasonal increase in daylength, as the spring initiation progresses polewards. In the SO, I_o varies accordingly with the time of initiation. A start in early austral summer in September encounters lower I_o of 15-20 mol photon m^{-2} d^{-1} compared with a later initiation in November, when the daylength has increased and I_o values have more than doubled, reaching 50 mol photon m^{-2} d^{-1}.

Global estimates of community compensation irradiance

Globally, the estimates of community compensation irradiance I_c (Fig. 4.3d) show a large contrast between the tropics and subtropics, displaying particularly high values, and the higher latitudes displaying almost an order of magnitude lower values (except in the Central NP, which presents high I_c values comparable to the tropics). The present estimates fall within the range of values reported by Siegel et al. (2002) for the NA, based on a similar approach to retrieve I_c. Poleward increase in I_c is observed, with low estimates of 0.5-1 mol photon m^{-2} d^{-1} around 35°N to 4.5-5 mol photon m^{-2} d^{-1} around 65°N. Similar range and distribution of I_c values are found within the surrounding waters of the Central NP and throughout most of the SO. The strickingly high I_c estimates (7-10 mol photon m^{-2} d^{-1}) for the Central NP result from the particularly shallow MLD (< 40 m) recorded at b_i in that region. In contrast, the high I_c estimations (7-15 mol photon m^{-2} d^{-1}) found sparsely within the SO, are the result of high I_o recorded in regions where the growing season started in late austral spring. I_c estimates are an order of magnitude higher in the tropics and subtropics with values ranging between 10 and 20 mol photon m^{-2} d^{-1}, and reaching up to 40 mol photon m^{-2} d^{-1} in places.

A high I_c indicates that the phytoplankton cells require a high minimum irradiance level to compensate the community respiration. Community compensation irradiance I_c must be differentiated from phytoplankton compensation irradiance I_{cphy}. I_{cphy} strictly indicates the capacity of the phytoplankton cells to compensate their own maintenance respiration, but not to compensate the total community respiration. I_{cphy} has mostly been determined in laboratory experiments, such as the compilation of Langdon (1988) for eight phytoplankton species. He showed large inter-species variability with values ranging between 0.1 and 3 mol photon m^{-2} d^{-1}. *In-situ* measurements of I_{cphy} are much more limited and relatively little is known about its spatial, vertical and temporal variability. The study of Marra (2004) along a mooring site at 50°N in the NA, revealed that I_{cphy} decreases with depth, ranging from 0.2-0.4 mol photon m^{-2} d^{-1} at 50 m to 0.02-0.09 mol photon m^{-2} d^{-1} at 150 m. The one-order of magnitude lower estimates reported at greater depth suggest the possible presence of phytoplankton community adapted to low irradiance level, i.e. a high initial slope α (Fig. 4.1) associated with a low I_{cphy}. The only *in-situ* measurements of total community compensation irradiance I_c come from the study of Riley (1957). He estimated I_c to 3.5 mol photon m^{-2} d^{-1} (the value was originally measured in g cal cm^{-2} min^{-1} and converted in mol photon m^{-2} d^{-1} by Siegel et al. (2002)) at 35°N along the subtropical border of the NA. This *in-situ* measurement is coherent with I_c calculated in the present study.

The large differences in I_c observed between tropical and subpolar regions might be explained by a differential adaptation of the plankton community to distinct environmental conditions. In the tropics and subtropics, irradiance levels remain high throughout the year. The phytoplankton community is therefore adapted to high-light intensity regime. Such photoadaptation is associated with high I_c to compensate high autotrophic respiration (Langdon, 1988). Furthermore, high I_c is also required to compensate high rates of bacterial respiration induced by warm water temperature (Robinson, 2008).

Hence, the retrieved I_c distribution suggests distinct community growth regimes

between the low- and mid-latitudes and the high-latitudes. The development of these distinct regimes is indicated in the shoaling/deepening of z_{mld} compared to z_{cr} (Fig. 4.4). Poleward of 35°, the deep winter mixing replenishes nutrient concentrations in surface waters. Shoaling of the mixed layer in spring allows phytoplankton cells to receive sufficient light supply, triggering net accumulation of biomass. This is illustrated by the fact that z_{mld} remains equal or shallower than z_{cr} (in red on Fig. 4.4) over the duration of the estimated growing season. Equatorward of 35°, light supply is rarely limiting. Quasi-permanent stratification maintains however low nutrients concentrations in surface waters, which limits phytoplankton growth. Although increase vertical mixing of nutrients (i.e. deeping the mixed layer) may trigger net accumulation of phytoplankton biomass, photoacclimation may also be responsible for the chlorophyll enhancement (McClain et al., 2004). This is illustrated by the fact that z_{mld} is generally deeper than z_{cr} (in blue on Fig. 4.4) over the duration of the estimated growing season.

4.5.2 Regional and seasonal variability in mixed layer integrated production P_{mld} and respiration R_{mld}

Spatial distribution and latitudinal seasonality of P_{mld} and R_{mld} are shown in Fig. 4.5a, b, c, d. In oligotrophic regions (McClain et al., 2004), seasonality in P_{mld} is limited and the annual average is low (< 60 g C m^{-2} y^{-1}). This annual average is at least two-times larger (> 120 g C m^{-2} y^{-1}) in the NA, the NP, the SO, the North Indian Ocean (IO), and in coastal and equatorial upwelling regions. In these regions, P_{mld} tends to be higher (> 150 g C m^{-2} y^{-1}) during the estimated growing season. The spatial distribution of R_{mld} differs from that of P_{mld}. Annual average R_{mld} is particularly high (> 200 g C m^{-2} y^{-1}) in the Central NP, along the 45°N and 60°N bands of the NA, along the 35-45°S band of the SO, in the Arabian Sea, as well as in the coastal and equatorial upwelling regions. Relatively low annual average R_{mld} (< 100 g C m^{-2} y^{-1}) are estimated in most of the remaining ocean. Seasonality in R_{mld} is observed at all latitudes and is separated in time and space from that of

P_{mld}. Poleward of 35°, R_{mld} is high (> 300 g C m^{-2} y^{-1}) outside of the estimated growing season and low (≈ 50-100 g C m^{-2} y^{-1}) during the growing season. In contrast, equatorward of 35°, R_{mld} is low (< 60 g C m^{-2} y^{-1}) outside of the estimated growing season and high (≈ 150-250 g C m^{-2} y^{-1}) during the growing season.

The P_{mld}:R_{mld} ratio provides informative indication on the equilibrium status of the pelagic ecosystem (Platt et al., 2009). Annual MLD integrated rates of production and respiration are plotted against one another in Fig. 4.6 for the world ocean. The strong positive correlation ($\rho = 0.69$, $P < 0.001$, $n = 13473$) observed between production and respiration agrees with previous studies based on *in-situ* datasets of volumetric and depth integrated estimates (del Giorgio et al., 1997; Duarte and Augusti, 1998; Williams, 1998; Williams et al., 2004; Robinson and Williams, 2005; Robinson, 2008). Major controversy arose about the value of the slope (Williams et al., 1999). The average P:$R < 1$ observed in volumetric estimates (del Giorgio et al., 1997; Duarte and Augusti, 1998) contrasted with the average P:$R > 1$ observed in depth integrated estimates (Williams, 1998). The method of analysis and potential "bias" in dataset coverage (towards oligotrophic or highly-productive regions) were suggested as explanations for the differences (Williams et al., 1999; Serret et al., 1999; del Giorgio and Duarte, 2002; Robinson and Williams, 2005). In the present analysis, the slope (1.32±0.01) is slightly but significantly greater than one ($t = 71$, $P < 0.001$, $\nu = 43$), suggesting global imbalance of the ecosystem towards net heterotrophy ($R > P$). Amongst the global estimates, depth integrated respiration is twice as variable as depth integrated production. Low- and mid-latitudes estimates follow closely the 1:1 line (Fig. 4.6). The NA and SO (south of 45°S) estimates remain below the 1:1 line, indicating net autotrophic balance in their systems. The particularly high respiration rates estimated for the Central NP and SO 35-45°S band are responsible for the shift in the slope towards $R > P$.

4.5.3 Regional and seasonal variability in mixed layer integrated net community production NCP_{mld}

The spatio-temporal imbalance between production and respiration is further characterised in Fig. 4.5e, f. Depth-integrated net community production (NCP_{mld}) is calculated as the difference between production (P_{mld}) and respiration (R_{mld}). Poleward of 35°, NCP_{mld} is positive (100-150 g C m^{-2} y^{-1}) during the estimated phytoplankton growing season. The balance is temporally dominated by net autotrophy (Zhai et al., 2008). The sequence is followed by net heterotrophic imbalance, persisting as long as phytoplankton growth is limited. In contrast, equatorward of 35°, NCP_{mld} is negative (− 50-90 g C m^{-2} y^{-1}) during the estimated growing season and positive (30-70 g C m^{-2} y^{-1}) outside of the growing season. This is at first counter-intuitive, because the phytoplankton population cannot increase unless it compensates for the community respiration. However, in oligotrophic regions, the estimated phytoplankton growing season is not representative of a biomass outburst, but rather a slight increase above the low annual average. In these regions, phytoplankton growth is not limited by light but by nutrient supply. Hence, the deepening of the mixed layer and sporadic inputs of allochthonous material might stimulate planktonic as well as bacterial populations. Increased phytoplankton production further enhance bacterial and zooplankton respiration, leading to negative NCP_{mld}. The seasonal imbalance remains relatively moderate throughout most of the low- and mid-latitudes compared with that in the high latitudes (Fig. 4.5f).

Extreme heterotrophic sequences are calculated in the Central NP, the SO 35-45° band, and the Arabian Sea (Fig. 4.5e, Table 4.2). Although negative NCP has been reported in some of these regions (Robinson and Williams, 1999; Williams et al., 2004), the explanation for the present extreme estimations of R_{mld} (> 500 g C m^{-2} y^{-1}) must lie in the method used to calculate z_{cr} and I_c. Indeed, outstandly high estimates of I_c, for reasons discussed in section 4.5.1, will result in overestimation of surface and depth-integrated respiration rates. Net autotrophy is observed in the highly productive regions of the NA, the Kurushio extension, the

Bering Sea, and in the SO between 30-35°S and south of 45°S with annually averaged $NCP_{mld} > 70$ g C m^{-2} y^{-1}. In the tropics and subtropics, the system oscillates between annual net heterotrophy and net autotrophy with relatively limited amplitude: $-50 < NCP_{mld} < 50$ g C m^{-2} y^{-1}. The persisting controversy and the lack of global-scale estimates of NCP make it difficult to evaluate the soundness of the present results. Nonetheless, the results can be compared with local and regional *in-situ* and modelled NCP estimates of Serret et al. (2009) and Zhai et al. (2009).

4.5.4 Comparison of calculated NCP_{mld} with regional *in-situ* and modelled estimates

The North Atlantic Drift (NADR) province

Databases of euphotic zone integrated NCP (NCP_{eu}) and particulate organic ^{14}C-derived primary production ($PO^{14}CP$) were compiled over two latitudinal (from 30°S to 45°N) transects of the Atlantic Ocean performed during the Atlantic Merdional Transect (AMT)-6 and -11 cruises (Serret et al., 2001, 2002, 2006). Using the cruises databases, Serret et al. (2009) developed the AMT-6 and AMT-11 models to predict NCP_{eu} from its relationship with $PO^{14}CP$. The models were calibrated with data from productive biogeochemical provinces (NADR, CNRY, BENG, ETRA, Longhurst (1998)) and oligotrophic provinces (SATL, NAST, Longhurst (1998)), that were crossed along the cruise tracks. Particular attention was given to the NADR province, as the seasonal variability of predicted NCP_{eu} could be compared with *in-situ* measurements from an 18-month survey performed at three stations in the Bay of Biscay (Serret et al., 1999). Fig. 4.7 (adapted from Serret et al. (2009)) presents the seasonal cycles of AMT-6 and AMT-11 predicted NCP_{eu} averaged throughout the NADR province, together with the seasonal cycles of NCP_{eu} and integrated O_2 saturation measured in the Bay of Biscay by Serret et al. (1999). The present study NCP_{mld} averaged throughout the NADR province were converted in mmol O_2 m^{-2} d^{-1} (O_2:C mole ratio of 175:127, Broecker and Peng (1982)) and then plotted on Fig. 4.7. The results agree with the range of NCP_{eu} measured

and predicted by Serret et al. (2009). However, NCP_{mld} shows relatively weaker seasonal variability compared with NCP_{eu}. Weaker NCP_{mld} amplitudes occur in the winter/spring months, when the mixed layer is significantly deeper (≈300 m) than the euphotic zone in the NADR province (Longhurst, 1998). Conversely, when the mixed layer and euphotic zone are approximately equal in summer/autumn, the present NCP_{mld} estimates match closely with the *in-situ* and AMT-6 predicted NCP_{eu}, suggesting that the present method derived from Sverdrup (1953) model might be of use to predict *NCP* in some regions of the ocean.

The Northwest Atlantic Shelf

The net change in phytoplankton biomass in the mixed layer (NCB_{mld}) is described by Zhai et al. (2008, 2009) as the difference between mixed layer depth integrated phytoplankton growth and total phytoplankton loss by respiration, mortality, grazing, sinking and effects of advection and mixing. Hence, whereas NCP_{mld} represents the potential of plankton community for export (Williams, 2000), NCB_{mld} embodies all community losses including export.

Assuming uniform vertical distribution of biomass (B) within the mixed layer, NCB_{mld} was formulated by Zhai et al. (2008, 2009) as:

$$NCB_{mld}(t) = \int_0^{z_{mld}(t)} \frac{\partial(\chi(t)B(z,t))}{\partial t}\, dz = z_{mld}(t)\frac{\partial(\chi(t)B(t))}{\partial t} \tag{4.16}$$

where $z_{mld}(t)$ is depth of mixed layer at time t, $B(t)$ is satellite-derived concentration of surface chlorophyll-a at t, $\chi(t) = 79B(t)^{-0.36}$ is the carbon-to-chlorophyll ratio proposed by Sathyendranath et al. (2009) optimised for the North Atlantic. Equation 4.16 was implemented in the present study using weekly climatology of chl-a and z_{mld} (see data section 4.4).

Fig. 4.8a,b present the seasonal and latitudinal variations in NCP_{mld} and NCB_{mld} for the Northwest Atlantic shelf (70-45°W,40-60°N). NCB_{mld} and NCP_{mld} agree in their range of values, but differ significantly in their temporal distributions. Negative NCP_{mld} is observed before initiation of the growing season (Fig. 4.8a), indicating net heterotrophy. At initiation, NCP_{mld} is close to zero as P_{mld} balances R_{mld} following

Sverdrup's hypothesis. Positive NCP_{mld} is then observed throughout the growing season. Between 42-52°N, net autotrophy persists after the end of the 'main' growing season for more than ten weeks, most likely during the automnal and 'secondary' growing season. In contrast, NCB_{mld} is positive only during the ascendant phase of the growing season (Fig. 4.8b). At peak amplitude, NCB_{mld} is close to zero as a brief equilibrium is observed between gain and loss of biomass. Negative NCB_{mld} is observed during the waning phase of the growing season. Outside of the growing season, NCB_{mld} weakly oscillates around zero, suggesting a relatively constant biomass in the region.

NCB_{mld} becomes negative when the loss of phytoplankton biomass in the mixed layer overcomes phytoplankton growth in that same layer. Intense grazing and sinking of large phytoplankton cells reduce significantly phytoplankton biomass in the mixed layer. In the waning phase of the growing season, the phytoplankton population is still growing but not at sufficient pace so as to compensate the losses from the layer. In such conditions, the system is not under net heterotrophic balance. The temporal differences between positive and negative phases of NCB_{mld} and NCP_{mld} come from the fact that the latter represents only the potential of the plankton community for organic export rather than the total plankton community losses.

Annual NCB_{mld} (+ 0.07 P C y^{-1}) is almost null, indicating a close balance between annual total loss and PP (Zhai et al., 2009). The effect of physical forcings and notably advection is suggested to be responsible for the slight net autotrophic imbalance of 0.07 P C y^{-1} in the region. Subtraction of the advection processes (+ 0.07 P C y^{-1}) from the annual NCP_{mld} (+ 0.23 P C y^{-1}) gives a net potential for export production of 0.16 P C y^{-1}. Particulate organic carbon export is estimated to 0.11 P C y^{-1} by the biogeochemical model of Schlitzer (2002) in the same region, giving a reasonable correspondance with the export fraction of NCP_{mld} derived from Sverdrup's model.

4.6 Concluding remarks

Plankton community respiration and net community production were calculated at global scale using the critical depth model of Sverdrup (1953). The model is based on the balance between depth-integrated production and respiration, occuring at the onset of the phytoplankton growing season when the depth of the mixed layer is equal to the critical depth. The model relied on the recent availability of global scale estimates of z_{mld}, PP, I_o and the timing of onset of the growing season. However, some of the basic assumptions associated with the model proved to have certain limitations.

One issue was the overestimation of annual R_{mld} in the Central NP, the SO 35-45°S band and the Arabian Sea, which resulted in calculation of global annual net heterotrophic imbalance of -5.9 Pg C y^{-1} (Table 4.2). The considerable interannual variability and low phytoplankton biomass seasonality present in the overestimated regions, hampered reliable estimation of z_{cr} and I_c, which are key parameters in Sverdrup's model. A similar issue was suggested in the tropics and subtropics where the growing season is not limited by light but by nutrient supply. In these regions, z_{cr} could potentially be deeper than the estimated value of z_{mld} at the onset of the growing season, which would result in potential overestimation of I_c and R_{mld}. However, stably permanent stratification in these regions has most likely limited the offset in z_{cr} estimations.

In spite of the model's limitations, specific regional patterns in I_c could be distinguished. Particularly high I_c were retrieved in the tropics and subtropics ($\approx$ 10-15 mol photon m^{-2} d^{-1}) compared to the high-latitudes, displaying almost an order of magnitude lower I_c ($\approx$ 0.5-3 mol photon m^{-2} d^{-1}). Relatively sparse field measurements of I_c impeded validation of the regional and seasonal variability observed in the present estimates.

Spatio-temporal displacement between net autotrophy ($P > R$) and net heterotrophy ($P < R$) was observed at all latitudes. Regions poleward of 30° showed

high annual net autotrophic imbalance ($\approx$ 50-120 g C m^{-2} y^{-1}) (except in the Central NP and the SO 35-45°S band where R_{mld} was overestimated). Although large spatial variability in the sign of NCP_{mld} was observed in regions equatorward of 30°, the amplitude of the variations remained relatively limited ($-$ 70 $< NCP_{mld} <$ +70 g C m^{-2} y^{-1}).

The range and seasonality of NCP_{mld} agreed with *in-situ* and model data reported by Serret et al. (1999, 2009) in the North Atlantic Drift province (Longhurst, 1998). An annual net heterotrophic imbalance of $-$ 1 Pg C y^{-1} was estimated for the whole tropics and subtropics (Table 4.2), with coastal and upwelling regions appearing as the main contributors. Duarte and Augusti (1998) reported that net heterotrophic imbalance occurs in 80% of the ocean's surface, supported by net autotrophy in the remaining 20% of the ocean. Allochthonus organic inputs of up to $\approx$ 9 Pg C y^{-1} are also suggested to be sufficient to sustain a net heterotrophic imbalance (del Giorgio and Duarte, 2002). The model showed relatively coherent results throughout the NA, where a net autotrophic imbalance of + 0.65 Pg C y^{-1} was calculated (Table 4.2). Comparison with the net change in phytoplankton biomass (Zhai et al., 2009) suggested that advection processes contribute to $\approx$ 30% of the NCP_{mld} estimates in the NA. Hence, net organic export is estimated to 0.45 Pg C y^{-1}, which appears coherent with the POC export of 0.34 Pg C y^{-1} from Schlitzer (2002) for the same region.

References

Antoine, D., André, J.-M., and Morel, A. (1996). Oceanic primary production 2. Estimates at global scale from satellite (coastal zone color scanner) chlorophyll. *Global Biogeochem. Cycles*, 10:57–69.

Behrenfeld, M. and Falkowski, P. G. (1997). Photosynthetic rates derived from satellite-based chlorophyll concentration. *Limnol. Oceanogr.*, 42:1–20.

Behrenfeld, M. J., Boss, E., Siegel, D., and Shea, D. (2005). Carbon-based ocean productivity and phytoplankton physiology from space. *Global Biogeochem. Cycles*, 19:doi:10.1029/2004GB002299.

Broecker, W. S. and Peng, T. H. (1982). *Tracers in the sea*. Eldigio Press, Palisades, New York. 690pp.

de Boyer Montégut, C., Madec, G., Fischer, A., Lazar, A., and Iudicone, D. (2004). Mixed layer depth over the global ocean: An examination of profile-based climatology. *J. Geophys. Res.*, 109:doi:10.1029/2004JC002378.

del Giorgio, P., Cole, J., and Cimbleris, A. (1997). Respiration rates in bacteria exceed phytoplankton production in unproductive aquatic ecosystems. *Nature*, 385:148–151.

del Giorgio, P. and Duarte, C. (2002). Respiration in the open ocean. *Nature*, 420:doi:10.1038/nature01165.

Duarte, C. and Augusti, S. (1998). The CO_2 Balance of Unproductive Aquatic Ecosystems. *Science*, 281:doi:10.1126/science.281.5374.234.

Hartmann, D. L., editor (1994). *Global Physical Climatology*. Academic Press, San Diego.

Henson, S., Robinson, I., Allen, J., and Waniek, J. (2006). Effect of meteorological conditions on interannual variability in timing and magnitude of the spring bloom in the Irminger Basin, North Atlantic. *Deep Sea Res., Part I*, 53:1601–1615.

Hu, C., Carder, K., and Muller-Karger, F. (2001). How precise are SeaWiFS ocean color estimates? Implications of digitization-noise errors. *Remote Sens. Environ.*, 76:239–249.

Langdon, C. (1988). On the causes of interspecific differences in the growth-irradiance relationship for phytoplankton. II. A general review. *J. Plankton Res.*, 10:1291–1312.

Longhurst, A. (1998). *Ecological Geography of the Sea*. Academic Press, Califoria.

Marra, J. (2004). The compensation irradiance for phytoplankton in nature. *Geophys. Res. Lett.*, 31:doi:10.1029/2003GL018881.

McClain, C. R., Signorini, S., and Christian, J. (2004). Subtropical gyre variability observedby ocean-color satellites. *Deep Sea Res., Part II*, 51:281–301.

Mélin, F. (2003). *Potentiel de la télédétection pour l'analyse des propriétés optiques du système océan-atmosphère et application à l'estimation de la photosynthèse phytoplanctonique*. PhD thesis, Université Toulouse III.

Peña, M. and Varela, D. (2007). Seasonal and interannual variability in phytoplankton and nutrient dynamics along Line P in the NE subarctic Pacific. *Prog. Oceanogr.*, 75:200–222.

Platt, T., Bird, D., and Sathyendranath, S. (1991a). Critical depth and marine primary production. *Proc. R. Soc. Lond., Ser. B*, 246:205–217.

Platt, T., Caverhill, C., and Sathyendranath, S. (1991b). Basin-Scale Estimates of Oceanic Primary Production by Remote Sensing: The North Atlantic. *J. Geophys. Res.*, 96:15,147–15,159.

Platt, T. and Sathyendranath, S. (1988). Oceanic Primary Production: Estimation by Remote Sensing at Local and Regional Scales. *Science*, 241:doi:10.1126/science.241.4873.1613.

Platt, T., White II, G., Zhai, L., Sathyendranath, S., and Roy, S. (2009). The phenology of phytoplankton blooms: Ecosystem indicators from remote sensing. *Ecol. Model.*, In press:doi:10.1016/j.ecolmodel.2008.11.022.

Riley, G. A. (1957). Phytoplankton of the North Central Sargasso Sea, 1950-52. *Limnol. Oceanogr.*, 2:252–270.

Robinson, C. (2008). Heterotrophic Bacterial Respiration. In Kirchman, D., editor, *Microbial Ecology of the Oceans, Second Edition*, pages 299–334. Wiley, New York.

Robinson, C. and Williams, P. (1999). Plankton net community production and dark respiration in the Arabian Sea during September 1994. *Deep Sea Res., Part II*, 46:745–765.

Robinson, C. and Williams, P. (2005). Respiration and its measurement in surface marine waters. In del Giorgio, P. and Williams, P., editors, *Respiration in Aquatic Ecosystems*, pages 147–180. Oxford University Press, Oxford.

Rochford, P., Kara, A., Wallcraft, A., and Arnone, R. (2001). Importance of solar subsurface heating in ocean general circulation models. *J. Geophys. Res.*, 106:30923–30938.

Sarmiento, J. L. and Gruber, N. (2006). *Ocean Biogeochemical Dynamics*. Princetown University Press.

Sarmiento, J. L., Slater, R., Barber, R., Bopp, L., Doney, S., Hirst, A., Kleypas, J., Matear, R., Mikolajewicz, U., Monfray, P., Soldatov, V., Spall, S., and Stouffer, R. (2004). Response of ocean ecosystems to climate warming. *Global Biogeochem. Cycles*, 18:doi:10.1029/2003GB002134.

Sathyendranath, S., Platt, T., Caverhill, C., Warnock, R., and Lewis, M. (1989). Remote sensing of oceanic primary production: computations using a spectral model. *Deep Sea Res.*, 36:431–453.

Sathyendranath, S., Stuart, V., Nair, A., Oka, K., Nakane, T., Bouman, H., Forget, M., Maass, H., and Platt, T. (2009). Carbon-to-chlorophyll ratio and growth rate of phytoplankton in the sea. *Mar. Ecol. Prog. Ser.*, 383:doi:10.3354/meps07998.

Schlitzer, R. (2002). Carbon export fluxes in the Southern Ocean: results from inverse modeling and comparison with satellite-based estimates. *Deep Sea Res., Part II*, 49:1623–1644.

Serret, P., Fernández, E., Álvarez-Sostres, J., and Anadón, R. (1999). Seasonal compensation of microbial production and respirationin a temperate sea. *Mar. Ecol. Prog. Ser.*, 187:43–57.

Serret, P., Fernández, E., and Robinson, C. (2002). Biogeographic differences in the net ecosystem metabolism of the open ocean. *Ecology*, 83:3245–3234.

Serret, P., Fernández, E., Robinson, C., Woodward, E., and Pérez, V. (2006). Local production does not control the balance between plankton photosynthesis and respiration in the open Atlantic Ocean. *Deep Sea Res., Part II*, 83:3245–3234.

Serret, P., Robinson, C., Fernández, E., Teira, E., and Tilstone, G. (2001). Latitudinal variation of the balance between plankton photosynthesis and respiration in the eastern Atlantic Ocean. *Limnol. Oceanogr.*, 46:1642–1652.

Serret, P., Robinson, C., Fernández, E., Teira, E., Tilstone, G., and Pérez, V. (2009). Predicting plankton net community production in the Atlantic Ocean. *Deep Sea Res., Part II*, 56:941–953.

Siegel, D., Doney, S., and Yoder, J. (2002). The North Atlantic spring phytoplankton bloom and Sverdrup's critical depth hypothesis. *Science*, 296:730–733.

Smetacek, V. and Passow, U. (1990). Spring Bloom Initiation and Sverdrup's Critical-Depth Model. *Limnol. Oceanogr.*, 35:228–234.

Sverdrup, H. U. (1953). On conditions for the vernal blooming of phytoplankton. *Cons. Int. Expor. Mer.*, 18:287–295.

Williams, P. (1998). The balance of plankton respiration and photosynthesis in the open oceans. *Nature*, 394:55–57.

Williams, P. (2000). Net production, gross production and respiration: what are the interconnections and what controls what? In Hanson, R. B., Ducklow, H. W., and Field, J. G., editors, *The changing ocean carbon cycle: a midterm synthesis of the Joint Global Ocean Flux Study*, pages 37–60. Cambridge University Press, Cambridge.

Williams, P., Bowers, D., Duarte, C., Augusti, S., del Giorgio, P., and Cole, J. (1999). Regional Carbon Imbalances in the Oceans. *Science*, 284:doi:10.1126/science.284.5421.1735b.

Williams, P., Moris, P., and Karl, D. (2004). Net communityproduction and metabolic balance at the oligotrophic ocean site, station ALOHA. *Deep Sea Res., Part I*, 51:doi:10.1016/j.dsr.2004.07.001.

Zhai, L., Platt, T., Tang, C., Dowd, M., Sathyendranath, S., and Forget, M. (2008). Estimation of phytoplankton loss rate by remote sensing. *Geophys. Res. Lett.*, 35:doi:10.1029/2008GL035666.

Zhai, L., Platt, T., Tang, C., Sathyendranath, S., Fuentes-Yaco, C., Devred, E., and Wu, Y. (2009). Seasonal and geographic variations in phytoplankton losses from the mixed layer on the Northwest Atlantic Shelf. *J. Marine Syst.*, submitted.

4.7 Tables

Table 4.1: Glossary of mathematical notations.

Notation	Quantity and description	Units
α	Initial slope of *P-I* curve	$mg\ C\ mol\ photon^{-1}$
b_i	Initiation of growing season	$week$
b_t	Timing of maximum amplitude	$week$
b_e	End of growing season	$week$
I	Irradiance in the Photosynthetically Active Range (PAR)	$mol\ photon\ m^{-2}\ d^{-1}$
I_c	Community compensation irradiance	$mol\ photon\ m^{-2}\ d^{-1}$
I_{cphy}	Phytoplankton compensation irradiance	$mol\ photon\ m^{-2}\ d^{-1}$
I_o	Incident irradiance in the PAR at the surface (z=0)	$mol\ photon\ m^{-2}\ d^{-1}$
k	Vertical attenuation for irradiance in the PAR	m^{-1}
k_{490}	Vertical attenuation for irradiance at 490nm wavelength	m^{-1}
NCB_{mld}	Integrated net change of phytoplankton biomass in the mixed layer	$g\ C\ m^{-2}\ y^{-1}$
NCP	Net community production	$g\ C\ m^{-2}\ y^{-1}$
NCP_{eu}	Integrated net community production in the euphotic zone	$g\ C\ m^{-2}\ y^{-1}$
NCP_{mld}	Integrated net community production in the mixed layer	$g\ C\ m^{-2}\ y^{-1}$
PP	Primary Production	$g\ C\ m^{-2}\ y^{-1}$
P_o	Primary Production at surface (z=0)	$g\ C\ m^{-2}\ y^{-1}$
P_{cr}	Integrated Primary Production from surface to z_{cr}	$g\ C\ m^{-2}\ y^{-1}$
P_{mld}	Integrated Primary Production in the mixed layer	$g\ C\ m^{-2}\ y^{-1}$
$P_{0.1\%}$	Integrated Primary Production at 0.1% light level	$g\ C\ m^{-2}\ y^{-1}$
R	Community respiration	$g\ C\ m^{-2}\ y^{-1}$
R_o	Community respiration at surface (z=0)	$g\ C\ m^{-2}\ y^{-1}$
R_{cr}	Integrated community respiration from surface to z_{cr}	$g\ C\ m^{-2}\ y^{-1}$
R_{mld}	Integrated community respiration in the mixed layer	$g\ C\ m^{-2}\ y^{-1}$
z	Depth	m
z_c	Sverdrup's compensation depth, where P_o=R_o	m
z_{cr}	Sverdrup's critical depth, where P_{cr}=L_{cr}	m
z_{mld}	Depth of the mixed layer	m
$z_{0.1\%}$	Depth at 0.1% light level	m

Table 4.2: Annual mixed layer depth-integrated primary production P_{mld}, community respiration R_{mld} and net community production NCP_{mld} averaged in different regions and over the global ocean. Positive NCP_{mld} indicates net autotrophic imbalance and negative NCP_{mld} indicates net heterotrophic imbalance. Estimates are in Pg C y^{-1}.

Region	P_{mld}	R_{mld}	NCP_{mld}
North Atlantic	2.87	2.22	+ 0.65
North Pacific	3.22	6.76	− 3.54
Southern Ocean	10.65	13.26	− 2.61
Tropics and subtropics	20.53	21.60	− 1.07
Global	38.06	44.00	− 5.94

4.8 Figures

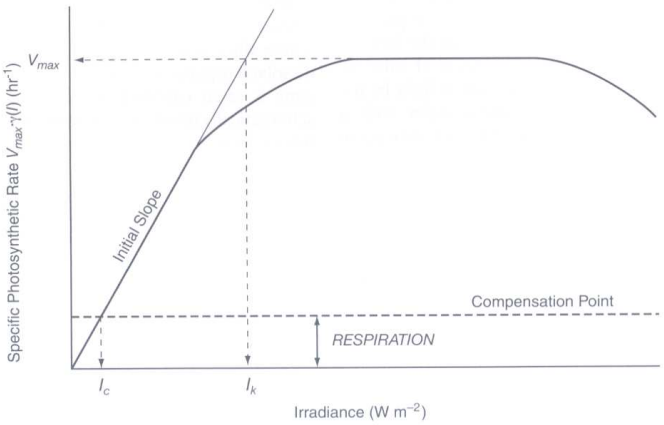

Figure 4.1: Schematic of the effect of irradiance range on the specific rate of photosynthesis (figure adapted from Sarmiento and Gruber (2006)). The intersection between the initial slope α and the specific rate of respiration indicates the minimum irradiance level required for net growth to occur. This level is called the compensation irradiance I_c.

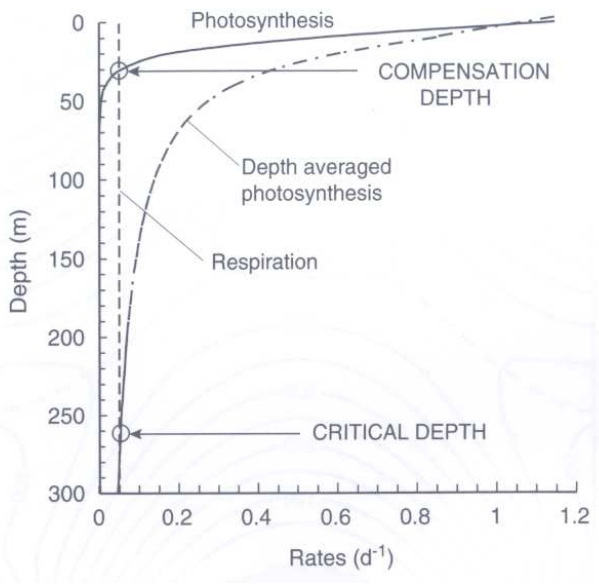

Figure 4.2: Schematic representation of the compensation depth and critical depth concepts as defined by Sverdrup (1953) (figure adapted from Sarmiento and Gruber (2006)). The rates of photosynthesis decrease exponentially with depth due to attenuation of the irradiance by absorption and scattering. The rates of respiration of the plankton community (i.e. phytoplankton, zooplankton and bacteria) are assumed to remain constant with depth. At compensation depth z_c, the rates of photosynthesis and respiration are equal. In a stratified water-column, net phytoplankton growth occurs at depth greater than z_c. In a mixed water-column, phytoplankton cells will spend time both above and below z_c and the depth-averaged rates of photosynthesis are estimated. The depth at which the averaged-depth rates of photosynthesis and respiration are equal is defined as the critical depth z_{cr}. Net phytoplankton growth occurs when the depth of the mixed layer is greater than z_{cr}.

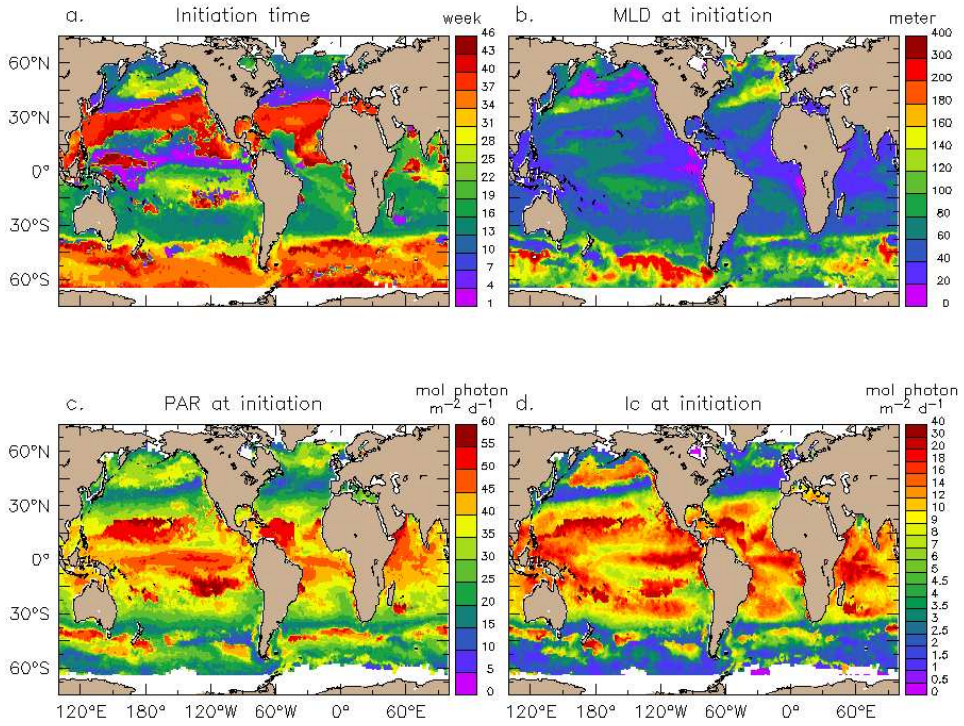

Figure 4.3: Spatial distribution of (a) week of initiation of growing (b_i; week 1 starting in January), (b) mixed layer depth at initiation (z_{mld} in meters), (c) incident irradiance in the PAR at initiation (I_o in mol photon m^{-2} d^{-1}), (d) community compensation irradiance (I_c in mol photon m^{-2} d^{-1}). b_i, z_{mld} and I_o are available as climatologies.

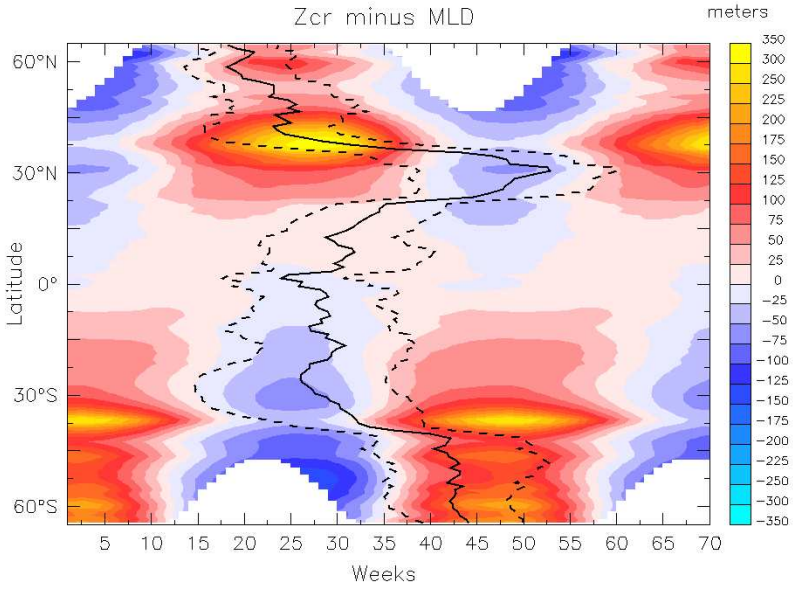

Figure 4.4: Difference between the Sverdrup critical depth z_{cr} and the mixed layer depth z_{mld} (climatology of de Boyer Montégut et al. (2004)) as a function of latitude and time. I_c is assumed to remain constant over time. Positive values indicate that z_{cr} is deeper than the mixed layer. Plain line indicates the time of peak amplitude of the phytoplankton growing season. Dashed lines indicate the time of initiation and end of growing season.

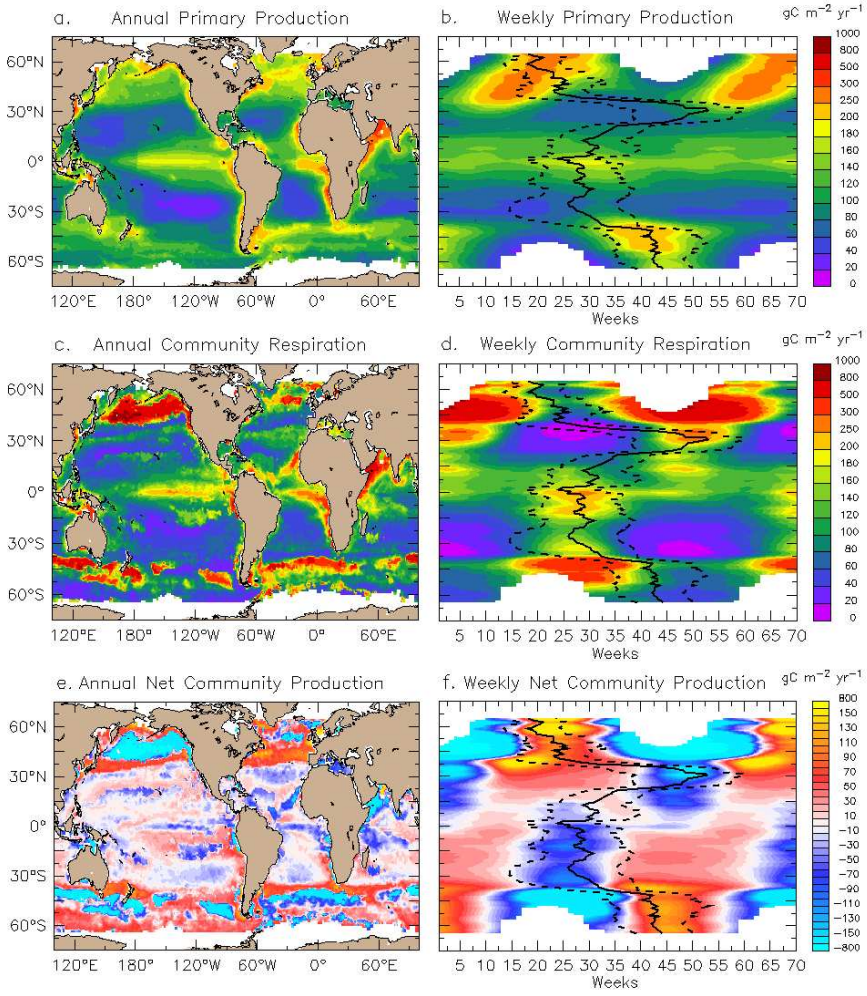

Figure 4.5: Spatial and temporal distribution of mixed layer depth-integrated (a, b) Primary Production (P_{mld} in g C m^{-2} y^{-1}); (c, d) Community respiration (R_{mld} in g C m^{-2} y^{-1}); (e, f) Net community production (NCP_{mld} in g C m^{-2} y^{-1}). Positive NCP_{mld} indicates net autotrophic imbalance ($P_{mld} > R_{mld}$). Negative NCP_{mld} indicates net heterotrophic imbalance ($P_{mld} < R_{mld}$). Plain line indicates the time of peak amplitude of the phytoplankton growing season. Dashed lines indicate the time of initiation and end of growing season.

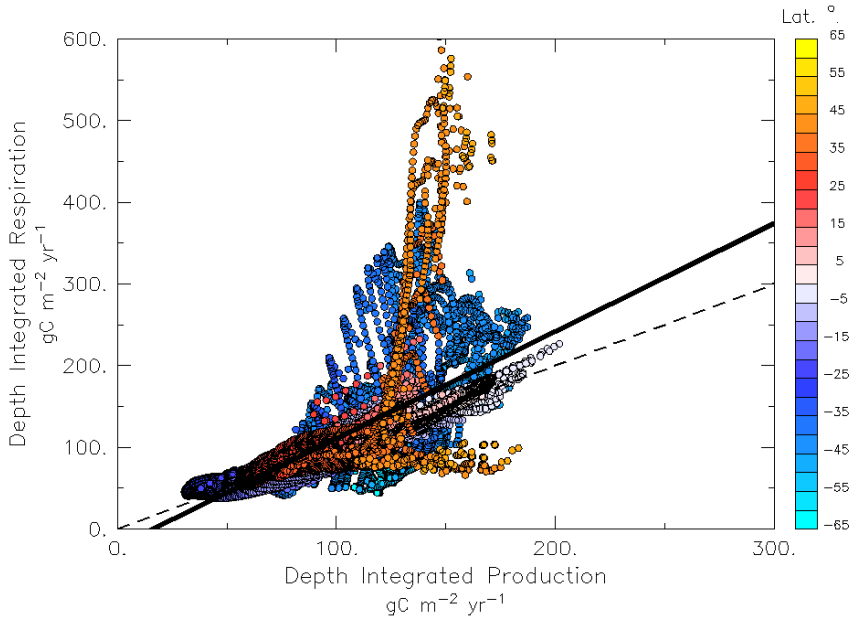

Figure 4.6: Mixed layer depth-integrated community respiration R_{mld} as a function of production P_{mld} in g C m^{-2} y^{-1}. Colour scale indicates the latitude of the data point (from 65°S to 65°N). The solid line is the fitted regression $R_{mld} = 1.3 \pm 0.01 P_{mld} - 21$, $\rho = 0.69$, $P < 0.001$, $n = 13473$. The likelihood of the slope is given at $\pm$ 1 σ. The dashed line represents equality between production and respiration rates.

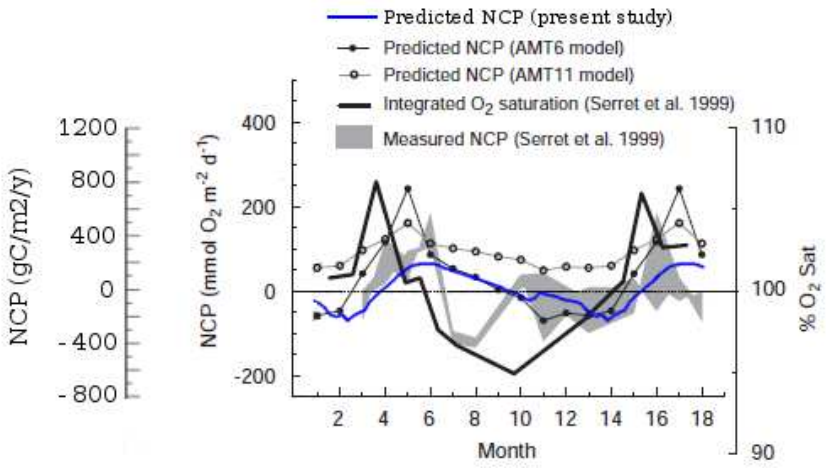

Figure 4.7: Mean seasonal cycles of present study mixed layer depth-integrated NCP_{mld} and Serret et al. (2009) modelled euphotic zone-integrated NCP_{eu} in the NADR province (Longhurst, 1998); and seasonal variation of the percentage of oxygen saturation integrated to the depth of the winter mixed layer at an off-shelf station in the southern Bay of Biscay measured by Serret et al. (1999). Shadowed trend shows the range of NCP_{eu} measurements across the Biscay shelf as reported by Serret et al. (1999). The figure is adapted from Serret et al. (2009). The present study NCP_{mld} averaged throughout the NADR province was converted in mmol O_2 m^{-2} d^{-1} (O_2:C mole ratio of 175:127, Broecker and Peng (1982)). The scale in g C m^{-2} y^{-1} is given for comparative information.

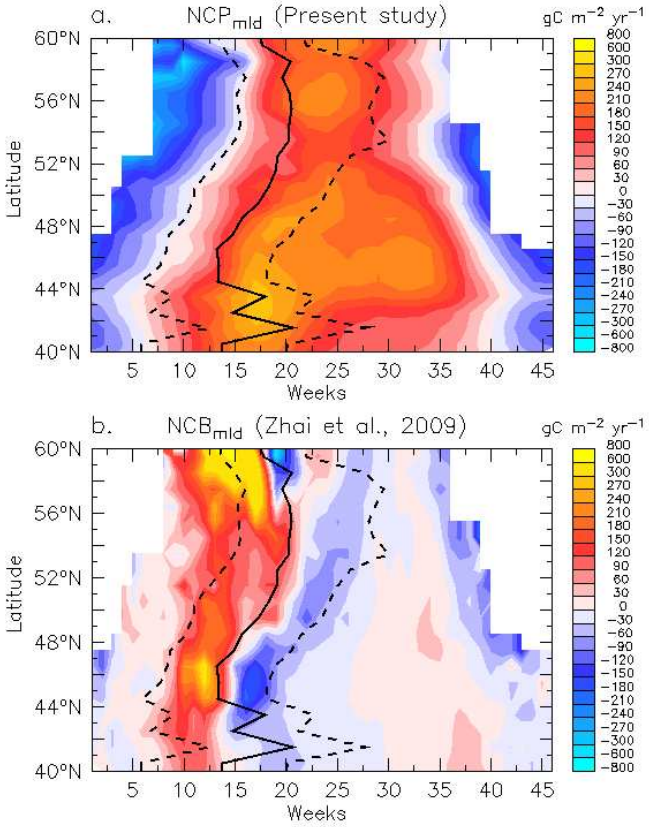

Figure 4.8: Mixed layer depth-integrated (a) net community production NCP_{mld} and (b) net change in phytoplankton biomass NCB_{mld} as a function of latitude and time. NCB_{mld} is calculated as per Zhai et al. (2009). Estimates are in g C m^{-2} y^{-1}. Plain line indicates the time of peak amplitude of the phytoplankton growing season. Dashed lines indicate the time of initiation and end of growing season.

Chapter 5

Conclusions

5.1 Global ocean phytoplankton phenology

This work presents a first assessment of phytoplankton phenology at the global scale. Distinct growth regimes are identified, associated with specific environmental conditions. Phytoplankton growing season begins in winter around 35° latitude in the subtropics, and propagates towards the poles to begin in late spring/early summer at 60° latitude. In latitudinal band, the time of initiation is tightly coupled with the seasonal increase in insolation and shallowing of the mixed layer. The duration appears to be limited by the conditions occurring at the end of the growing season, indicating nutrient depletion in surface waters. The duration shortens towards the poles ($<$ 10 weeks) and is generally associated with high biomass maximum ($>$ 1.5 mg m^{-3}) characteristic of intense blooms.

In contrast, equatorwards of 35°, light is rarely limiting, and the phytoplankton growing season is triggered and limited by nutrient supply controlled by ocean mixing. Phytoplankton biomass remains low ($<$ 0.5 mg m^{-3}) throughout a relatively long growing season ($>$ 15 weeks). However, at these latitudes, a permanent stratification of surface waters might prevent seasonal development of phytoplankton. Regions with low or no seasonality are more difficult to characterise with the method of the phenology developed in the present study. In these regions, if any growth occurs, a particularly long growing season is generally estimated, whereas if no growth occurs, the method can detect extremely low pulses in chlorophyll and interpret a growing season of one to two weeks. The tropics are therefore particularly challenging to track and can show extreme interannual variability in the estimated duration of growing season.

5.2 Interannual and decadal variability in phytoplankton growing season

The 1998-2007 decade of observations shows large interannual variability in duration of growing season by up to ± 10 weeks in some regions. Significant negative

linear trends in duration ($-$ 10% yr^{-1} on average) are observed in the tropics and subtropics, the eastern North Atlantic and the Southern Ocean (SO) south of 50°S. Regions showing a significant increase in duration (+ 8% yr^{-1} on average) occupy a smaller fraction of the ocean and include the Greenland Sea and part of the SO 35-45°S band. The major El Niño that occured in 1997-1998 at the beginning of the time series strongly enhanced phytoplankton biomass and primary production (Behrenfeld et al., 2001, 2006). Hence, the estimated reduction in duration over the 1998-2007 period is largely influenced by this event and might not reflect long-term trends.

Using satellite observations from the sensors CZCS and SeaWiFS, we estimate that North of 45°S, the phytoplankton growing season increased by 2.4 weeks on average between the periods 1979-1986 and 1998-2008. Over more than 70% of the global ocean, the regional lengthening (shortening) of the phytoplankton growing season are associated with geographic increases (decreases) in sea-surface temperature (SST). Large regional increases in SST enhance upper-ocean stratification and limit the supply of nutrient (Bopp et al., 2001, 2005; Behrenfeld et al., 2006), leading to the expansion of oligotrophic and permanently-stratified waters (Sarmiento et al., 2004; Polovina et al., 2008).

5.3 Impact of biological changes on the ocean carbon cycle

Global ocean duration in phytoplankton growing season is shown to be linearly related to carbon export flux. A decrease in carbon export of 0.6 Pg C y^{-1} (excluding the SO) is inferred from the increase in duration over two decades between 1979-1986 and 1998-2008. On this timescale, approximately 75% of the changes in export flux are reflected directly in changes in sea-to-air CO_2 flux (Moore et al., 2006; Giraud et al., 2008), so as to weaken the oceanic CO_2 sink by -0.4 Pg C y^{-1} North of 45°S. This indicates a rapid response of marine ecosystem to global change and

emphasises its importance and significant impact on the oceanic carbon cycle.

However, limited CZCS data coverage in the SO impedes the extension of the above conclusions to the global ocean. In fact, recent decadal increase in winds in the Southern Ocean would suggest enhanced nutrient supply (Le Quéré et al., 2007), and thus a different operating mechanism. Using remote sensing data of Phytoplankton Functional Types (PFTs) (Alvain et al., 2005) and results from a biogeochemistry model that includes several PFTs (Le Quéré et al., 2007), we have shown that changes in PFT community composition in response to environmental changes may act to partially counterbalance the weakening of the SO sink of CO_2 (Alvain et al., 2009) caused by the strengthening of the surface winds. Assessment of the specific contribution of each PFT to export production appears critical to improve understanding of, and quantify the impact of changes in biology on the ocean carbon cycle. This is one of the perspectives that I wish to explore in my future research.

5.4 Phytoplankton phenology applications

5.4.1 Resolving Sverdrup's critical depth model

Knowledge of the time of initiation b_i of the phytoplankton growing season allows us to estimate the key parameters of Sverdrup (1953) critical depth model and predict mixed layer integrated plankton community respiration R_{mld} and net community production NCP_{mld} at the global scale. Although the method of estimation of b_i presents some limitations in regions of low phytoplankton biomass seasonality, NCP_{mld} estimates agree with *in-situ* observations and model results in the tropical and North Atlantic regions. Thus, the method may be use to assess the trophic balance (i.e. heterotrophic or autotrophic) of some regions of the global ocean.

5.4.2 Assessing global ocean ecosystem-biogeochemical models

Most recent ocean ecosystem-biogeochemical models show a significant development in the representation of ecosystem processes and include several PFTs (Moore et al., 2002; Gregg et al., 2003; Le Quéré et al., 2005). This increased biological complexity allows to address pressing questions and hypotheses on climate change impacts on marine ecosystems. Hence, model results and projections are subject to international scrutiny and assessment of model skills has become essential. For this purpose, a suite of metrics has been identified to compare comprehensively model results with *in-situ* and remote sensing observations. The metrics include: graphical techniques, statistical analysis (root mean square, correlation), difference fields and Taylor diagrams (Doney et al., 2009). Although considerable effort has been devoted to the selection and implementation of the metrics, the variables themselves have not been developed to the same extent. Amplitude and annual chlorophyll concentrations are commonly used to assess phytoplankton biomass performance in the models (Gregg et al., 2009). Estimating phenological variables such as the times of initiation, peak amplitude and duration of the growing season in models would allow for a systematic evaluation of model representations of phytoplankton seasonal cycles. This is another perspective that I would be particularly interested to pursue in the future using different global ocean ecosystem-biogeochemical models.

5.4.3 Monitoring marine ecosystems

In the present work, we show that phytoplankton phenology is affected by changes in climate over recent decades. Phytoplankton are at the base of the food chain and the timing of their life cycle events is critical to the recruitment and year-class strength of zooplankton and fish populations (Platt et al., 2003; Koeller et al., 2009). Shifts in timing can induce decoupling of phenological relationships between phytoplankton and larvae, and ultimately lead to extinction of some higher trophic level species (Hughes, 2000). Thus, changes in phytoplankton phenology have important

socioeconomic impacts, especially when they affect the commercially exploited fish stocks (Hays et al., 2005). Global monitoring of phytoplankton phenology is extremely useful to assess and predict future directional changes in marine ecosystems in response to changes in climate.

References

Alvain, S., Le Quéré, C., Racault, M.-F., Beaugrand, G., and Bopp, L. (2009). Rapid shift in phytoplankton ecosystem due to climate variability. In preparation.

Alvain, S., Moulin, C., Dandonneau, Y., and Bréon, F. (2005). Remote sensing of phytoplankton groups in case 1 waters from global SeaWiFS imagery. *Deep Sea Res., Part I*, 52:1989–2004.

Behrenfeld, M., O'Malley, R., Siegel, D., McClain, C., Sarmiento, J., Feldman, G., Milligan, A., Falkowski, P., Letelier, R., and Boss, E. (2006). Climate-driven trends in contemporary ocean productivity. *Nature*, 444:doi:10.1038/nature05317.

Behrenfeld, M. J., Randerson, J. T., McClain, C. R., Feldman, G. C., Los, S. O., Tucker, C. J., Falkowski, P. G., Field, C. B., Frouin, R., Esaias, W. E., Kolber, D. D., and Pollack, N. H. (2001). Biospheric primary production during an ENSO transition. *Science*, 291:doi:10.1126/science.1055071.

Bopp, L., Aumont, O., Cadule, P., Alvain, S., and Gehlen, M. (2005). Response of diatoms distribution to global warming and potential implications: A global model study. *Geophys. Res. Lett.*, 32:doi:10.1029/2005GL023653.

Bopp, L., Monfray, P., Aumont, O., Dufresne, J.-L., LeTreut, H., Madec, G., Terray, L., and Orr, J. (2001). Potential impact of climate change on marine export production. *Global Biogeochem. Cycles*, 15:81–100.

Doney, S., Lima, I., Moore, J., Lindsay, K., Behrenfeld, M., Westberry, T., Mahowald, N., Glover, D., and Takahashi, T. (2009). Skill metrics for confronting global upper ocean ecosystem-biogeochemistry models against field and remote sensing data. *J. Marine Syst.*, 76:95–112.

Giraud, X., Le Quéré, C., and da Cunha, L. (2008). Importance of coastal nutrient supply for global ocean biogeochemistry. *Global Biogeochem. Cycles*, 22:doi:10.1029/2006GB002717.

Gregg, W. W., Friedrichs, M., Robinson, A., Rose, K., Schlitzer, R., Thompson, K., and Doney, S. (2009). Skill assessment in ocean biological data assimilation. *J. Marine Syst.*, 76:16–33.

Gregg, W. W., Ginoux, P., Schopf, P. S., and Casey, N. W. (2003). Phytoplankton and iron: validation of a global three-dimensional ocean biogeochemical model. *Deep Sea Res., Part II*, 50:3143–3143.

Hays, G., Richardson, A., and Robinson, C. (2005). Climate change and marine plankton. *Trends Ecol. Evol.*, 20:doi:10.1016/j.tree.2005.03.004.

Hughes, L. (2000). Biological consequences of global warming: is the signal already apparent? *Trends Ecol. Evol.*, 15:56–61.

Koeller, P., Fuentes-Yaco, C., Platt, T., Sathyendranath, S., Richards, A., Ouellet, P., Orr, D., Skúladóttir, U., Wieland, K., Savard, L., and Aschan, M. (2009). Basin-Scale Coherence in Phenology of Shrimps and Phytoplankton in the North Atlantic Ocean. *Science*, 324:doi:10.1126/science.1170987.

Le Quéré, C., Harrison, S. P., Prentice, I. C., Buitenhuis, E. T., Aumont, O., Bopp, L., Claustre, H., da Cunha, L. C., Geider, R., Giraud, X., Klaas, C., Kohfeld, K. E., Legendre, L., Manizza, M., Platt, T., Rivkin, R. B., Sathyendranath, S., Uitz, J., Watson, A. J., and Wolf-Gladrow, D. (2005). Ecosystem dynamics based on plankton functional types for global ocean biogeochemistry models. *Glob. Change Biol.*, 11:doi:10.1111/j.1365–2486.2005.01004.x.

Le Quéré, C., Rödenbeck, C., Buitenhuis, E., Conway, T., Langenfelds, R., Gomez, A., Labuschagne, C., Ramonet, M., Nakazawa, T., Metzl, N., gillett, N., and Heimann, M. (2007). Saturation of the Southern Ocean CO_2 sink due to recent climate change. *Science*, 316:doi:10.1126/science.1136188.

Moore, J., Doney, S., Lindsay, K., Mahowald, N., and Michaels, A. (2006). Nitrogen fixation amplifies the ocean biogeochemical response to decadal timescale variations in mineral dust deposition. *Tellus*, 58B:560–572.

Moore, J. K., Doney, S. C., Kleypas, J. A., Glover, D. M., and Fung, I. Y. (2002). An intermediate complexity marine ecosystem model for the global domain. *Deep Sea Res., Part II*, 49:403–462.

Platt, T., Fuentes-Yaco, C., and Frank, K. (2003). Spring algal bloom and larval fish survival. *Nature*, 423:398–399.

Polovina, J., Howell, E., and Abecassis, M. (2008). Ocean's least productive waters are expanding. *Geophys. Res. Lett.*, 35:doi:10.1029/2007GL031745.

Sarmiento, J. L., Slater, R., Barber, R., Bopp, L., Doney, S., Hirst, A., Kleypas, J., Matear, R., Mikolajewicz, U., Monfray, P., Soldatov, V., Spall, S., and Stouffer, R. (2004). Response of ocean ecosystems to climate warming. *Global Biogeochem. Cycles*, 18:doi:10.1029/2003GB002134.

Sverdrup, H. U. (1953). On conditions for the vernal blooming of phytoplankton. *Cons. Int. Expor. Mer.*, 18:287–295.